Effects of aerosol on shallow convective clouds

George Spill

St Edmund Hall

University of Oxford

A thesis submitted for the degree of

Doctor of Philosophy

Trinity 2021

Acknowledgements

I would like to begin by thanking my supervisor, Philip Stier, for his guidance, support, and insight, which were invaluable throughout this project and in developing my own research ideas. I would also like to thank my co-supervisor, Paul Field, for his support and assistance, most particularly in the face of innumerable technical hurdles. Without their time and experience, none of this work would have been possible.

Particular thanks are also due to Guy Dagan, for his ideas, support, and peerless feedback. I would like to thank all the members of the Climate Processes group with whom I have had the pleasure of sharing our section of corridor. The enthusiasm and exciting work being carried out have been sources of inspiration throughout my DPhil.

I would like to thank Ilan Koren and Lesley Gray for examining this thesis, and for an interesting and enjoyable discussion during the viva.

I am grateful to both the Natural Environment Research Council, and the UK Met Office for funding this project, and to UK Research and Innovation for their further support. I am grateful, too, for having been part of the Oxford Doctoral Training Program in Environmental Research.

I would like to thank all those at St Edmund Hall who have made it such an incredible place to spend my time at Oxford. Special thanks must go to St Edmund Hall Boat Club, in particular my crewmates and coaches, from whom I have learned many valuable lessons, and of whom there are far too many to list.

I would like to express my gratitude to my parents, Jane and Stephen, for their boundless love and support throughout my time at Oxford, and for encouraging me to pursue my academic interests. Finally, I would like to thank Rebecca Preece for her love and support, as well as her encouragement and belief in me.

Abstract

Clouds and aerosols are deeply significant components of the Earth's atmosphere and climate system. Yet, aerosol-cloud interactions, particularly for shallow convective clouds, remain poorly understood and highly uncertain. Many varied, and often conflicting, hypotheses of aerosol effects on shallow clouds have been proposed, reflecting the myriad pathways and mechanisms through which they interact. This thesis uses high-resolution, large-domain simulations to investigate the effects of aerosol on shallow convective clouds. Large-domain simulations are performed to capture the large-scale behaviour of the cloud field in response to aerosol perturbations. Increased aerosol is found to lead to decreases in domain-mean precipitation, increases in domain-mean liquid water path, and little impact on cloud fraction or the frequency of higher precipitation rates, in contrast to existing research. It is hypothesised that these differences are due to differing approaches to the model setup. Idealised and realistic simulations of trade wind cumuli are performed, producing starkly different cloud fields and responses to increases in aerosol. The idealised simulations experience significant changes in their thermodynamic evolution along with convective deepening, in contrast with little change in the thermodynamic evolution of the realistic simulations. Detailed investigation of the properties and life-cycle of individual clouds highlights the different responses of clouds with different characteristics to changes in aerosol. Cloud lifetimes are directly quantified using a cloud tracking algorithm, displaying little change in response to increased aerosol. Shallow clouds occur less frequently, while congestus clouds may become deeper. Increased aerosol notably delays the onset of precipitation, and reduces the probability of precipitation. This analysis emphasises the importance of representing the diversity present in realistic trade wind cloud fields.

Contents

List of Figures

Preface

Whether looking up at the sky from the Earth's surface, or looking down on our planet from space, the prevalence of clouds throughout the atmosphere is clear. So, too, is the rich variety in their appearance and behaviour, inevitably leading one to wonder at the importance they must have in the climate. From Aristotle's *Meteorologica* to the pioneering work of Lamarck (1802) and Howard (1803), and on to modern atmospheric science, and from the poems of Goethe to the paintings of John Constable, clouds have intrigued, captivated, and inspired.

Clouds and aerosols play hugely significant roles in the atmosphere and climate system. Clouds are responsible for transporting moisture, energy, and momentum through the atmosphere, and between the atmosphere and the Earth's surface. They exert a radiative effect through reflecting incoming short wave radiation, and emitting long wave radiation at a range of temperatures. Aerosols serve as condensation nuclei for the formation of cloud droplets, and so are an integral part of understanding cloud behaviour, but also are associated with their own radiative effects. Cloud processes range from microphysics on micrometer scales, up to mesoscale systems on horizontal scales of hundreds of km, while processes across these scales may have profound impacts on one another. This is key, not only to the rich and exciting behaviours of clouds, but also to the difficulty in studying and understanding them, which persists in current research. This thesis is motivated by both the importance of clouds, and their scientifically compelling nature.

The following section will provide a brief overview of the structure of the thesis, and of each chapter.

Structure of the thesis

Chapter 1: This chapter will outline the scientific concepts underpinning cloud physics, as well as the various methodologies employed in the study of clouds, with a specific focus on shallow convective clouds and their representation in numerical models. The roles of clouds and aerosols in the atmosphere are discussed in detail, along with the current state of research in shallow clouds and aerosol-cloud interactions. Based on this discussion, the research questions that this thesis aims to explore are outlined. Furthermore, the models and methodologies employed in the thesis are discussed in detail.

Chapter 2: Simulations of the effects of aerosol on shallow cumuli in large domains are presented, using the case study outlined in the previous chapter. Simulations are carried out using the Met Office Unified Model (UM), characterised particularly by high spatial resolution and the large, nested domains employed. A series of simulations with idealised aerosol perturbations are performed. The analysis focuses on the effect of these perturbations on the characteristics of domain mean properties such as cloud fraction, liquid water path, and precipitation.

Chapter 3: A comparison of idealised and realistic simulations of shallow cumuli is presented, with a focus on their respective responses to aerosol perturbations. These are performed based on the findings of Chapter 2, and their context amid existing research. The analysis focuses on comparing the effect of different approaches to large scale forcing and domain boundaries on the response of the simulations.

Chapter 4: This chapter builds on Chapter 3, and extends the analysis of the realistic simulations using a cloud tracking algorithm. This allows for a detailed inspection of the effect of aerosol perturbations on the properties of individual clouds, and how these vary over the cloud life-cycle.

Chapter 5: Finally, the results of the previous chapters are summarised. The conclusions of the thesis and their relation to existing and future research are discussed. The chapter concludes by suggesting new potential questions and avenues of research arising from the findings of the thesis.

Chapter 1

Introduction

1.1 Atmospheric aerosols

Atmospheric aerosols are defined as any solid or liquid particles suspended in the atmosphere. They are either emitted directly into the atmosphere, in which case they are referred to as primary aerosols, or can be formed by precursor gases, and are referred to as secondary aerosols. Aerosols may be classified according to their chemical properties, or else by physical characteristics such as shape, density, and size, which can vary from nanometres to several micrometres (Lohmann et al., 2016). They are a significant component of the atmosphere, directly affecting the radiation budget through scattering and absorption (Ångström, 1962; McCormick & Ludwig, 1967), as well as affecting the thermal profile of the atmosphere via these processes (Grassl, 1973; Markowicz et al., 2002; Davidi et al., 2012).

Aerosols further impact the state of the atmosphere through interactions with clouds, either in their role as cloud condensation or ice nuclei, or through cloud responses to the aforementioned radiative cooling and warming (Twomey, 1977; Albrecht, 1989; Boucher et al., 2013a; Lohmann et al., 2016; Seinfeld & Pandis, 2016).

Atmospheric aerosols have a large variety of both natural and anthropogenic sources. Natural emissions of aerosols include sea salt, mineral dust, wildfire smoke, as well as organic aerosols from biogenic sources (Andreae, 2007; Carslaw et al., 2010). Biogenic emissions include both primary, such as pollen or plant debris, as well as secondary aerosols from emissions of gases such as dimethyl sulphide from plankton (Boucher et al., 2013a; Cavalli et al., 2004; Korhonen et al., 2008). Volcanoes, through degassing and eruptions, are also a significant source of aerosols, primarily sulphates (Lohmann et al., 2016; Gettelman et al., 2015). Anthropogenic emissions of aerosols and aerosol precursors are strongly associated with industrial processes and the burning of fossil fuels, and include sulphates, nitrates, and black carbon (Boucher et al., 2013a). These aerosol species, along with other organic carbon species, are also components of anthropogenic biomass burning aerosol, produced by vegetation fires and the use of biofuels (Andreae, 2019; Haywood et al., 2021). Black carbon is particularly important for its ability to absorb solar radiation (Stier et al., 2007), while species such as sulphates and nitrates are primarily associated with scattering (Charlson et al., 1992; Boucher et al., 2013a).

Many aerosol species evidently share both natural and anthropogenic sources. Aerosols typically have lifetimes in the atmosphere of a few days in the case of coarse primary aerosol particles, up to a little over a week for smaller secondary aerosol particles (Seinfeld & Pandis, 2016). There are therefore very few regions of the atmosphere that may be considered pristine, making an assessment of aerosol conditions before the onset of significant anthropogenic emissions very difficult (Andreae, 2007). This is additionally complicated by nonlinearities in aerosol processes caused by aerosol emissions, such that anthropogenic emissions of carbonaceous aerosol disproportionately contribute to aerosol number close to source regions, while anthropogenic sulphate emissions disproportionately contribute far from source regions and contribute less than proportionately close to

source regions (Stier et al., 2006).

Furthermore, localised emissions and large-scale transport contribute to significant variability in the spatiotemporal distribution of aerosols (Schutgens et al., 2017; Zhang et al., 2012; Koffi et al., 2016). These factors are key contributors to the uncertainty associated with estimates of radiative forcing due to anthropogenic aerosol (Carslaw et al., 2013; Watson-Parris et al., 2020). Indeed, aerosol radiative forcing, through direct interactions with radiation and through aerosol-cloud interactions, is the largest source of uncertainty in estimates of anthropogenic radiative forcing of the atmosphere, despite its significance in offsetting some of the forcing due to greenhouse gases (Myhre et al., 2013). The Intergovernmental Panel on Climate Change (IPCC) 5th Assessment Report (AR5) describes the distinction between *forcings*, where agents such as aerosol act directly on the global radiation budget, and *rapid adjustments*, where an agent causes changes to another component of the climate system, such as cloud cover, thus impacting the radiation budget (Boucher et al., 2013a). The net forcing resulting from the combination of RF and rapid adjustments is then known as the *effective radiative forcing* (ERF). The radiative forcing (RF) due to aerosol-radiation interactions (RF_{ari}) is often referred to as the aerosol direct effect. When considered along with rapid adjustments, that have previously been known as semi-direct effects, the result is the ERF due to aerosol-radiation interactions (ERF_{ari}). The RF due to aerosol-cloud interactions (RF_{aci}) refers to the impact of instantaneous aerosol-induced changes in cloud albedo on the radiation budget. When combined with rapid adjustments, we have the ERF due to aerosol-cloud interactions (ERF_{aci}). In practice, it is very difficult to separate RF_{aci} from the rapid adjustments due to other aerosol-cloud interactions, and so typically only ERF_{aci} is quantified (Boucher et al., 2013a).

In this thesis, the primary importance of aerosols is in their ability to act as cloud condensation nuclei, discussed in detail in section 1.1.1. Through this, they

have the potential to modify and affect many cloud properties. These aerosol-cloud interactions will be explored in more detail in section 1.3.

1.1.1 Aerosols as cloud condensation nuclei

Aerosols in the atmosphere serve an essential purpose in facilitating the formation of cloud droplets. They act as condensation nuclei for water vapour to condense into liquid droplets, which would otherwise not be possible via homogeneous nucleation. The processes by which this formation of droplets occurs are known as Köhler theory (Köhler, 1936). The Kelvin equation describes the relationship between the vapour pressure over the curved surface of a droplet of radius r, $e_S(r)$, with that over a flat surface, $e_S(\infty)$:

$$e_S(r) = e_S(\infty) \exp\left(\frac{2\sigma v_l}{kTr}\right), \tag{1.1}$$

where σ is the surface tension of water, v_l is the volume occupied by a molecule in the liquid phase, k is the Boltzmann constant, and T the temperature. For brevity, we may write this as

$$e_S(r) = e_S(\infty) \exp\left(\frac{A}{r}\right), \tag{1.2}$$

where A is a curvature factor given by

$$A = \frac{2\sigma v_l}{kT}. \tag{1.3}$$

The Kelvin equation states that, for a given substance, the vapour pressure over a curved surface is always greater than that over a flat surface. In order for cloud droplets to grow via homogeneous nucleation then, they must overcome

this effect. Defining the saturation ratio

$$S = \frac{e_S(r)}{e_S(\infty)}, \tag{1.4}$$

the Kelvin equation suggests saturation ratios far higher than those observed in the atmosphere in order for cloud droplets to grow in this way (Lohmann et al., 2016).

However, the presence of soluble aerosol particles in the atmosphere can alter this. Raoult's law describes how soluble material dissolved in water reduces the saturation vapour pressure over the flat surface of a solution, e_S^{sol}:

$$\frac{e_S^{sol}(\infty)}{e_S(\infty)} = \frac{n_w}{n_{sol} + n_w}, \tag{1.5}$$

where n_w and n_{sol} are the number of water molecules and solute molecules in the solution, respectively. For a dilute solution, this may be approximated using a Taylor expansion as

$$\frac{e_S^{sol}(\infty)}{e_S(\infty)} \approx 1 - \frac{n_{sol}}{n_w}. \tag{1.6}$$

n_w and n_{sol} may be written as

$$n_w = \frac{N_A m_w}{M_w}, \text{ and } n_{sol} = \frac{i N_A m_s}{M_s}, \tag{1.7}$$

where N_A is Avogadro's constant, i is the Van 't Hoff factor, m_w and m_s are the masses of water and the solute, and M_w and M_s are the molecular weights of water and the solute.

A droplet of radius r has a mass

$$m_{droplet} = m_w + m_s. \tag{1.8}$$

Again approximating for a dilute solution, the mass of the solute may be neglected, so that

$$m_{droplet} \approx m_w = \frac{4}{3}\pi r^3 \rho_w, \tag{1.9}$$

where ρ_w is the density of water.

Applying Raoult's law for a droplet thus yields

$$\frac{e_S^{sol}(r)}{e_S(r)} = 1 - \frac{B}{r^3}, \tag{1.10}$$

where

$$B = \frac{3im_sM_w}{4\pi\rho_w M_s}. \tag{1.11}$$

Combining the competing effects of the Kelvin equation and Raoult's law yields

$$\frac{e_S^{sol}(r)}{e_S(\infty)} = \frac{e_S^{sol}(r)}{e_S(r)}\frac{e_S(r)}{e_S(\infty)} = \left(1 - \frac{B}{r^3}\right)\exp\left(\frac{A}{r}\right). \tag{1.12}$$

A Taylor expansion of the exponential term allows this to be written, for small values of A/r,

$$\frac{e_S^{sol}(r)}{e_S(\infty)} \approx \left(1 - \frac{B}{r^3}\right)\left(1 + \frac{A}{r}\right) \tag{1.13}$$

$$= 1 + \frac{A}{r} - \frac{B}{r^3} - \frac{AB}{r^4}. \tag{1.14}$$

This can be further simplified since, for droplets larger than 0.1 µm, both A/r and $B/r^3 << 1$, and therefore so is their product, the last term. This leads to the Köhler equation

$$\frac{e_S^{sol}(r)}{e_S(\infty)} = S = 1 + \frac{A}{r} - \frac{B}{r^3}. \tag{1.15}$$

For a given aerosol, this equation can describe a Köhler curve, which describes the saturation ratio over a droplet, given its radius. The maximum of the Köhler curve, which roughly separates the regimes dominated by the Raoult and Kelvin effects, describes what is known as the activation or critical saturation ratio, S_c, and radius, r_c. Setting the derivative of 1.15 to zero yields

$$r_c = \sqrt{\frac{3B}{A}}, \quad S_c = 1 + \sqrt{\frac{4A^3}{27B}}. \tag{1.16}$$

This activation saturation ratio S_c, for a given solute and corresponding Köhler curve, is the saturation required for a droplet to grow to the macroscopic sizes of cloud droplets. Fig 1.1 shows some examples of Köhler curves for particles of different dry radii. For $S < S_c$, a droplet is in a stable equilibrium with its surroundings, and may only grow to the size along its Köhler curve corresponding to S, and will not be activated.

Cloud condensation nuclei (CCN) are those members of the atmospheric aerosol population that have the potential to be activated. CCN must therefore be defined at a fixed supersaturation. The activated CCN population is determined by both the aerosol population and properties, as well as the properties of the surrounding atmospheric environment that determine the supersaturation; including humidity, temperature, and vertical air velocity.

The processes described thus far have been limited to warm phase formation of cloud droplets. However, it is also possible for certain aerosol particles to act as

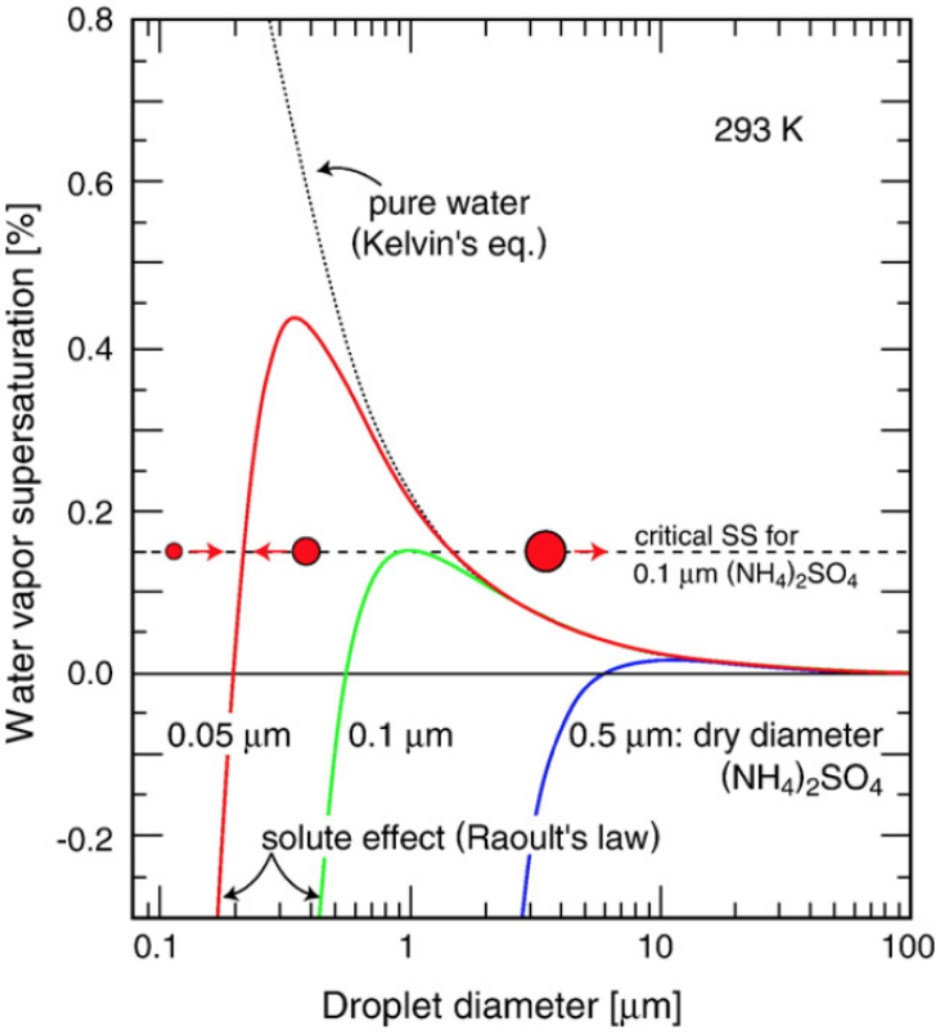

Figure 1.1: Köhler curves showing the vapour pressure equilibrium between a droplet and the environment, for three ammonium sulphate particles of varying dry diameter. The curves demonstrate the combination of the Raoult and Kelvin effects. The horizontal dashed black line shows the supersaturation required for the activation into a cloud droplet of a 0.1 µm particle (from Andreae and Rosenfeld (2008) after Seinfeld and Pandis (2016)).

ice nulcei (IN) in the formation of cloud ice through heterogeneous ice nucleation (Lohmann et al., 2016). Ice nucleation processes are still poorly understood, though the subset of the aerosol population that is able to act as IN may be determined in part by factors such as surface structure, or functional chemical groups (Kanji et al., 2017). This thesis, however, will focus on warm phase clouds, and thus the details of ice nucleation processes will not be important.

1.1.2 Representation in numerical models

Aerosols may be represented in atmospheric numerical models in a number of different ways. The approaches vary depending on the particular application, and the levels of complexity can vary significantly. Bulk schemes are the most simple, making use of predefined size ranges to categorise aerosol (Neale et al., 2010). Linear superpositions of lognormal distributions have been shown to be effective at characterising components of the aerosol size spectrum (Whitby, 1978). For a given component or mode i, these have the form

$$n_N(r)\ln(r) = \frac{dN_i}{dr} = \frac{N_i}{\sqrt{2\pi}\ln\sigma_i}\exp\left(-\frac{(\ln r - \ln r_i)^2}{2\ln^2\sigma_i}\right), \tag{1.17}$$

where $n_N(r)$ is the aerosol number density as function of radius, r, N_i is the aerosol number, r_i is the median particle radius, and σ_i is the standard deviation. Modal schemes use a sum of these lognormal distributions to describe a number of aerosol size modes (Stier et al., 2005; Mann et al., 2012). Sectional, or bin, schemes are the most complex, discretising aerosol sizes into a series of bins (Zhang et al., 2004; Yu et al., 2015). These are, however, much more computationally expensive compared to other approaches (Mann et al., 2012).

The modes typically represented in modal schemes, shown in fig. 1.2, are also useful more generally for understanding aerosol distributions, and the processes

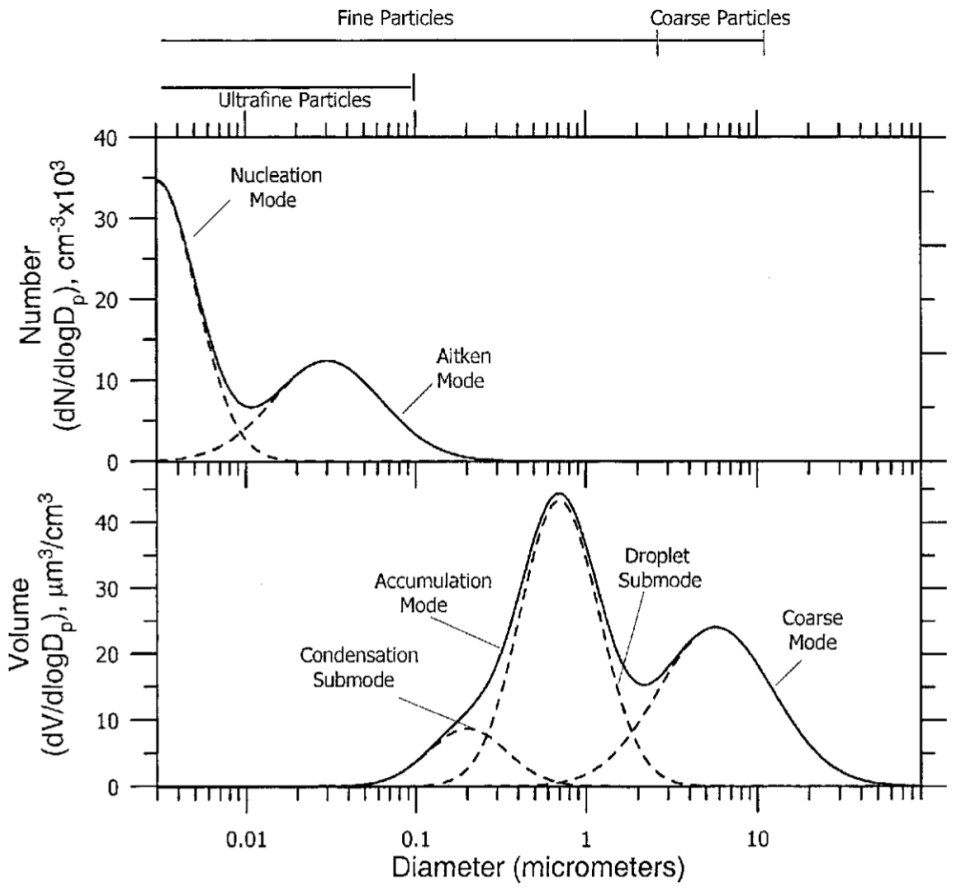

Figure 1.2: Typical number and volume distributions of atmospheric aerosol shown by the solid lines, with contributions of different aerosol modes shown by dotted lines (from Seinfeld and Pandis (2016)).

associated with the different components. The nucleation mode refers to particles with diameters up to around 10 nm, formed through nucleation of supersaturated vapours (Seinfeld & Pandis, 2016). The Aitken mode refers to the range 10 to 100 nm. The accumulation mode comprises the range 0.1 to 2.5 µm, and is named for the tendency for particles to accumulate in this size range as a result of coagulation of smaller particles and less efficient removal mechanisms (Seinfeld & Pandis, 2016). Above 2.5 µm is the coarse mode, comprising such species as sea salt and dust.

No detailed and fully interactive aerosol scheme will be used in this the-

sis. However, a cloud microphysics scheme with some interactive treatment of aerosols will be employed, and is discussed in more detail in section 1.5. This overview of aerosol representations will thus prove useful in informing later discussions.

1.2 Clouds

Clouds are defined as consisting of particles of liquid water or ice, or both, suspended in the atmosphere (World Meteorological Organization, 2017). They are an ubiquitous feature of Earth's atmosphere, covering on average more than two thirds of the surface (King et al., 2013; Stubenrauch et al., 2013). It is no surprise, then, that clouds are deeply significant components of the atmosphere and climate system, contributing to many important atmospheric processes. Cloud processes range from micrometre scale microphysics through to circulations on scales of hundreds of kilometres. This fact is key to both the rich multitude of cloud behaviours, as well as the difficulty in understanding and representing them in global climate models.

Clouds, and the associated precipitation, are major contributors to the hydrological cycle, as well as the processing and deposition of atmospheric aerosol (Lohmann et al., 2016). Additionally, the vertical motions associated with clouds are responsible for transport of heat and moisture in the atmosphere. They further impact the global radiation budget, interacting with both short- and longwave radiation (Cotton et al., 2011). The longwave cloud radiative effect (LWCRE) is primarily determined by cloud-top temperature, while the shortwave cloud radiative effect (SWCRE) is determined by the cloud albedo. The longwave and shortwave effects are around $28\,\mathrm{W\,m^{-2}}$ and $-46\,\mathrm{W\,m^{-2}}$, respectively, leading to a global net cloud radiative effect of around $-18\,\mathrm{W\,m^{-2}}$ (Loeb et al., 2018). This is largely owing to the prevalence of low-level stratocumulus

and cumulus clouds in the marine boundary layer, with high albedos and warm cloud-top temperatures (Cotton et al., 2011; Stephens et al., 2012).

Given the integral role of clouds in the atmosphere, there is much interest in understanding how they may respond to perturbations to the climate. This is especially salient due to their role in processes of great importance to humanity, including precipitation and extreme events, such as storms and flooding. *Feedbacks* in the climate system refer to changes in a component of the climate in response to increases in global mean surface temperature, that may act to amplify or dampen this change in temperature (Boucher et al., 2013a). However, cloud feedbacks in a warming climate, and responses to aerosol perturbations, constitute some of the largest sources of uncertainty in climate sensitivity (Bony et al., 2004; Bony & Dufresne, 2005; Boucher et al., 2013a; Bony et al., 2015). This is particularly true of low, shallow clouds, which will be discussed in more detail in 1.2.1.

The definition of a cloud given above by the World Meteorological Organisation (WMO) is rather general, and serves to emphasise the dependence on microphysics that is common to all cloud types. However, it does little to describe the morphological and dynamical characteristics of clouds, or the rich variety of behaviours they may exhibit. The definitions of specific genera of cloud given in the International Cloud Atlas (World Meteorological Organization, 2017) go further in this regard, detailing ten genera, and many further species and varieties of clouds. A schematic of the ten genera is shown in fig. 1.3, and it is instructive to consider several of the main types, their characteristics, and the roles they play in the atmosphere.

Before doing so, however, it is also useful to consider the atmospheric conditions under which clouds may develop. It is important to note that, while the fundamental equations for the thermodynamics of dry and moist air are well understood, numerical models are required to make a number of simplifications

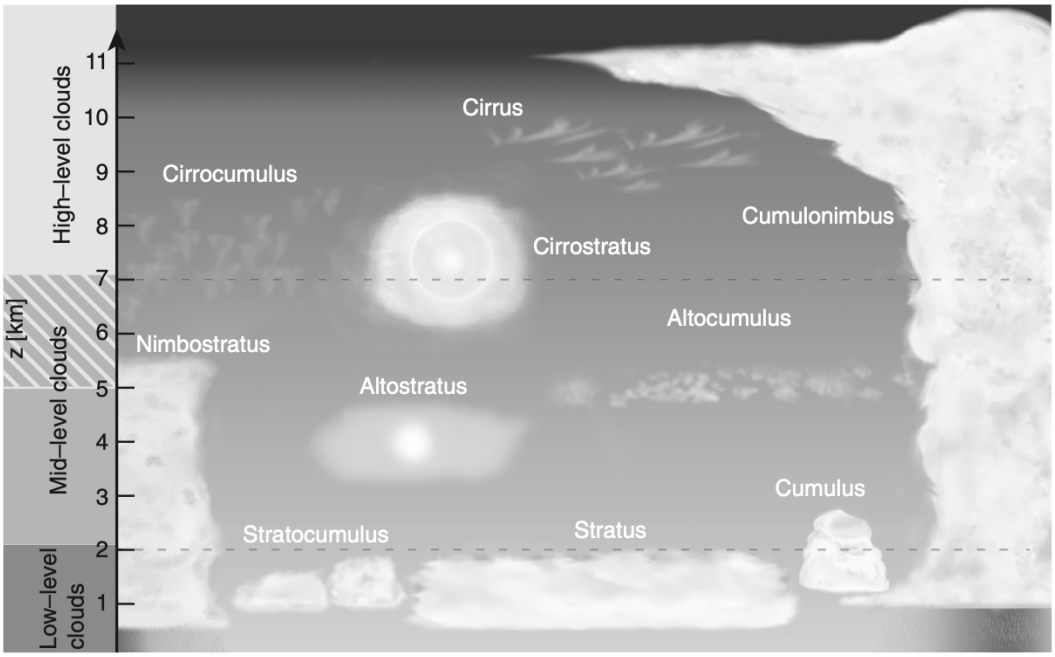

Figure 1.3: A schematic figure of the ten cloud genera defined by the WMO (from Lohmann et al. (2016)).

and assumptions. This is due to the breakdown of the continuum hypothesis for hydrometeors such as liquid droplets or ice crystals, and due to the difficulty in accounting for the continuous phase changes that occur in clouds. However, we can nonetheless gain a good understanding of the relevant processes by employing one of two assumptions: reversible thermodynamics, or pseudoadiabatic thermodynamics. Under an assumption of reversible thermodynamics, total water is conserved following air motion; that is, the material derivative of the total water mixing ratio is 0, and thus all condensate is considered to move with the air. In stark contrast, the pseudoadiabatic assumption is that condensate produced by a moist adiabatic process is immediately removed from the air upon formation, via idealised instantaneous precipitation. For the purposes of this discussion, we will proceed with the pseudoadiabtic assumption.

The buoyancy, B of a parcel of air is given by

$$B = -g\frac{\rho - \rho_0}{\rho} = -g\frac{\rho^{'}}{\rho}, \tag{1.18}$$

where g is the gravitational acceleration, ρ is the density of the air, and $^{'}$ denotes the deviation from a reference state in hydrostatic balance, ρ_0, such that the vertical derivative of pressure, p, is given by

$$\frac{dp}{dz} = -g\rho_0. \tag{1.19}$$

The potential temperature, θ, may be defined as

$$\theta \equiv T\left(\frac{p}{p_{00}}\right)^{\frac{R_a}{c_{pa}}}, \tag{1.20}$$

where T is temperature, p_{00} is a reference pressure (typically 1000 hPa), R_a is the gas constant for air, and c_{pa} is the specific heat capacity of air at constant pressure. Considering this along with the ideal gas equation,

$$p = \rho R_a T, \tag{1.21}$$

allows us to write 1.19 as

$$B = g\frac{\theta^{'}}{\theta_0}. \tag{1.22}$$

We can begin to account for the presence of condensate by modifying the definition of density, and by defining the virtual temperature, T_v, so that

$$\rho = \rho_a(1 + q_H), \tag{1.23}$$

and

$$T_v \approx T(1 + 0.61 q_v), \tag{1.24}$$

where q_H is the hydrometeor mixing ratio, and q_v is the water vapour mixing ratio. The equation of state is thus now

$$p = \rho R_d T_v, \tag{1.25}$$

where R_d is the gas constant for dry air. The buoyancy may now be approximately written as

$$B \approx g \left(\frac{T^{'}}{T_0} - \frac{p^{'}}{p_0} + 0.61 q_v^{'} - q_H \right). \tag{1.26}$$

A useful form of the equations of motion in the atmosphere is that resulting from the anelastic approximation. This assumes that buoyancy is a significant component of the vertical momentum equation, that the characteristic vertical displacement of an air parcel is comparable to the density scale height, and that horizontal variations are small compared to the reference state. Following Bannon (1996), the anelastic momentum equation can be written

$$\frac{D\mathbf{u}}{Dt} = -\frac{1}{\rho_0} \nabla p^{'} + B\mathbf{k} - 2\mathbf{\Omega} \times \mathbf{u} + \frac{\mathbf{F}}{\rho_0}. \tag{1.27}$$

Taking the vertical component,

$$\frac{dw}{dt} = -\frac{1}{\rho_0} \frac{\partial p^{'}}{\partial z} + B, \tag{1.28}$$

for a dry parcel with $p \approx p_0$, we have

$$\frac{dw}{dt} - B = 0. \tag{1.29}$$

Expanding a Taylor series around a small change in height, δz, for 1.22 we find

$$\frac{\delta B}{\delta z} = -\frac{g}{\theta_0}\frac{\partial \theta_0}{\partial z}. \tag{1.30}$$

Defining the Brunt-Väisälä frequency

$$N_0^2 = \frac{g}{\theta_0}\frac{\partial \theta_0}{\partial z}, \tag{1.31}$$

and substituting into 1.29, yields

$$\frac{d^2\delta z}{dt^2} = -N_0^2 \delta z. \tag{1.32}$$

We therefore find that for $\frac{\partial \theta_0}{\partial z} < 0$, a displaced parcel will accelerate in the direction of displacement, that is, the atmosphere is unstable. For $\frac{\partial \theta_0}{\partial z} > 0$, however, we find oscillatory solutions, and the atmosphere is stable, while for $\frac{\partial \theta_0}{\partial z} = 0$ the atmosphere is in a neutral equilibrium.

Atmospheric stability can be similarly determined through examining the lapse rate, Γ, defined

$$\Gamma = -\frac{dT}{dz}. \tag{1.33}$$

For an idealised dry air parcel rising adiabatically, the dry adiabatic lapse rate

follows from the equation of state, and the assumption of hydrostatic equilibrium,

$$\Gamma_d = \frac{g}{c_p} \approx 9.81\,\mathrm{K\,km^{-1}}. \tag{1.34}$$

From its definition, we can write the vertical gradient of the potential temperature in terms of Γ_d, and the ambient lapse rate, Γ,

$$\frac{1}{\theta_0}\frac{\partial \theta_0}{\partial z} = \frac{1}{\theta_0}\frac{\partial}{\partial z}\left(T\left(\frac{p}{p_{00}}\right)^{\frac{R_a}{c_{pa}}}\right) \tag{1.35}$$

$$= \frac{1}{T}\frac{\partial T}{\partial z} - \frac{R_a}{pc_{pa}}\frac{\partial p}{\partial z} \tag{1.36}$$

$$= \frac{1}{T}\frac{\partial T}{\partial z} + \frac{R_a}{pc_{pa}}g\rho \tag{1.37}$$

$$= \frac{1}{T}(\Gamma_d - \Gamma). \tag{1.38}$$

In this dry case, then, we can see that for $\Gamma < \Gamma_d$ the atmosphere is stable, while for for $\Gamma > \Gamma_d$ the atmosphere is unstable, and neutral if the two lapse rates are equal. In the presence of moisture, however, the release of latent heat by condensation must also be considered. To find the saturated adiabatic lapse rate, following Lohmann et al. (2016), the first law of thermodynamics may be written

$$dq = c_p dT - \frac{dp}{\rho} + L dq_s, \tag{1.39}$$

where q_s is the saturation specific humidity. Dividing by $c_p dz$, and rearranging, we find

$$\frac{dT}{dz} = -\frac{L}{c_p}\frac{dq_s}{dT}\frac{dT}{dz} - \Gamma_d. \tag{1.40}$$

From this, we find the saturated adiabatic lapse rate, Γ_s,

$$\Gamma_s = \Gamma_d \left(1 + \frac{L}{c_p}\frac{dq_s}{dT}\right)^{-1}. \tag{1.41}$$

The release of latent heat in the rising parcel reduces the rate at which it cools, thus, Γ_s is always less than Γ. These two lapse rates allow us to consider more general criteria for atmospheric stability:

$$\begin{aligned} \Gamma < \Gamma_s &\qquad \text{Absolutely stable} \\ \Gamma_s < \Gamma < \Gamma_d &\qquad \text{Conditionally unstable} \\ \Gamma_d < \Gamma &\qquad \text{Absolutely unstable} \end{aligned}$$

In the conditionally unstable case, a parcel undergoing dry adiabatic ascent will be cooler than the ambient air, and thus stable, while a parcel undergoing saturated adiabatic ascent will be warmer than the ambient air, and thus unstable.

Stratiform clouds, such as *stratus*, *nimbostratus*, and *stratocumulus*, are typically layered, with a significant horizontal extent (Lohmann et al., 2016). They may produce drizzle in clean air masses with low aerosol concentrations, such as over the oceans, and often have lifetimes of several hours (Lohmann et al., 2016; Cotton et al., 2011). Stratus clouds are typically formed in statically stable air by large-scale vertical air motions (Yau & Rogers, 1996). In contrast, the dynamics of stratocumuli are driven by convective instability resulting from radiative cooling at the cloud top, where they are typically capped by a strong temperature inversion (Wood, 2012). Stratocumuli cover large portions of the atmosphere, commonly forming extensive decks over subtropical oceans (Wood, 2012). This, coupled with their reflection of incoming shortwave radiation, leads them to have a significant net negative radiative effect (Hartmann et al., 1992; Chen et al., 2000; Wood, 2012).

Convective clouds, such as *cumulus* and *cumulonimbus*, are characterised by their morphology; with vertical development in the form of towers or mounds, and bouyancy-driven vertical motion. They form in unstable air, when a buoyant air parcel rises through air sufficiently moist for droplet activation and condensation to occur (Lohmann et al., 2016). This activation and condensational growth releases latent heat, leading to additional buoyancy of the parcel and allowing the convection to develop. Shallow convective clouds are typically limited to this warm phase regime, and develop in conditionally unstable air. As the focus of this thesis, they are discussed in more detail in section 1.2.1. If the rising air parcel is buoyant enough to reach the freezing level, however, then additional latent heat release from the freezing of cloud droplets can further enhance vertical motion, leading to the development of deep *cumulonimbus* clouds. Deep convective clouds are an important component of the hydrological cycle, both through vertical transport of moisture to the troposphere, and through their significant contribution to regional precipitation. They are also strongly associated with large-scale circulations such as the Hadley cell (Cotton et al., 2011).

Cirrus clouds are an example of high clouds, composed almost entirely of ice crystals. They are often characterised by a wispy, fibrous appearance, particularly in the latter stages of their development (Houze, 2014). Cirrus anvils are also associated with deep convective clouds and mesoscale convective systems (Sassen et al., 2009). High clouds typically exert a net positive radiative effect, due to their cold temperature and low albedo, though thicker anvil cirrus may have a negative effect due to their greater optical thickness (Cotton et al., 2011).

1.2.1 Shallow convective clouds

Shallow cumuli are the most prevalent cloud type on Earth by number (Rossow & Schiffer, 1999; Sassen & Wang, 2008); ubiquitous throughout the trade winds,

the easterly ocean surface winds so named for their historical importance in maritime navigation and commerce. Cumulus clouds can be further sub-categorised into *humulis*, *mediocris*, and *congestus*, according to their vertical development, though cumulus humilis and mediocris are often referred to together simply as cumulus. Warm cumuli may have vertical extents of less than 1km for the shallowest clouds, up to around 6km for congestus (Cotton et al., 2011). The lifetimes of cumulus clouds can vary from as short as 10 minutes to longer than an hour, typically increasing for clouds with greater vertical development. Vertical velocities can range from a few $\mathrm{m\,s^{-1}}$ in the convectively weakest clouds, up to $10\mathrm{m\,s^{-1}}$ in congestus clouds, and liquid water contents are typically in the range of 0.3 - $2.5\mathrm{g\,m^{-3}}$. Despite having often been idealised as non-precipitating (Stevens, 2005), many studies have found that warm precipitation from shallow clouds is, in fact, extremely common, and forms a significant component of rainfall over tropical and subtropical oceans (Short & Nakamura, 2000; Lau & Wu, 2003; Schumacher & Houze, 2003; Masunaga & Kummerow, 2006; Nuijens et al., 2009).

The atmospheric structure typical of the trades is characterised by the presence of large-scale subsidence, and of a temperature inversion, which may cap smaller cumuli (Lohmann et al., 2016; Stevens, 2005). Shallow cumuli interact with their thermodynamic environment by warming the cloud layer through condensation, transporting moisture to the inversion layer above, and cooling both the inversion and the sub-cloud layer through the evaporation of detraining cloud droplets and precipitation (Hartmann et al., 1992; Zhu & Bretherton, 2004; Neggers et al., 2007). Sufficiently high buoyancy may allow cumuli to develop further and penetrate the trade inversion, where the vertical transport of moisture and cloud-top cooling contributes to conditioning the atmosphere for the development of deeper convection further into the tropics (Stevens, 2005).

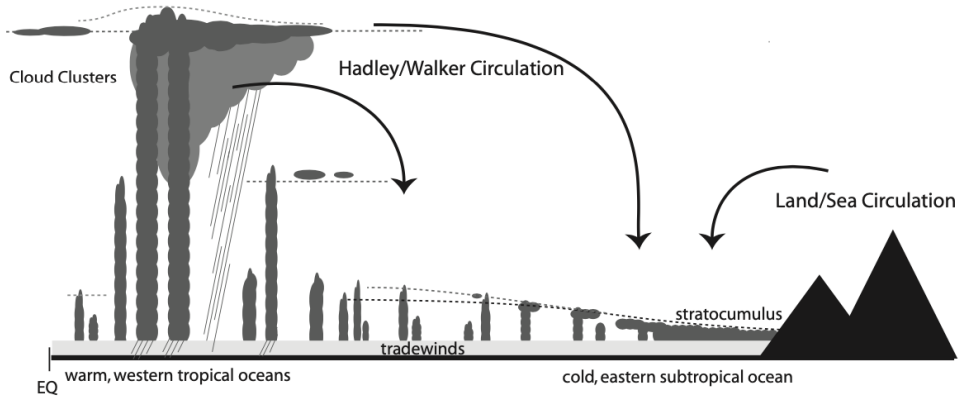

Figure 1.4: A schematic of clouds along a classic trade wind trajectory. From Stevens (2005).

A schematic cartoon in fig. 1.4 illustrates the structure of clouds in the trade winds.

While shallow cumuli are individually small in size, their existence in large fields of clouds lends an additional component to their dynamical behaviour. Shallow cloud fields have been found to exhibit a number of regimes of organisation, including streets, arcs, and clusters (Malkus & Riehl, 1964; Nair et al., 1998; Seifert & Heus, 2013). Recently, machine learning approaches to pattern recognition and image classification have suggested the existence of more complex patterns of organisation of shallow cloud fields (Rasp et al., 2020; Denby, 2020). The factors influencing this mesoscale organisation are an area of active research, but may include cold pools, gravity waves, radiative cooling, and cycles of developing and consuming instability (Zuidema et al., 2012; Seifert & Heus, 2013; Naumann et al., 2017; Dagan et al., 2018b). Convective cold pools form due to the evaporation of precipitation in downdraughts, with the evaporatively-cooled air spreading out at the surface as a density current (Simpson, 1969; Charba, 1974). The expanding gust fronts of such cold pools can create favourable conditions for the development of new clouds (Li et al., 2014; Vogel et al., 2021). In

cycles of developing and consuming instability, clouds develop due to instability driven by surface fluxes, but subsequently produce precipitation which acts to stabilise the atmosphere and reduce cloudiness, before surface fluxes begin to again drive the development of instability (Dagan et al., 2018b). Organised cloud fields may differ markedly in their cloud amount, as well as in their radiative properties (Vogel et al., 2020; Denby, 2020). Bony et al. (2020) find that certain patterns of organisation can have net cloud radiative effects that differ by a factor of 2, driven by differences in cloud amount. Further, they find that variability in the occurrence of such patterns may depend on the estimated inversion strength, which has been predicted to increase over the tropical Atlantic in a warmer climate (Qu et al., 2015). Patterns of spatial organisation of shallow convective clouds may therefore be extremely significant in influencing the low-cloud feedback.

The coupling between shallow clouds and large-scale circulations is of great interest due to its importance for climate sensitivity. Indeed, feedbacks associated with these clouds are responsible for most of the uncertainty in climate sensitivity in climate models (Bony et al., 2004; Bony & Dufresne, 2005; Medeiros et al., 2008; Vial et al., 2013; Boucher et al., 2013a; Medeiros et al., 2015; Bony et al., 2015). Shallow convective mixing of the lower troposphere by boundary layer clouds over the ocean is a key component of this uncertainty (Bony et al., 2015). This mixing may act to dry the marine boundary layer, reducing low-cloud amount, and leading to a positive low-cloud feedback (Sherwood et al., 2014). Another significant component of the uncertainty in understanding the behaviour of shallow clouds is how they are affected by changing atmospheric aerosol, which will be discussed in detail in section 1.3.

1.2.2 Representation of shallow clouds in numerical models

Representing clouds in general circulation models (GCMs) is a great challenge, due to the limitations imposed by the need for coarse resolutions, with horizontal grid lengths of tens to hundreds of km. In such models, all convective clouds must be parameterised, commonly using mass flux models (Tiedtke, 1989; Gregory & Rowntree, 1990). These models are limited in their applicability to precipitating shallow clouds, as well as in their representation of cloud amount, with no representation of cloud organisation (Cotton et al., 2011). They are further limited in their ability to represent the highly non-linear effects of aerosol. Convection parameterisations may also be used alongside cloud cover parameterisations based on, for example, relative humidity (Sundqvist et al., 1989; Smith, 1990). Alternative approaches to parameterise clouds include higher-order closure schemes (Golaz et al., 2002; Larson & Golaz, 2005), as well as so-called super-parameterisations. Under this approach, 2D cloud-resolving models are embedded in each column of a GCM (Khairoutdinov & Randall, 2001; Grabowski, 2001). However, the embedded models are still too coarse to resolve shallow cumulus or stratocumulus clouds.

Convection-permitting or cloud-resolving models (CRMs) with grid spacings on the order of a few km are so named since they are able to explicitly resolve features of deep convective systems (Langhans et al., 2012). These are also referred to as storm-resolving models (SRMs). Global CRMs or SRMs are beginning to be employed (Satoh et al., 2017; Satoh et al., 2019; Stevens et al., 2019b), and aim to represent convective processes far more realistically than the current generation of climate models. However, these are still too coarse to explicitly represent shallow convection or boundary layer clouds; a goal that is still out of reach for global simulations (Schneider et al., 2017).

Large eddy simulations (LES), with resolutions on the order of tens to hundreds of metres, are able to resolve the largest turbulent eddies, containing most of the energy and scalar flux of a flow. These models are able to explicitly represent most of the structure of shallow convective clouds and their dynamics (Khairoutdinov et al., 2009; Bryan et al., 2003; McGee & van den Heever, 2014). However, sub-grid turbulence must still be parameterised, along with a number of other important processes, notably the cloud microphysics (vanZanten et al., 2011; Guichard & Couvreux, 2017). Furthermore, they typically do not include a radiation scheme (Guichard & Couvreux, 2017), though, recently, some studies have done so (Seifert et al., 2015). LES are limited-area models, and, due to computational limitations, have commonly been performed with small domain sizes of tens of km. Recently, however, advancements in computing capabilities have allowed LES in much larger domains (Schalkwijk et al., 2015; Heinze et al., 2017). Limited-area models require a decision to be made regarding the boundaries of the domain, with LES often employing doubly-periodic lateral boundary conditions. However, this choice may not allow for large-scale behaviour to be fully represented (Guichard & Couvreux, 2017), and further suggests an underlying assumption that cloud fields or atmospheric conditions are similar over large scales, such that the cycling of clouds through a domain can be considered representative of new clouds entering the domain. Additionally, large-scale forcing must be imposed through prescribed tendencies of temperature, moisture, and surface fluxes, all of which are typically constant. These potential limitations of periodic limited-area models will be one of the topics of investigation in Chapter 3.

The modelling approaches employed in this thesis will be discussed in more detail in section 1.5.

1.2.3 Cloud microphysical processes and their representation in numerical models

Microphysical processes are those processes that affect the droplet size distribution, and thus the formation and evolution of cloud and precipitation particles. These include condensational growth, collision and coalescence, freezing, melting, and evaporation, amongst many others. Microphysics is also closely tied to the dynamical and thermodynamic behaviour of clouds, in particular due to the exchange of latent heat from phase changes of cloud water (Morrison et al., 2020). Furthermore, microphysical properties such as particle shape, size, and number, are important determinants of cloud radiative properties. The large number of processes through which hydrometeors interact is key to the complexity that characterises cloud microphysics. Modelling microphysics is further complicated by the number of hydrometeors, which can typically be on the order of $10^8\,\mathrm{m}^{-3}$ in a cloudy air volume (Morrison et al., 2020). Directly simulating each hydrometeor is therefore impractical due to the computational cost, and cloud microphysics must be parameterised in almost all atmospheric models.

There are two main approaches to microphysics parameterisations: bulk schemes, and bin schemes (Khain et al., 2015).

Bulk microphysics schemes make use of prescribed, semi-empirical particle size distributions (PSDs) for different classes of hydrometeors such as cloud droplets, rain, ice, graupel, and snow. Typically, these PSDs are gamma functions of the particle radius, with prescribed intercept, slope, shape parameters (Khain et al., 2015). Bulk schemes are able to be computationally efficient due to their consideration of the moments of the PSDs, which describe various properties of the hydrometeor class. For a given hydrometeor class, single- or one-moment schemes consider the first moment of the PSD, the mass mixing ratio. Double- or two-moment schemes will additionally include the zeroth moment of the PSD,

the number concentration. Additional moments may also be considered to give more information about the hydrometeor properties, such as radar reflectivity, given by the third moment. Schemes including the hydrometeor number concentration have the notable advantage of being able to model the effect of aerosols on cloud droplets (Khain et al., 2015; Morrison et al., 2020).

In bin microphysics schemes no a priori information about PSDs is required. Instead, these schemes explicitly calculate the PSDs from microphysical equations for some number of mass bins. Though they allow a detailed treatment of individual processes, this, along with the often large number of mass bins, means that bin schemes are much more computationally expensive compared to bulk schemes - typically by at least an order of magnitude, or more (Khain et al., 2015; Morrison et al., 2020).

Alternative methods have been developed to attempt to bridge the gap between the efficiency of bulk schemes and the detail of bin schemes. One method has been to employ a bin approach for warm-phase processes, and a bulk approach for the ice-phase (Onishi & Takahashi, 2012). Another approach, known as bin-emulating, employs process rates calculated offline by a bin scheme, which are then incorporated into a bulk scheme via lookup tables (Saleeby & Cotton, 2008). Super-droplet schemes employ a particle-based, probabilistic approach to cloud microphysics. In this method, super-droplets are defined to represent many individual droplets with the same attributes (Shima et al., 2009). These super-droplets are then considered to behave just as an individual droplet might, with the exception of the coalescence process, for which a stochastic treatment is employed (Shima et al., 2009; Shima et al., 2020). This approach allows for detailed treatment of microphysical processes, while potentially reducing the computational demand and numerical diffusion compared to multi-dimensional bin schemes (Shima et al., 2009; Grabowski et al., 2018; Shima et al., 2020).

In this thesis, the focus is on shallow, warm clouds, and therefore the important microphysical processes are in the warm phase. Once a droplet has been activated, it will continue to undergo condensational growth. However, this growth rate is inversely proportional to the droplet radius, and thus slows as the droplet grows (Lohmann et al., 2016), making it insufficient for the formation of precipitation. Droplets also grow by collision-coalescence, whereby colliding droplets may coalesce to form a larger droplet. Differential settling of droplets of different sizes allows collisions to take place. A number of possible outcomes are possible when droplets collide: they can coalesce to form a single droplet, they can rebound from the collision, or they can coalesce before splitting into a larger number of smaller droplets. The geometry of droplet collisions can be understood by considering a collision occurring between a larger and a smaller droplet in calm air. When separated by a small distance, the trajectory of the smaller droplet will be altered due to the airflow around the larger droplet, tending to avoid a collision. Thus, the effective collision cross-section is smaller than the geometric cross-section of the two droplets, and the ratio of these cross-sections may define a collision efficiency. For relatively larger small droplets, their increased inertia will result in a tendency to deviate from the airflow around the large droplet, increasing the collision efficiency. However, as the relative speed of the droplets decreases as their sizes become more similar, the increased time for a collision to occur can slightly decrease the collision efficiency (Lohmann et al., 2016). In order for collisions to occur, the droplet size spectrum must be wide enough for droplets to have sufficiently varying fall speeds. Condensation causes a narrowing of the size spectrum (Howell, 1949), however. A number of mechanisms to enable collision-coalescence have been proposed, including the influence of giant CCN (GCCN) (Johnson, 1982a; Feingold et al., 1999) and of turbulence. Very large soluble aerosol particles, GCCN, may broaden the droplet size distribution, forming droplets large enough for collision-coalescence to occur.

Turbulence, meanwhile, may enhance collision efficiencies and collection kernels due to changes in fall speeds and horizontal motion (Pinsky & Khain, 1997; Khain & Pinsky, 1997). A falling droplet may also capture other droplets via wake capture, whereby reduced aerodynamic resistance in the wake of the falling droplet may be sufficient for a droplet in the wake to reach higher a fall speed and lead to a collision (Hu et al., 1998; Lohmann et al., 2016).

Collision-coalescence is the dominant pathway by which drizzle and rain droplets develop in warm clouds (Lohmann et al., 2016; Lau & Wu, 2003). The initial stage, during which cloud droplets grow into drizzle droplets, is known as autoconversion. The further growth of these larger droplets by collisions with cloud droplets is known as accretion. An additional component, self-collection, refers to the collision-coalescence of droplets of a similar size.

A number of approaches are employed to represent these processes in microphysics schemes. Bulk schemes often make use of a saturation adjustment for condensation and evaporation, in contrast to the explicit calculation of diffusional growth and supersaturation in bin schemes. Under the saturation adjustment approach, the supersaturation is adjusted to zero at the end of each time-step, with excess water vapour relative to the saturation mixing ratio condensed to cloud water (Lebo et al., 2012; Khain et al., 2015). This approach assumes that the model time-step is sufficiently longer than the condensation/evaporation timescale. However, in convective updraughts, supersaturations rarely fall to zero due to increased vertical velocity and a decrease in droplet concentration due to collision-coalescence processes (Lebo et al., 2012; Khain et al., 2015). Employing saturation adjustment under such conditions can lead to enhanced condensation and latent heating at lower levels, potentially overestimating vertical velocities and convective precipitation, and thus limiting the ability of aerosol to impact buoyancy at higher levels (Lebo et al., 2012; Khain et al., 2015). Thus, the use of saturation adjustment may reduce the sensitivity of bulk schemes to changes

in aerosol. Many of the processes that may be affected by aerosol, discussed in section 1.3, are associated with droplet and precipitation formation, and the resulting thermodynamic changes. The use of saturation adjustments is therefore one of the most important limitations of bulk schemes in their application to studying aerosol cloud interactions.

Bin microphysics schemes describe the evolution of the droplet size distribution (DSD) due to collision-coalescence by solving the stochastic collection equation (Pruppacher & Klett, 2012; Khain et al., 2015). Bulk schemes, however, typically consider autoconversion and accretion separately, due to the separation of cloud and drizzle droplets into distinct hydrometeor classes. Self-collection, meanwhile, is often not included. It is common for bulk parameterisations of autoconversion and accretion to be formulated empirically from results from explicit calculations in bin schemes (Khairoutdinov & Kogan, 2000; Khain et al., 2015). They can therefore be limited in the scope of their applicability, since the explicit solutions upon which they are based are often calculated for a relatively small number of simulations. These differing representations of autoconversion are a significant source of uncertainty in comparing bulk schemes (Gilmore & Straka, 2008; White et al., 2017). However, it is also important to note that the use of similar schemes may provide a false sense of agreement.

1.3 Aerosol effects on clouds and precipitation

Clouds play an extensive role in the atmosphere, and aerosols play a fundamental role as CCN in the formation of clouds. In doing so, aerosols may modify cloud properties in a number of ways, affecting both the micro- and macrostructure. Changes in cloud radiative properties or cloudiness due to aerosol, often referred to as aerosol indirect effects, are highly relevant to anthropogenic forcing of the climate system (Boucher et al., 2013a; Seinfeld et al., 2016; Lohmann &

Feichter, 2005). Furthermore, the IPCC note in their 5th Assessment Report (AR5) that aerosol-cloud interactions are the largest source of uncertainty in anthropogenic radiative forcing (Boucher et al., 2013a; Myhre et al., 2013). Understanding aerosol-cloud interactions, then, is of great significance in furthering our understanding of our climate system.

Reutter et al. (2009) describe the differences between aerosol-limited and updraught-limited clouds. In aerosol-limited clouds, supersaturations and activated CCN fractions are high. In contrast, updraught-limited clouds have low supersaturations, and low fractions of activated CCN. These regimes represent the extremes of a likely range of conditions (Reutter et al., 2009; Sheffield et al., 2015). An increase in aerosol in an aerosol-limited cloud will, for a given cloud liquid water content, lead to an increase in droplet number, and a decrease in droplet radius, and vice versa for a decrease in aerosol (Twomey, 1977). The increase in cloud albedo that results from an increase in aerosol concentration is known as the Twomey effect, and is responsible for the radiative forcing due to aerosol cloud interactions (RF_{aci}) introduced in section 1.1. Albrecht (1989) argued that smaller droplets resulting from increased aerosol reduces precipitation efficiency, thus leading to an increase in the cloud lifetime, known as the lifetime effect. However, this simple argument is linked with a number of important microphysical and dynamical behaviours of clouds. Stevens and Feingold (2009) note that it has led to a number of distinct hypotheses regarding so-called lifetime effects, many of which may bear little relation to cloud lifetime as such, and furthermore may be regime- or time-dependent (Saleeby et al., 2015; Lee et al., 2012). The extent of these hypotheses will be discussed in more detail in section 1.3.1. The complex interdependence between different aerosol-cloud interactions makes it difficult for them to be considered entirely separately. These interactions and their impact on clouds and aerosols constitute the rapid adjustments of clouds to changes in aerosol. The effective radiative forcing due to aerosol-cloud

interactions (ERF_{aci}) introduced by the IPCC AR5 is then the combination of the Twomey effect, and rapid adjustments (Boucher et al., 2013a).

While this introduction has centred around warm clouds, as the focus of this thesis, it should also be noted that similar principles underscoring aerosol-cloud interactions are also relevant for mixed- and ice-phase clouds, where hydrometeor properties may be affected by aerosol acting as as either CCN or IN (Ekman et al., 2007; Seinfeld et al., 2016). The greater number of microphysical processes in mixed- and ice-phase clouds adds a large amount of complexity to understanding the aerosol-cloud interactions, and indeed, many of the processes themselves are poorly understood (Seinfeld et al., 2016).

Aerosols may further affect clouds through their interactions with radiation; heating due to absorbing aerosol, such as black carbon, can affect the environment in which clouds develop, and therefore the evolution of the clouds themselves (Ackerman et al., 2000; Koren et al., 2004). This is known as the *semi-direct effect* (Hansen et al., 1997). Observations have shown that increases in smoke can reduce cloudiness and inhibit cumulus convection (Koren et al., 2004), but can also lead to thickening of stratocumulus (Wilcox, 2010). However, it has also been found that the sign of the semi-direct effect for low clouds may depend on the location of the absorbing aerosol relative to the cloud layer. When absorbing aerosol is located at low levels within the cloud layer, the enhanced diabatic heating leads to reductions in relative humidity that reduce cloudiness (Ackerman et al., 2000). In contrast, when the absorbing aerosol is located above the cloud layer, cloudiness can be enhanced (Johnson, 1982a; Perlwitz & Miller, 2010; Stjern et al., 2017). Model diversity and uncertainty is large, however, and observational constraints of atmospheric heating profiles have suggested significant decreases in low cloud cover, leading to a positive semi-direct effect (Allen et al., 2019). Furthermore, semi-direct effects on different cloud types, such as stratocumulus or cirrus, can have both positive and negative contributions to

the total effect due to the clouds' differing radiative properties (Fan et al., 2016). Aerosol-cloud-radiation interactions are thus extremely complex and important to explore. The focus of this thesis, however, is on the effect of aerosols in their role as condensation nuclei.

Aerosol-cloud interactions are bidirectional; processes and pathways exist such that each may affect the other. Clouds may remove aerosol through a number of processes known collectively as wet scavenging, or wet deposition (Seinfeld & Pandis, 2016). Nucleation scavenging removes interstitial aerosol through the activation of CCN to cloud droplets, which may then be removed from the atmosphere via precipitation. Cloud and rain droplets can further collect aerosol both in and below the cloud. Additionally, aerosol particles may be resuspended if the associated hydrometeor evaporates. The importance of aerosol chemistry and size for droplet activation, as well as the facilitation of aerosol formation in aqueous reactions in droplets, therefore means that cloud processing of aerosols can significantly influence the characteristics of the aerosol population (Seinfeld & Pandis, 2016).

1.3.1 Aerosol effects on shallow convective clouds

Aerosol-cloud interactions are highly regime-dependent; varying between cloud type, and subject to confounding by meteorological variability (Khain et al., 2008; Stevens & Feingold, 2009; van den Heever et al., 2011). This section explores the state of research on the effects of aerosol on shallow convective clouds, which are the subject of this thesis. The interactions of cumulus clouds with aerosol have been the subject of both intense investigation and debate for many years, and remain poorly understood (Tao et al., 2012).

Observational studies of shallow convection have often focused on the trade wind region of the Atlantic near Barbados, with the area having been the sub-

ject of several field campaigns: the Barbados Oceanographic and Meteorological Experiment (BOMEX) (Davidson, 1968), the Rain in Shallow Cumulus over the Ocean (RICO) campaign (Rauber et al., 2007), the Barbados Aerosol Cloud Experiment (BACEX) (Jung et al., 2013), the Next-generation Aircraft Remote-sensing for Validation studies (NARVAL) expeditions (Stevens et al., 2019a), and the Elucidating the Role of Cloud-Circulation Coupling in Climate ($EUREC^4A$) field study (Stevens et al., 2021). The establishment of the Barbados Cloud Observatory (Stevens et al., 2016) has also contributed to the wealth of data available for study in the area. The popularity of the region for such investigation is largely due to the prevalence of undisturbed trade wind cumuli. Furthermore, Medeiros and Nuijens (2016) find that the clouds in the region may be representative of clouds in other trade wind regions. Measurement campaigns have, however, also explored other trade wind regions, such as the Sulu sea (Reid et al., 2016).

Field campaigns have also served as the foundation for many modelling studies of trade wind cumuli, including model intercomparisons (Abel & Shipway, 2007; Jiang et al., 2006; Xue et al., 2008; Jiang et al., 2009; vanZanten et al., 2011; Seifert & Heus, 2013; Saleeby et al., 2015; Seifert et al., 2015; Heiblum et al., 2016; Dagan & Chemke, 2016; Dagan et al., 2018b; Yamaguchi et al., 2019). Measurements taken during the campaigns provide information for models, typically large eddy simulations, to be initialised and forced, while also allowing them to be validated.

Central to the uncertainty in aerosol-cloud interactions in warm clouds is the coupling between microphysical impacts of increased aerosol, and resulting changes in macrophysical cloud characteristics. Increased aerosol may, for a given liquid water content, reduce droplet size and thus reduce the precipitation efficiency (Albrecht, 1989). However, this may not be the case if the aerosol size distribution is altered. An increase of GCCN, such as sea salt particles,

may suppress the activation of smaller condensation nuclei via competition for water vapour (O'Dowd et al., 1999), and furthermore may facilitate the initiation of warm rain processes by being activated directly to drizzle or rain droplets (Johnson, 1982b).

Stevens and Feingold (2009) hypothesised that systems of shallow clouds may be 'buffered'. That is, that such complex systems may compensate for the impact by a perturbation, such as aerosol, on one process via other pathways. One such buffering pathway they describe is that of convective invigoration and deepening; that is, an increase in vertical development and stronger updraught speeds. They describe a mechanism for the invigoration of shallow cumuli by increasing aerosol, whereby higher droplet numbers delay the onset of precipitation, allowing more moisture to be lofted to the cloud top. The increased evaporation at the cloud top destabilises the cloud layer, enabling greater vertical development of the cloud. Deeper clouds are more able to produce heavier rain, potentially compensating for the initial reduction in precipitation.

Koren et al. (2014) describe the warm-phase invigoration of convection by aerosol as an extension of the aerosol-limited regime. In this regime, the droplet number and surface area available for condensation are small, limiting the mass of condensed water. Compared to this regime, an increase in aerosol reduces droplet size, but allows more water to be condensed, enhancing latent heating and leading to greater vertical development (Lebo & Seinfeld, 2011; Koren et al., 2014; Sheffield et al., 2015).

There have been a number of observational studies employing satellite data showing an invigoration effect on shallow clouds; with greater cloud top heights, as well as cloud fraction, with increased aerosol (Kaufman et al., 2005; Yuan et al., 2011; Koren et al., 2014; Mace & Abernathy, 2016). Gryspeerdt et al. (2016), however, suggest that much of the relationship between aerosol optical depth and cloud fraction may be explained by meteorological covariability. Jung

et al. (2016), meanwhile, use aircraft data from a number of measurement campaigns to explore the precipitation susceptibility of shallow clouds. Precipitation susceptibility, S_0, is defined as $S_0 = -\frac{dlnR}{dlnN_d}$, where R is the precipitation rate and N_d is the droplet number, and it is typically evaluated for a fixed or limited range of liquid water path. Jung et al. (2016) find that the precipitation susceptibility is small for both shallow, non-precipitating cumuli, and deeper precipitating cumuli, while it is greater for intermediate-depth clouds.

Modelling studies have suggested a range of possible aerosol effects on cumulus convection; sometimes consistent, but often conflicting. Xue et al. (2008) and Jiang et al. (2006) both find that, while increased aerosol has little impact on cloud lifetime or top height, it does lead to a decrease in precipitation, and suggest an enhancement of evaporation and entrainment feedbacks. Xue et al. (2008) further note that such feedbacks may lead to a non-monotonic relationship between cloud fraction and aerosol, such that cloud fraction increases with aerosol up to a threshold, beyond which enhanced evaporation reverses the trend.

A similar non-monotonic relationship between aerosol loading and invigoration is found by Dagan et al. (2017) and Liu et al. (2019). Convective invigoration and deepening of cumuli has been found in a number of modelling studies (Lee et al., 2012; Seifert et al., 2015; Saleeby et al., 2015; Dagan et al., 2017; Yamaguchi et al., 2019), though often with conflicting details. Lee et al. (2012) find that increased aerosol initially causes clouds to be deeper, but over time this reverses, with unperturbed clouds becoming relatively deeper, and eventually the cloud fields become statistically similar, albeit with lower precipitation with increased aerosol. Seifert et al. (2015) argue that systems of trade wind cumuli tend towards a quasi-equilibrium state, similar to radiative convective equilibrium, but modified by advective forcing of temperature and moisture, and large-scale subsidence. In such a system, a transient stage exists during which aerosol-induced

deepening buffers the initial reduction in precipitation by modifying the thermodynamic environment. This allows deeper clouds to develop and produce higher peak precipitation rates, ultimately leading to similar precipitation rates in the quasi-equilibrium stage. However, Dagan et al. (2018a) argue that such a regime is not realistic, with lifetimes of shallow cloud fields typically much shorter than the time required for simulations to reach equilibrium. Large eddy simulations typically require more than 24 hours to reach a quasi-equilibrium (Dagan et al., 2018a; Seifert et al., 2015; Yamaguchi et al., 2019). However, using satellite and reanalysis data, Dagan et al. (2018a) find that the characteristic timescale for shallow convective cloud field lifetime is less than 12 hours. From observations of trade wind clouds at the Barbados Cloud Observatory, Nuijens et al. (2014) conclude that only a few hours are required for fields of cumuli to appear markedly different. Notably differing characteristics of the fields are number, depth, and size of clouds, as well as whether they are precipitating, and whether cumuli exist alongside stratiform-type clouds. Vial et al. (2019), too, note the diversity present in large-scale trade wind cloud fields, as well as the importance of diurnal variations in small non-precipitating cumuli, deeper precipitating cumuli, and accompanying stratiform clouds.

van den Heever et al. (2011) use simulations of radiative-convective equilibrium, and find that increased aerosol leads to fewer shallower cumuli, but invigoration of the congestus mode of convection, with stronger updraughts, and increased liquid water path and precipitation. The combined result is a weak domain-mean response, with little change in cloud fraction, due to the opposite effects on different clouds. This effect on smaller clouds is also found by Seifert et al. (2015), while Sheffield et al. (2015) note the invigoration of congestus. Saleeby et al. (2015) explore the aerosol-cloud dynamic-thermodynamic feedback by employing LES without imposing large-scale forcing, and simulating a case with cumuli, stratocumuli, and deeper convective clouds. They, too, find

that increased aerosol reduces the number of shallower cumuli, and that cumuli able to penetrate the inversion precipitate more heavily, though not sufficiently to overcome the reduction in domain-mean precipitation, due in part to the erosion of the stratiform layer present in their simulations.

Several studies have also noted the impact of aerosol-driven changes in precipitation on the organisation of shallow cloud fields. Precipitation may lead to cold pool outflows, which can drive the formation of new convective cells and contribute to mesoscale organisation (Xue et al., 2008; Zuidema et al., 2012; Seifert & Heus, 2013). The effect of increased aerosol on reducing precipitation may disrupt this process, however (Xue et al., 2008; Seifert et al., 2015; Dagan et al., 2018b). Yamaguchi et al. (2019) also investigated the role of wind shear on clean and perturbed simulations of trade wind cumuli. Regardless of shear, they find that increased aerosol leads to deeper clouds and a reduced cloud fraction. However, shear mutes the deepening such that precipitation is reduced, while in its absence, deepening leads to an increase in precipitation with aerosol.

1.4 Aims and purpose

The result of the diverse range of outcomes found in simulations of aerosol-cloud interactions in the trade winds is that these interactions are still poorly understood. It is clear that the large-scale behaviour of cloud fields is an important aspect, both in terms of mesoscale organisation (Seifert et al., 2015; Dagan et al., 2018b), and in terms of the diversity of cloud types that may occur in such fields, and their potentially differing response to aerosol. This may include shallow and congestus modes of cumulus convection, as well as stratiform clouds (Nuijens et al., 2014; van den Heever et al., 2011; Saleeby et al., 2015). Furthermore, meteorological conditions and large-scale forcing are highly relevant, as they underscore the dynamic and thermodynamic environment in which clouds develop

and aerosol-cloud interactions occur (Kaufman et al., 2005; Gryspeerdt et al., 2016; Dagan et al., 2016).

The vast majority of the modelling studies of trade wind cumuli discussed in the previous section employed highly idealised large eddy simulations. Typically, such an approach uses a high horizontal resolution of tens of metres, at the cost of requiring the domain size to be limited to tens of km, limiting the representation of the mesoscale structure of the cloud field. The common approach of applying doubly-periodic boundary conditions may present additional disadvantages in representing the large-scale behaviour, as discussed in section 1.2.2. Furthermore, the imposition of constant large-scale forcing of subsidence, temperature, and moisture over relatively long simulations of a few days (Seifert et al., 2015; Yamaguchi et al., 2019), limits the expression of transient large-scale behaviour that is indicated by observations (Dagan et al., 2018a). The significance of diurnal variations found by Vial et al. (2019) suggests another possible limitation of LES in representing shallow cloud fields, in that they do not typically include a radiation scheme, but rather account for radiative influences on heating or cooling by directly applying temperature tendencies.

This thesis aims to advance the existing understanding of aerosol effects on shallow convective clouds by exploring these limitations using large-domain, realistic simulations, and aims to answer the following questions:

- How do aerosol perturbations affect trade wind cloud fields in large domains?
- How do aerosol effects on shallow convective clouds differ in simulations with idealised and realistic representations of domain boundaries and large-scale forcing?
- How are the different components of shallow cloud fields affected by aerosol perturbations?

1.5 Methods

In this thesis, interactions between aerosol and shallow convective clouds are investigated using numerical models; specifically, the effects on these clouds of changes in aerosol concentration. While the specific simulation setups are described in detail in each chapter, the framework is similar, and it is useful to discuss it here in general.

The simulations presented herein are based on case studies from the RICO field campaign, and are supplemented by observational data from the campaign. The model (discussed in more detail in section 1.5.1) is run to produce a baseline simulation for the case in question. In order to investigate the effect of changes in aerosol concentrations, further simulations with perturbed aerosol are performed. These perturbations to the aerosol concentration are idealised; simply multiplying the baseline conditions by some factor of 10. This approach is taken in order to avoid introducing complications that may result from changes in factors such as the vertical distribution of aerosol, or aerosol properties. Thus, the approach allows the focus to be on the effect of changes in aerosol concentration.

1.5.1 Model

Throughout this thesis, simulations are performed using the Met Office Unified Model (UM). A central feature of the UM is that it is 'seamless'; the same model may be used, in different configurations, across a wide range of spatial and temporal scales, with a great deal of flexibility in how the model may be configured. Of particular concern are the representations of clouds, convection, microphysics, and sub-grid turbulence.

The majority of simulations presented in this thesis were performed with horizontal resolutions of approximately 500m, with some simulations at 100m. This

is more coarse than the highest resolutions currently employed by LES, but allows for large simulation domains. While core cloud updraughts will be resolved, finer-scale processes such as entrainment of air into clouds at their boundaries may be poorly represented. At this resolution, the UM is configured without employing a cloud or convection scheme. Representation of clouds and convection is then a result of resolved processes, in addition to a sub-grid turbulence scheme, and a microphysics scheme. Turbulence is represented using a 3D Smagorinsky-type scheme, originally developed for the Met Office Large Eddy Model (LEM) and implemented in the UM to improve the representation of sub-grid mixing for resolutions finer than approximately 1km (Boutle et al., 2014). The vertical coordinate is stretched, such that the resolution is higher in the boundary layer and becomes more coarse with increasing height. The simulations presented herein use a vertical coordinate with 70 levels below a model top of 40km, 30 of which are below 3km.

The UM can be configured to use the Cloud-Aerosol Interactive Microphysics (CASIM) scheme. CASIM is a multi-moment bulk microphysics scheme, allowing vertical profiles of aerosol concentrations to be prescribed, and further allowing explicit treatment of aerosol-cloud interactions. Hydrometeor size distributions are given by gamma distributions with prescribed shape parameters, and have two prognostic moments; the mass mixing ratio and number concentration. The autoconversion of cloud droplets to rain, and droplet accretion, follow Khairoutdinov and Kogan 2000. It is important to note that, as a bulk scheme, CASIM may be limited in representing the effect of aerosol due to the use of a saturation adjustment. However, the short time steps of only 2-3s required for prognostic treatment of supersaturation (Morrison & Grabowski, 2008) present significant computational challenges for large simulations, while the longer time steps of 15s used herein improve the suitability of the saturation adjustment approximation.

Two possible schemes for droplet activation were considered: from Abdul-Razzak and Ghan (2000) (ARG) and from Shipway (2015). Typically, schemes aim to find an expression for the peak supersaturation, since no more droplets will be activated at cloud base above this. Secondary activat5ion above cloud base is also possible, however, due to either increasing updraught strength or entrainment (Warner, 1969a, 1969b; Lasher-Trapp et al., 2005). The ARG scheme approximates the maximum supersaturation by setting the rate of change of the supersaturation to zero, and then neglecting effects of curvature, gas kinetics, and solute in the droplet growth rate. Two separate expressions for maximum supersaturation, for 'low' and 'high' critical supersaturations, are then combined, with coefficients determined by fitting to numerical simulations (Abdul-Razzak & Ghan, 2000). In contrast, the Shipway scheme applies an updated version of Twomey's approximation for the integral of the supersaturation, which is then used along with the application of lookup tables to find the maximum supersaturation (Shipway, 2015).

A number of studies have found that the ARG scheme consistently underestimates the number of activated droplets, and has too much competition for water vapour (Simpson et al., 2014; Connolly et al., 2014; Shipway, 2015). Shipway (2015) shows that this is particularly apparent for typical marine aerosol scenarios, and is worsened at higher updraught velocities. These limitations are also apparent when compared with other schemes, including the Shipway scheme, as well as in comparison with the full numerical solution of the supersaturation time evolution. Given the focus of this thesis on clouds in a marine environment, the Shipway scheme was chosen.

Aerosols in CASIM are described by a log-normal distribution for each of the soluble and insoluble fine, accumulation, and coarse modes. The mass and number mixing ratios are also carried as prognostic variables. Aerosol fields are

advected by the model, with initial and lateral boundary conditions being set by the prescribed profiles.

CASIM provides two possible treatments of aerosol-cloud interactions. The first, and the method used for this work, is the passive coupling. In this mode, processes such as droplet activation depend upon the aerosol fields, but these fields are not affected by cloud processes. The second option offered by CASIM is the processing mode, in which the aerosol fields are modified by in-cloud microphysical processes including droplet activation and ice nucleation, as well as evaporation and sublimation.

It should be noted again that the effects of aerosol perturbations on clouds have been shown to be sensitive to the details of microphysics schemes (White et al., 2017). In this thesis, however, simulations are performed using only one microphysics scheme, and therefore uncertainty relating to such sensitivities is not investigated in detail.

Simulation domains may also be flexibly configured in the UM. The primary configuration employed in this thesis features a limited-area domain nested inside a global driving model. The global configuration is initialised using operational analysis or reanalysis data, and provides boundary conditions for the nested domain. This allows the nested domain to have open boundaries, in addition to time-varying, realistic forcing of the large-scale properties of the domain. While this approach allows a great deal more realism to be introduced to the simulations, it does create a potential limitation in that many distinct simulations may be required to fully explore the range of possible atmospheric conditions and resulting behaviour of clouds and aerosols.

An additional configuration is employed in Chapter 3. The UM can be configured in an idealised setup, akin to those used for LES. In this case, the domain features doubly-periodic lateral boundaries, with large-scale forcing given by constant prescribed tendencies of temperature and moisture. The concurrent use of

these two configurations will allow the second research question noted previously to be explored effectively, by directly comparing approaches using a single model.

Chapter 2

Effects of aerosol in simulations of realistic shallow cumulus cloud fields in a large domain

This chapter is based on an article published in Atmospheric Chemistry and Physics, with some minor changes:

Spill, G., Stier, P., Field, P. R., and Dagan, G. (2019). Effects of aerosol in simulations of realistic shallow cumulus cloud fields in a large domain. *Atmospheric Chemistry and Physics*, 19(21), 13507–13517. doi: 10.5194/acp-19-13507-2019.

I designed the study together with the co-authors. I carried out the simulations and analyses presented, with input from the co-authors. I wrote the manuscript, and underwent the peer-review process, with contributions and approval from the co-authors.

Abstract

Previous study of shallow convection has generally suffered from having to balance domain size with resolution, resulting in high-resolution studies which do not capture large scale behaviour of the cloud fields. In this work we hope to go some way towards addressing this by carrying out cloud-resolving simulations on large domains. Simulations of trade wind cumulus are carried out using the Met Office Unified Model (UM), based on a case study from the Rain In Cumulus over the Ocean (RICO) field campaign. The UM is run with a nested domain of 500km with 500m resolution, in order to capture the large-scale behaviour of the cloud field, and with a double-moment interactive microphysics scheme. Simulations are run using baseline aerosol profiles based on observations from RICO, which are then perturbed. We find that the aerosol perturbations result in changes to the convective behaviour of the cloud field, with higher aerosol leading to an increase (decrease) in the number of deeper (shallower) clouds. However, despite this deepening, there is little increase in the frequency of higher rain rates. This is in contrast to the findings of previous work making use of idealised simulation setups. In further contrast, we find that increasing aerosol results in a persistent increase in domain mean liquid water path and decrease in precipitation, with little impact on cloud fraction.

2.1 Introduction

Shallow cumuli are the most common cloud type on Earth (Rossow & Schiffer, 1999; Sassen & Wang, 2008); they are ubiquitous throughout the trade winds, yet their behaviour is still poorly understood. These small, warm, shallow convective clouds have an important part in regulating the thermodynamics and dynamics of their environment; warming the cloud layer through condensation,

transporting moisture to the inversion layer above, and cooling both the inversion and the sub-cloud layer through the evaporation of detraining cloud droplets and precipitation (Hartmann et al., 1992; Zhu & Bretherton, 2004; Neggers et al., 2007).

Trade wind shallow cumuli are of great interest in the context of a changing climate. In particular due to their coupling to circulation, as well as their radiative properties; reflecting shortwave radiation whilst emitting longwave radiation at a similar temperature to the surface due to their low, warm cloud tops. The myriad of ways in which they interact with their environment means there is still much uncertainty in how they may respond to perturbations to the climate. Indeed, low-cloud feedbacks are responsible for most of the uncertainty in climate sensitivity (Bony et al., 2004; Bony & Dufresne, 2005; Medeiros et al., 2008; Vial et al., 2013; Boucher et al., 2013b; Medeiros et al., 2015).

Aerosol particles in the atmosphere can act as cloud condensation nuclei (CCN) allowing the formation of cloud droplets (Köhler, 1936). Changes in aerosol concentration can therefore have significant impacts on the properties of clouds. For example, for a given liquid water content, an increase in CCN will lead to a greater number of smaller droplets. Smaller, more numerous droplets scatter more shortwave radiation back to space, and thus this results in an increase in the cloud albedo (Twomey, 1977). Additionally, the shift in the droplet size distribution may affect the formation of precipitation in shallow clouds by inhibiting the development of larger droplets (Albrecht, 1989).

Aerosol-induced changes in the precipitation efficiency of clouds can also lead to impacts on convection. Suppressed precipitation can result in increased condensation warming the lower part of the cloud layer, and increased evaporation of detraining droplets cooling the upper part. This destabilisation of the cloud layer can lead to an invigoration and deepening of the convection (Albrecht, 1993; Stevens & Feingold, 2009; Dagan et al., 2016; Sheffield et al., 2015).

Cloud fields may be affected in other ways; changing precipitation characteristics may affect the formation of cold pools, for example, which can have an impact on the development of new convection, and contribute to the mesoscale organisation of the field of shallow clouds (Seifert & Heus, 2013; Seigel, 2014; Seifert et al., 2015).

A number of studies (Xue et al., 2008; Jiang et al., 2010) have seen significant aerosol effects such as those described above. However, several others (van den Heever et al., 2011; Seifert et al., 2015) have also shown effects where parts of the system respond to perturbations in such a way as to offset the initial aerosol effect. Stevens and Feingold (2009) described these as buffering effects, and proposed possible buffers that may be relevant for cloud-aerosol interactions, including, for example, convective deepening and invigoration. They describe a mechanism for the deepening of shallow cumuli by increasing aerosol, whereby higher droplet numbers delay the onset of precipitation and increase evaporation at the cloud top. This destabilises the cloud layer, enabling greater vertical development of the cloud, which can then produce heavier rain, potentially compensating for the initial reduction in precipitation.

There have been a number of observational studies showing an invigoration effect on shallow clouds (Kaufman et al., 2005; Yuan et al., 2011; Koren et al., 2014), while modelling studies have shown seemingly conflicting results. Jiang and Feingold (2005) and Xue et al. (2008) both find that increasing aerosol actually suppresses convection in warm, shallow clouds, while Dagan et al. (2017) and Altaratz et al. (2014) argue for a 'turning point' between suppression and invigoration of convection, depending on local conditions and specific cloud properties. van den Heever et al. (2011) find that even within a cloud field the response varies: with shallower clouds being suppressed, and deeper clouds penetrating the trade inversion experiencing invigoration. A similar result is obtained by Seifert et al. (2015), who find a reduction in the number of small clouds due

to an evaporative feedback from aerosol-suppression of precipitation. Both van den Heever et al. (2011) and Seifert et al. (2015) find that, though there are aerosol effects on cloud populations and properties such as rain rate, over a large area and after a long time these effects are minor. In contrast, Saleeby et al. (2015) find that a reduction in shallower cumuli and stratocumulus, along with an increase in deeper cumuli, leads to a reduction in domain accumulated precipitation with increased aerosol.

Much of the behaviour of convective clouds is constrained or driven by local conditions — heating, water budgets, or large scale subsidence for example — many of which may contribute to so-called buffering effects (Seifert et al., 2012), raising the possibility that cloud responses to aerosol are regime dependent or regionally dependent.

Despite much work on the subject, there is still a great deal of uncertainty and debate over the response of shallow convection to perturbations such as changes in aerosol (Tao et al., 2012). Typical modelling studies of shallow convection make use of high-resolution large eddy simulations (LES), or cloud resolving models (CRM). These models explicitly resolve convection, but until recently have only been run on limited area domains, of the order of tens of kilometres, due to computational limitations.

In this work we begin to extend the investigation of shallow convection by making use of the Met Office Unified Model's capabilities to run high resolution simulations on large domains in order to study the effect of aerosol perturbations over entire cloud fields on spatial scales on the order of hundreds of kilometres. Additionally, the use of a double moment cloud microphysics scheme, described below, allows aerosol concentration to be perturbed directly since activation processes are included, rather than using cloud droplet number as a proxy. We aim to investigate the character of the response of shallow convection to aerosol perturbations in simulations of realistic weather systems, and whether and why this

may differ from that seen in idealised simulations.

2.2 Model and case description

The Rain in Cumulus over the Ocean (Rauber et al., 2007) campaign was carried out over a period of November 2004 - January 2005, in a region of the trade winds in the western Atlantic off the Caribbean. This has been, and is, an ideal region for studies of shallow cumuli due to their prevalence, as well as the absence of upstream islands meaning that clouds observed here are likely to be highly representative examples of shallow cumuli.

Aircraft and shipborne measurements across the campaign region were supported by ground-based systems as well as radiosondes. The aerosol profiles used in this work were based on measurements from one of the NSF/NCAR C-130Q campaign aircraft flights from 19/01/2005 (Stossmeister, 2008). Vertical profiles, shown in Fig. 2.1, of Aitken and accumulation mode aerosol number concentration were derived from a fit to this data, and allowed to decay exponentially with height (e-folding height = 1km) above 5km.

A global configuration of the Unified Model (UM) UM vn10.8 (Walters et al., 2017), GA6.1, at resolution N768 (~25km x ~17km at midlatitudes) is run from operational analysis initial conditions, and used as a driving model to provide the lateral boundary conditions for a ~500km x ~500km nested region, centred on 17.5°N, 61.8°W. The nested region has a horizontal resolution of ~500m x ~500m and a stretched vertical coordinate system with 70 levels below 40km. This nested configuration allows for the simulations to capture the transient features and forcing for the specific case, due to the open boundaries and driving global model. The resolution in the nested region is expected to resolve most of the relevant convection, since the case in question was characterised by the presence of towering cumulus and congestus (Abel & Shipway, 2007), and in-

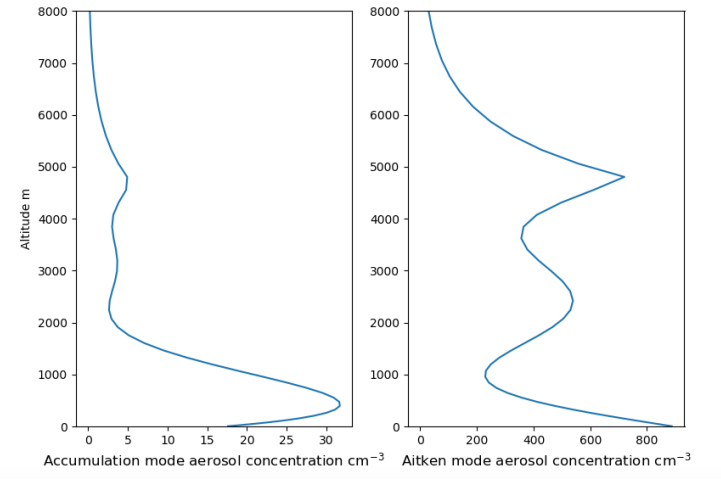

Figure 2.1: Vertical profiles of accumulation and Aitken mode aerosol concentration used in the baseline simulation.

spection of the simulations shows that this is indeed the case. A model time step of 15s is used, with prognostic and diagnostic radiation time steps of 900s and 300s. The simulations are initialised for 00:00 UTC 19 January 2005, and are run for 48h. The nested simulations are run without a parameterised convection scheme, and the operational microphysics scheme is replaced in favour of the double-moment Cloud AeroSol Interactive Microphysics (CASIM) scheme (Shipway & Hill, 2012; Grosvenor et al., 2017; Miltenberger et al., 2018a). A number of size modes for insoluble and soluble aerosol are available; however we use only the soluble Aitken and accumulation modes, with the profiles shown in Fig. 2.1. These profiles are used to initialise the domain, and as lateral boundary conditions. Aerosol may be advected through the domain, but the coupling to cloud processes is one-way. That is, aerosols affect droplet activation, but we do not include cloud processing and removal of aerosol, such as activation scavenging or precipitation washout. Here, CASIM is run with a sub-grid cloud fraction scheme based on that of Smith (1990), which parameterises the sub-grid variability in relative humidity. Its implementation in CASIM is described in Grosvenor et al. (2017). Additionally, we choose to apply the droplet activation

scheme from Shipway (2015), rather than CASIM's default scheme from Abdul-Razzak and Ghan (2000). This decision was based on the findings of a number of studies that the latter consistently underestimates the number of activated droplets for very high aerosol concentrations, and has too much competition for water vapour (Simpson et al., 2014; Connolly et al., 2014; Shipway, 2015). Shipway (2015) shows that this is particularly apparent for typical marine aerosol scenarios.

Four simulations with different aerosol number concentrations were carried out: a baseline case UM_CASIM, and three with the aerosol profiles perturbed by factors of 0.1, 10, and 100, labelled as UM_CASIM_0.1, UM_CASIM_10, and UM_CASIM_100, respectively.

2.3 Results and discussion

2.3.1 Structure and evolution of simulation

Figure 2.2 shows the evolution of a number of domain-averaged quantities over the simulation period for the baseline case, not including a 6h spin-up. Average profiles of liquid water potential temperature and specific humidity are shown in Fig. 2.3, which compare well to those used as initial profiles used in the GEWEX Cloud System Study (GCSS) RICO model intercomparison study (vanZanten et al., 2011), as well as those shown in Nuijens et al. (2009) and those obtained from simulations such as in Seifert and Heus (2013). Qualitative visual inspection reveals the transient meteorological features and characteristics of the cloud field over the simulated period. Some example snapshots are shown in Fig. 2.4.

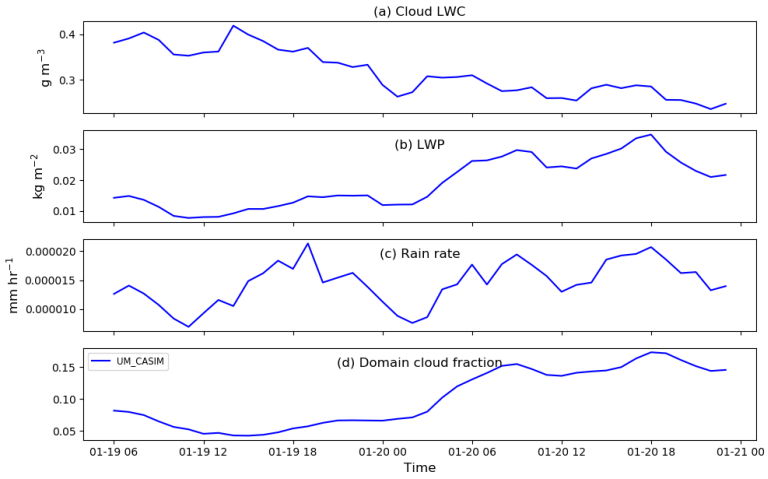

Figure 2.2: Time series of domain-averaged (a) cloud liquid water content (in-cloud only), (b) liquid water path, (c) rain rate, and (d) cloud fraction, all for the baseline case UM_CASIM. A liquid water content threshold of 0.01 g m^{-3} is used to define a cloudy gridbox.

2.3.2 Aerosol perturbations

In Fig. 2.5, time series of a number of domain-averaged quantities, excluding an initial 6h spin-up period, show that even when considered across a large domain there is a marked response to the aerosol perturbations.

Figure 2.5a shows the domain average of in-cloud liquid water, with a liquid water threshold of 0.01 g m^{-3} used to define a cloud. The cloud liquid water content (LWC) and domain liquid water path (LWP) both increase monotonically as the aerosol concentration is increased, while the rain rate decreases. Despite significant effects on other domain-wide parameters, there seems to be only a modest reduction of the domain-wide cloud fraction from aerosol perturbations.

Concurrently with the responses in average cloud LWC, we see similar trends in the domain average vertical profiles of liquid water mixing ratio in Fig. 2.6. The peak in liquid water is increased and is shifted to a higher altitude. Additionally, the liquid water mixing ratio becomes significantly greater at higher

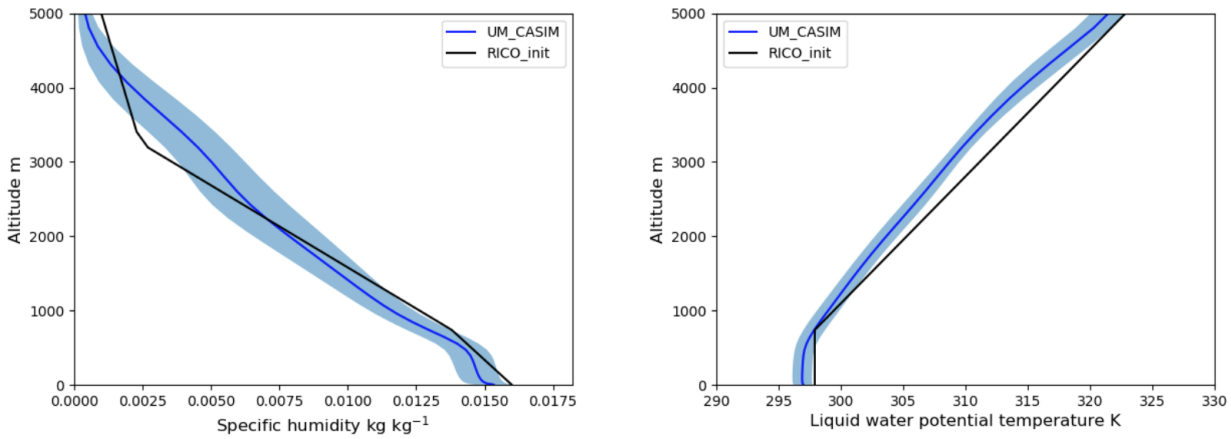

Figure 2.3: Domain-averaged vertical profiles of liquid water potential temperature and specific humidity for the baseline case, compared to the RICO initial setup, with the standard deviation of the baseline shaded.

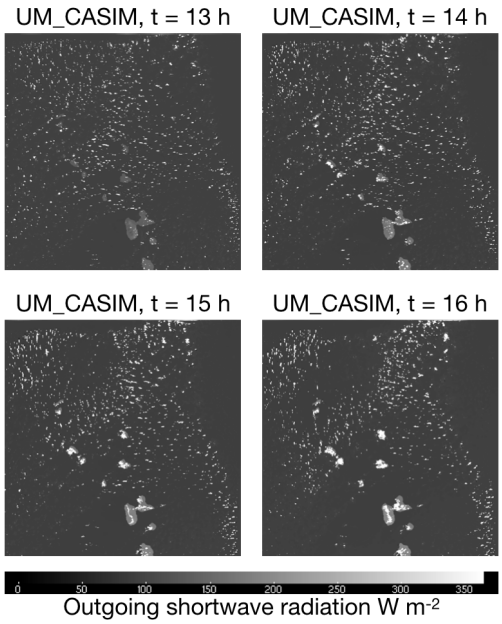

Figure 2.4: Snapshots of outgoing shortwave radiation showing the structure of the cloud field in the afternoon of the first day of the UM_CASIM simulation.

altitudes. The changes in these profiles indicate a deepening response to increasing aerosol. This may also be inferred from the profiles of cloud fraction (Fig. 2.6). As aerosol is increased, the cloud fraction is reduced at lower altitudes but

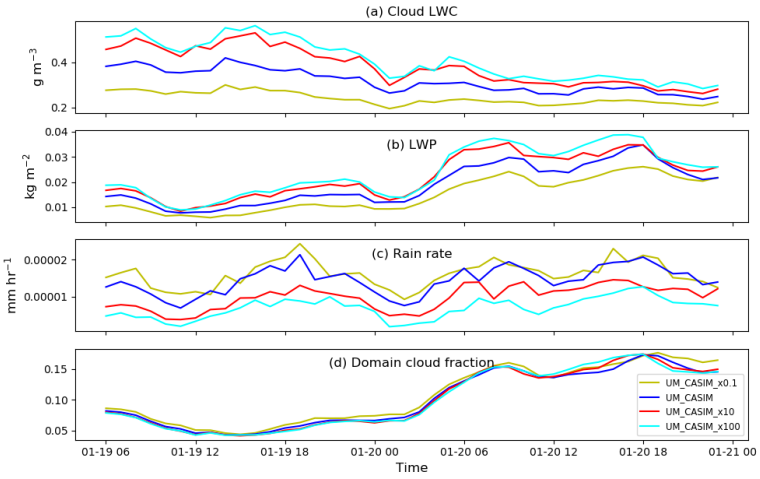

Figure 2.5: Time series of domain-averaged (a) cloud liquid water content (in-cloud only), (b) liquid water path (LWP), (c) rain rate, and (d) cloud fraction. A liquid water content threshold of 0.01 g m^{-3} is used to define a cloudy gridbox.

increases at higher altitudes. Additionally, the lowest aerosol case, UM_CASIM_-0.1, produces a cloud fraction profile which does not have the same pronounced double peaks seen in the other cases. An invigoration response is also evident in the profiles of updraught speed in Fig. 2.6. The updraught speeds show little change below 1.5km; however, there are marked responses above 1.5km with updraughts increasing in strength with aerosol. This increase, along with smaller droplets under the higher aerosol conditions having smaller fall velocities, leads to more water being lifted higher in the atmosphere (Koren et al., 2015), as can be seen in the vertical profiles of liquid water. It is important to note that an in-cloud mean in used for the updraught profiles, and therefore at the highest altitudes they are due to only a small number of clouds.

An increase in aerosol loading will generally lead to an increase in the cloud droplet number concentration. Under such an increase, combined with the increase in liquid water path, we would expect the cloud albedo to also increase. In Fig. 2.7 we show the synthetic cloud albedo, calculated following Seifert and

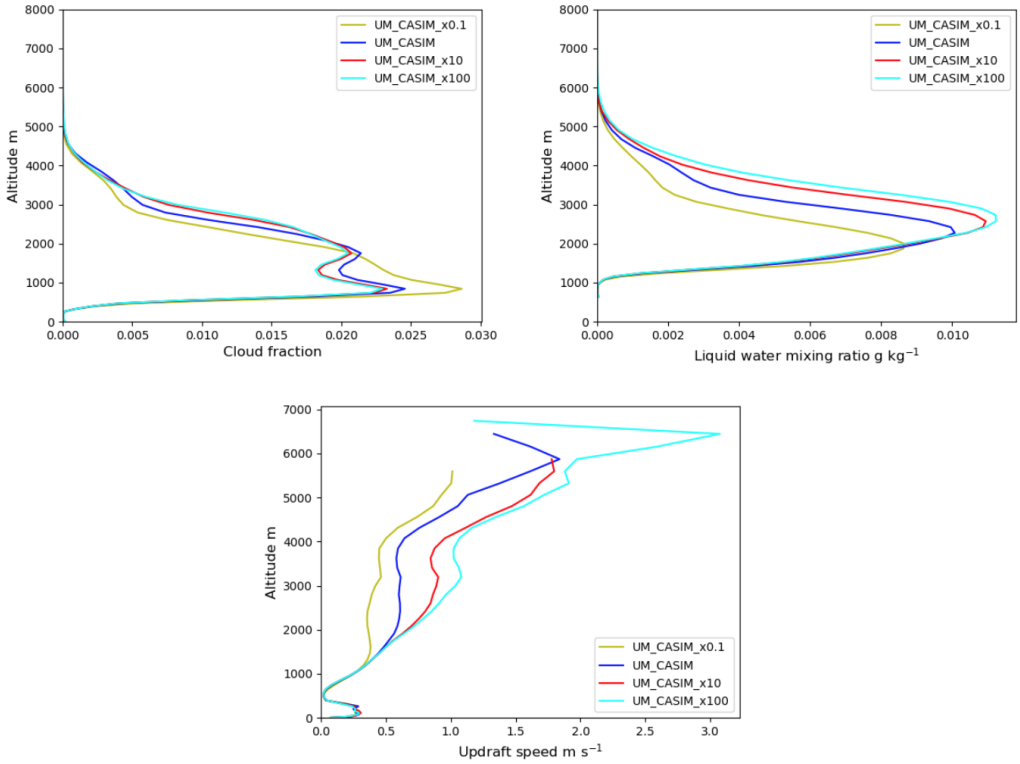

Figure 2.6: Vertical profiles of domain-average liquid water mixing ratio (top left) and cloud fraction (top right), calculated for all columns, and updraught speed (bottom), calculated for cloudy columns only.

Heus (2013), as

$$A = \frac{\tau}{6.8 + \tau} \tag{2.1}$$

where τ is an estimate of optical depth given by $0.19LWP^{5/6}N^{1/3}$, depending on the cloud liquid water path, LWP, and cloud droplet number concentration, N (Zhang et al., 2005). This shows that there is indeed a significant increase in the cloud albedo with higher aerosol loads. This change is sufficient to lead to an increase in the domain-wide scene albedo, in spite of the slight reduction in cloud fraction with higher aerosol. This is shown in Fig. 2.8, where the scene

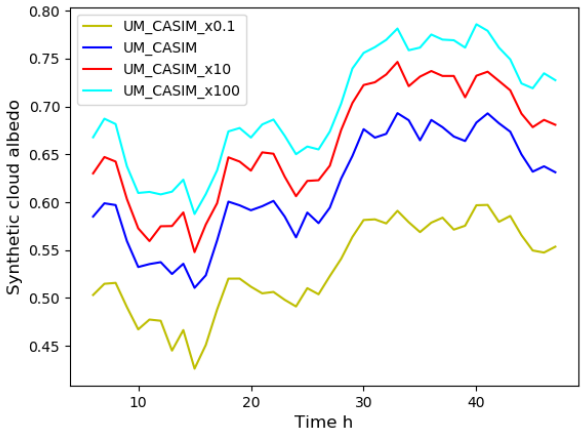

Figure 2.7: Time series of mean synthetic cloud albedo. This is calculated for cloudy columns only using an estimate of the cloud optical depth, as shown in equation 1.

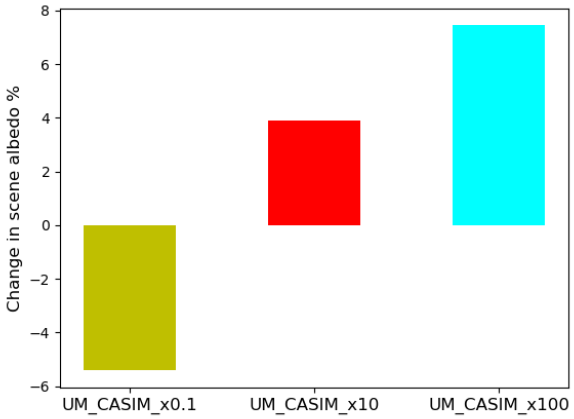

Figure 2.8: Percentage change in scene albedo for each of the perturbed aerosol simulations, relative to the baseline UM_CASIM case, calculated using time and domain mean synthetic cloud albedo and cloud fraction, as shown in equation 2.

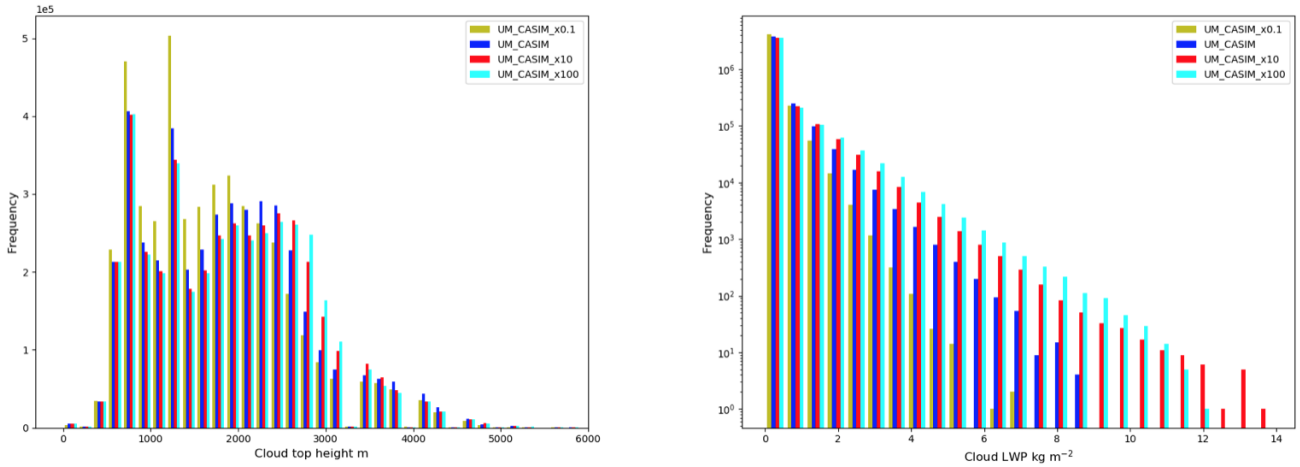

Figure 2.9: Histograms of cloud top height (left), calculated as the highest cloudy grid box in a cloudy column, and of total column liquid water path (right), calculated using only columns containing cloud.

albedo is calculated as

$$A_{\text{scene}} = CA + (1 - C)A_{\text{b}} \tag{2.2}$$

where C is the cloud fraction, and A_{b} is the background albedo. Following Seifert et al. (2015), we assume this to be the albedo of the sea surface at high zenith angles and set it to be 0.05.

The distributions of cloud top height (CTH) shown in Fig. 2.9 also indicate a shift in the convective behaviour with aerosol perturbations: with increasing aerosol resulting in a suppression of the frequency of occurrence of clouds with lower CTHs and an increase in the prevalence of higher CTHs.

The distributions of LWP in Fig. 2.9 also indicate a deepening response to aerosol: as the aerosol is increased, low LWPs become less frequent, while the tail of the distribution grows and extends to higher values.

The joint histograms of cloud top-height and liquid water path also shown in

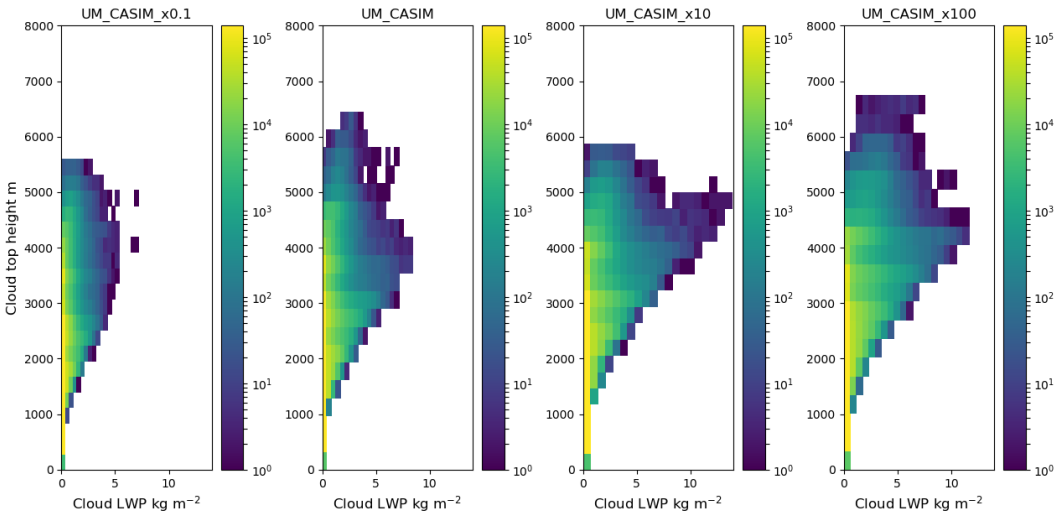

Figure 2.10: Joint histograms showing frequency of occurrence of liquid water path and cloud top height for each simulation, with aerosol increasing from left to right along the figure.

Fig. 2.10 give a clearer view of the effect: with higher aerosol concentrations come higher peak LWPs, indicating deeper clouds, as well as larger numbers of higher LWP clouds. However, it is also clear from these histograms that throughout all the simulations, the cloud fields are dominated in terms of occurrence by the shallowest clouds with lower CTHs.

With the change in the convective behaviour of these clouds comes an effect on the precipitation. As shown in Fig. 2.11, lower aerosol concentrations result in higher frequencies of drizzle and lower rain rates, while these are suppressed for higher aerosol concentrations, as is the onset of precipitation. This effect is responsible for the reduction in the domain-averaged precipitation in Fig. 2.2. There does not appear to be a consistent response in the frequency of the highest rain rates; however, due to the rarity of these events it is difficult to draw firm conclusions.

We can attempt to gain a greater insight into the change in convection by inspecting the thermodynamic environment in which the clouds are developing.

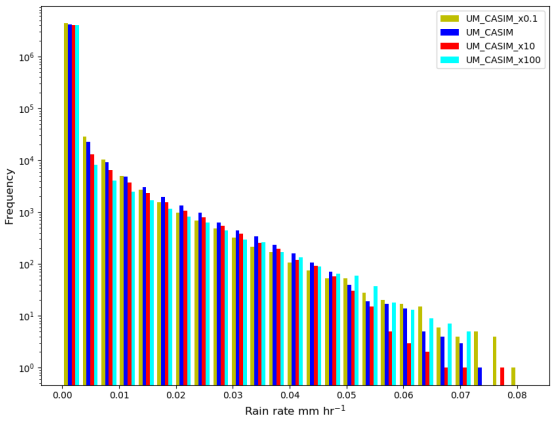

Figure 2.11: Histograms of rain rate, taken for all columns containing clouds.

In Fig. 2.12 we see that the variation in the mean specific humidity and liquid water potential temperature is far less across the aerosol perturbations than the standard deviation in the baseline case. We can visualise the change in thermodynamic structure through the simulation in more detail using the plots shown in Fig. 2.13. Here we show the difference between the domain average temperature or specific humidity at a given time and that at the beginning of the analysis period. We can see that though there are some differences between the simulations they are not very large. The minor changes reflect the deepening of convection but also demonstrate that the deepening and invigoration is not sufficient to significantly affect the thermodynamic structure in such a way as to promote further deepening.

2.4 Conclusions

We have presented results from a set of large-domain simulations with perturbed aerosol loadings. Simulations based on particular, realistic days of the RICO field campaign were run using the Met Office Unified Model, in a 500km × 500km domain with 500m resolution, nested in a global driving model. Our

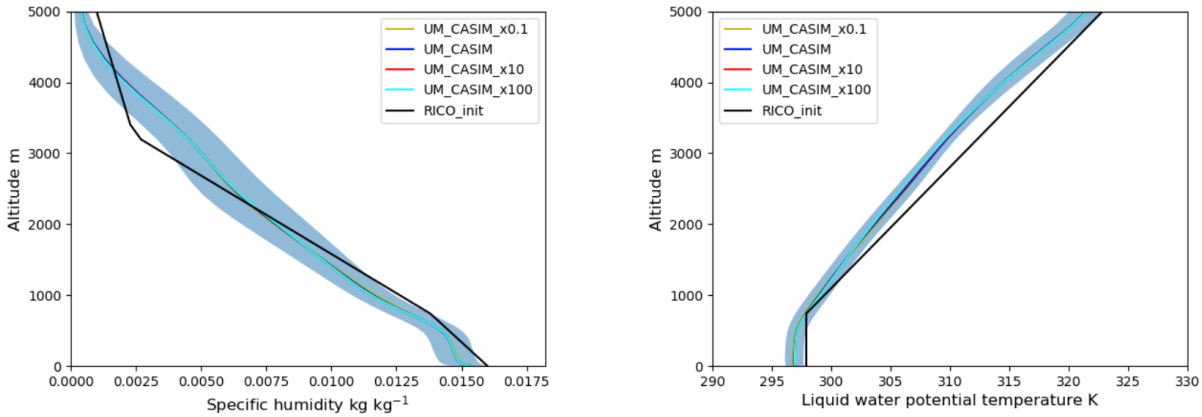

Figure 2.12: Average vertical profiles of liquid water potential temperature and specific humidity for each aerosol concentration, compared to the RICO initial setup as in Fig. 2.2, with the standard deviation of the baseline case shaded.

findings show that for a large domain without periodic boundary conditions, with realistic synoptic weather subject to large-scale forcing and energy and water budgets, changes in aerosol concentration can have significant effects. The impacts of aerosols on cloud microphysics are sufficient to result in persistent changes in the behaviour of the cloud field. We find that increasing aerosol suppresses the onset of precipitation, and leads to deepening and invigoration of convection. Increased aerosol loading results in a suppression of the shallow mode of convection, and invigoration of mid-level and deeper clouds. There is little change however in the updraught strength at low altitudes, in contrast to the substantially increased updraught speeds higher in the atmosphere. In spite of the convective deepening and invigoration, domain-averaged precipitation is still reduced throughout the simulations with increased aerosol, with little discernible change to the frequency of high rain rates. Examination of the thermodynamic structure of the simulations reveals that it is in fact highly resilient and is not significantly affected by the changes to the cloud field.

Previous studies of the effects of aerosols on convection which have made

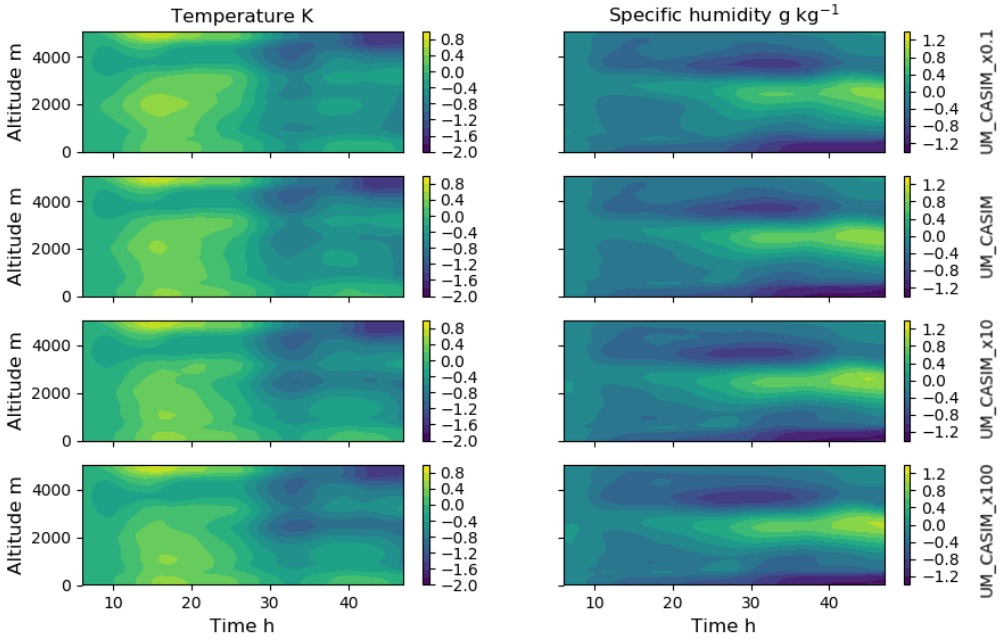

Figure 2.13: Hovmöller plots showing the temporal evolution of domain mean temperature (left) and specific humidity (right). These show the difference between the mean temperature or specific humidity at each time in the simulation and the first time point after the 6h spin-up. Each row is for a different simulation, with aerosol increasing from top to bottom down the figure.

use of more idealised modelling setups, making use of prescribed forcings and periodic boundaries, have also found invigoration and deepening as a result of increasing aerosol, as well as suppression of the shallowest clouds. However, our results differ from these in several ways. van den Heever et al. (2011) and Seifert et al. (2015) both find similar suppression and invigoration effects on different parts of the cloud population, as well as on characteristics of the precipitation rate distribution. However they conclude that the domain-wide effect is minimal, with small impacts on domain average or equilibrium properties. This is in agreement with our own findings for cloud cover but is in contrast to those for precipitation, where we find a persistent decrease in rain rates with higher

aerosol. Further, while Seifert et al. (2015) find that reduced cloud cover with higher aerosol compensates for the Twomey effect to produce only a minor change in scene albedo in equilibrium conditions, we find that there is a clear increase in scene albedo with increasing aerosol. Lee et al. (2012) argue that differences in aerosol have significant effects on the thermodynamic environment and development of instability, which in turn affects development of the cloud field. Our findings, however, are of thermodynamic conditions which are not significantly affected by aerosol.

Additionally, Dagan et al. (2017) find that there exists an optimum aerosol loading for convective invigoration and deepening, above which the trend reverses and increasing aerosol leads to suppression. In contrast, we find monotonic deepening and invigoration. Our results here do not preclude the possibility of an optimum loading or turning point, although in this case it is likely that such a point would be far above realistic aerosol concentrations, given the perturbations we applied.

It is important to note that the standard picture of buffering of aerosol effects on shallow convection appears to require some equilibrium state of the cloud field. In idealised simulations this state is reached under different aerosol loadings by affecting the convective development and precipitation characteristics to varying degrees. However, in the real atmosphere with constantly varying cloud fields subject to large scale advection, no such equilibrium exists. Dagan et al. (2018a) show that the characteristic timescale of shallow convective cloud fields is less than 12h, much less than the time required to reach an equilibrium state (Seifert et al., 2015). Here we have presented simulations of such a transient case, which suggest a quite different response: one in which cloud fields do not respond dramatically to restore an equilibrium but instead are altered persistently within the constraints of the transient thermodynamic conditions.

Given the apparent differences between idealised, limited-area large eddy sim-

ulations, and those presented here, it seems clear that work is required to elucidate the sources of these differences. LES studies performed on large domains will be necessary, as well as direct comparison of idealised and realistic model setups. It will be important to discern which differences are due to the choice of model, and which are due to the idealised or realistic nature of the simulations. In future work we aim to make such a comparison through the use of idealised and realistic configurations of the same model. We hope that the simulations and results we have discussed here will provide a starting point for this direction of investigating anthropogenic perturbations to shallow cumuli, and ultimately the climate.

Chapter 3

Contrasting responses of idealised and realistic simulations of shallow cumuli to aerosol perturbations

This chapter is based on an article published in Geophysical Research Letters, with some minor changes:

Spill, G., Stier, P., Field, P. R., and Dagan, G. (2020). Contrasting responses of idealised and realistic simulations of shallow cumuli to aerosol perturbations. *Geophysical Research Letters*, 48(13), e2021GL094137. doi: 10.1029/2021GL094137.

I designed the study together with the co-authors. I carried out the simulations and analyses presented, with input from the co-authors. I wrote the manuscript, and underwent the peer-review process, with contributions and approval from the co-authors.

Abstract

Shallow clouds remain greatly significant in improving our understanding of the atmosphere. Using the Met Office Unified Model, we compare highly idealised simulations of shallow cumuli with those using more realistic domains, with open lateral boundaries and varying large-scale forcing. We find that the realistic simulations are more capable of representing the cloud field on large spatial scales, and appear to limit the aerosol perturbations leading to impacts on the thermodynamic conditions. Aerosol perturbations lead to changes in the cloud vertical structure, and thermodynamic evolution of the idealised simulations; a central feature of behaviour seen previously in idealised simulations. Modelling approaches with open boundaries and time-varying forcing may allow for improved representation of shallow clouds in the atmosphere, and greater understanding of how they may respond to perturbations.

Plain Language Summary

Clouds, and shallow clouds in particular, are responsible for much uncertainty in our understanding of the atmosphere, and the response of the climate system to anthropogenic perturbations. The representation of shallow clouds in models has long been a challenge due to the myriad processes and scales involved; from micrometre cloud droplets, to cloud fields of tens or hundreds of km, leading to many computational difficulties. Here we present and compare a number of simulations using different approaches. We show that certain modelling choices allow for an improved representation of shallow cloud fields on large scales, and also show a different response to aerosol perturbations, with implications for future development of estimations of the effects of aerosol on shallow clouds.

3.1 Introduction

Shallow cumuli play a number of important roles in trade wind regions, affecting both their local environment, and the climate as a whole. Low cloud feedbacks are responsible for much of the uncertainty in estimates of climate sensitivity (Bony et al., 2004; Bony & Dufresne, 2005; Medeiros et al., 2008; Vial et al., 2013; Boucher et al., 2013b; Medeiros et al., 2015). One intensely studied aspect of shallow cumuli is how they are affected by changes in atmospheric aerosol, which facilitate the formation of cloud droplets by acting as cloud condensation nuclei (CCN) (Köhler, 1936). While certain aerosol effects on clouds are well understood, many questions, on scales varying from microphysical to entire cloud fields, remain open.

Higher concentrations of CCN lead to a greater number of smaller droplets, for a given liquid water content (Twomey, 1977). The greater droplet surface area increases scattered shortwave radiation, and thus cloud albedo. Smaller droplets due to increased aerosol may inhibit precipitation (Albrecht, 1989), and lead to longer cloud lifetimes. However, mechanisms have also been proposed for aerosol causing shorter lifetimes due to evaporation and entrainment feedbacks (Small et al., 2009).

Stevens and Feingold (2009) discuss 'buffering' effects in the response of clouds to aerosol perturbations, where systems respond to offset the effect of the perturbation. For example, increased aerosol may suppress precipitation, allowing more moisture to be lifted to the cloud top, enhancing evaporative cooling and destabilising the cloud layer, causing clouds to deepen and produce more precipitation. Convective invigoration and deepening due to aerosol are supported by both observations and modelling (Albrecht, 1993; Yuan et al., 2011; Koren et al., 2014; Sheffield et al., 2015; Dagan et al., 2016; Kaufman et al., 2005), however some find suppression of convection (Jiang & Feingold, 2005; Xue et al.,

2008). van den Heever et al. (2011) find that deeper cumulus modes, such as congestus, may be invigorated while the shallowest clouds are suppressed. Dagan et al. (2017) and Altaratz et al. (2014) suggest invigoration or suppression may depend on the magnitude of the aerosol perturbation, as well as local conditions. Seifert et al. (2015) discuss the deepening response of trade wind cumuli to aerosol perturbations as a transient effect, altering the thermodynamic environment, and eventually leading to a similar quasi-equilibrium cloud field. This quasi-equilibrium is considered as a regime of subsiding radiative-convective equilibrium (RCE), where prescribed large-scale forcings alter the state compared to traditional RCE. However, Dagan et al. (2018a) find that typical cloud field lifetimes are much less than the time required to reach equilibrium, suggesting that such quasi-equilibrium behaviour is unrealistic.

Much modelling work on shallow cumuli has used large eddy simulations (LES), typically with small domains on the order of tens of km, periodic lateral boundaries, and constant prescribed tendencies of winds, moisture, and thermodynamics. An alternative approach may be employed, whereby a global driving model supplies the forcing for a nested high resolution domain (Klocke et al., 2017; Miltenberger et al., 2018b; Spill et al., 2019). Spill et al. (2019) find a similar form of cloud response to aerosol perturbations, however the convective deepening does not impact the thermodynamic state of the domain significantly, and no equilibrium cloud field is produced, in contrast to findings such as those of Seifert et al. (2015).

Here we build on Spill et al. (2019) by directly comparing this approach with one that is more idealised, similar to LES, using different configurations of the Met Office Unified Model (UM) to account for model uncertainty. We investigate the approaches' representation of the cloud field, and their response to aerosol perturbations, on large scales.

3.2 Methods

Our simulations are based on the Rain in Cumulus over the Ocean (Rauber et al., 2007) (RICO) campaign. RICO has long been a popular choice for studying shallow convection due to the prevalence of trade wind cumuli in the region, and the availability of data for model initialisation and evaluation. Our case is initialised for 00:00UTC 19 January 2005, following Abel and Shipway (2007), with domains centred on 17.5°N, 57°W. All simulations are run for 96h, including a 12h spin-up.

Several configurations of the Met Office Unified Model are applied, with large domains of ~500km × ~500km, a horizontal resolution of ~500m × ~500m, and a stretched vertical coordinate system with 70 levels below 40km, and 30 levels below 3km. The UM uses a 3D Smagorinsky-type turbulence scheme (Boutle et al., 2014), and no convection scheme is enabled. The 'realistic' setup uses a nested domain with open lateral boundaries, with boundary conditions supplied hourly by an external global driving configuration of the UM (vn11.1, GA6.1), run from ERA Interim (Dee et al., 2011) initial conditions. The 'idealised' setup has periodic lateral boundaries, and constant large-scale tendencies of temperature and moisture are applied, as in most LES studies. Domain mean profiles of temperature, moisture, and winds from the realistic simulations are used to initialise the idealised simulations. Constant surface sensible and latent heat fluxes of 10.58 W m^{-2} and 93.17 W m^{-2} are prescribed, based on mean values of the time-varying fluxes in the realistic simulations. Horizontal advection of moisture, and large-scale subsidence are applied below 10km following Abel and Shipway (2007), along with a cooling rate, a significant component of which is to account for radiative cooling (vanZanten et al., 2011). Idealised simulations are therefore performed both with and without a radiation scheme, to provide an extra point of comparison between idealised and realistic configurations. However,

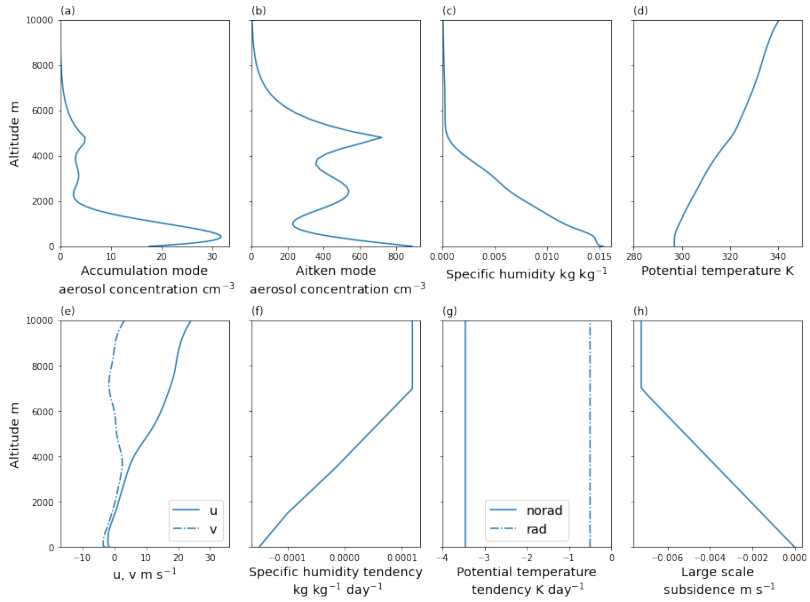

Figure 3.1: Profiles of prescribed aerosol and idealised initial conditions and tendencies: (a,b) baseline accumulation and Aitken mode aerosol concentrations, (c, d, e) initial specific humidity, temperature, and winds (f, g) tendencies of specific humidity and temperature (for idealised simulations with and without radiation schemes), (h) applied large-scale subsidence.

the scheme does not have a diurnal cycle, differing from the realistic simulations. Following Seifert et al. (2015), an advective cooling rate is applied in simulations including a radiation scheme. Profiles of idealised initial conditions and applied tendencies are shown in Figure 3.1.

Small domain idealised simulations are also performed, to more closely relate this comparison to existing LES studies. These have a domain of ~50km × ~50km, a horizontal resolution of ~100m × ~100m, and include the radiation scheme. At this higher spatial resolution it is likely that more convection and turbulence will be resolved, which may affect the response to aerosol perturbations due to improved resolution of updraughts and entrainment.

We use the double-moment microphysics scheme CASIM (Shipway & Hill, 2012; Grosvenor et al., 2017; Miltenberger et al., 2018b), with a droplet activa-

Simulation	Domain size		Horizontal resolution		Lateral boundaries		Radiation scheme	Aerosol	
	~500km ×~500km	~50km ×~50km	~500m ×~500m	~100m ×~100m	Open	Periodic		Baseline	Perturbed (×10)
nested	Y		Y		Y		Y	Y	
nested_x10	Y		Y		Y		Y		Y
id_500km_norad	Y		Y			Y		Y	
id_500km_norad_x10	Y		Y			Y			Y
id_500km_rad	Y		Y			Y	Y	Y	
id_500km_rad_x10	Y		Y			Y	Y		Y
id_50km_rad		Y		Y		Y	Y	Y	
id_50km_rad_x10		Y		Y		Y	Y		Y

Table 3.1: Summary of simulation names and configurations.

tion scheme from Shipway (2015). The configuration of CASIM has a one-way coupling between cloud and aerosol, in which aerosol fields affect droplet activation and may be advected, but are not affected by cloud microphysical processes. Aerosol profiles based on measurements during RICO, as described in Spill et al. (2019) and shown in Figure 3.1, are used for initial and lateral boundary conditions. Simulations are run with baseline aerosol profiles, and profiles perturbed by a factor of 10. The simulation names, along with key aspects of their configurations, are summarised in table 1.

3.3 Results

Satellite snapshots from the days of the simulations (Figure 3.2) show a great deal of structure and variability in the cloud field on large scales, including large features, even in this region that typifies trade wind cumuli. Comparing these with snapshots of the cloud fields from the realistic and idealised simulations in

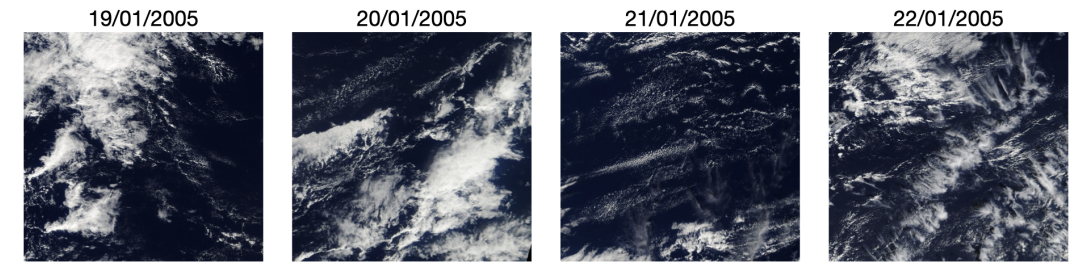

Figure 3.2: Satellite snapshots (Terra, MODIS, Corrected Reflectance, True Color, Bands 1-4-3) for the simulation days, showing the same domain as the nested simulations, from NASA Worldview Snapshots (https://worldview.earthdata.nasa.gov/).

Figure 3.3, the large domain idealised simulations (Figures 3.3c-3.3f) produce a much more uniform cloud field than the realistic case (Figures 3.3a and 3.3b) and the satellite snapshots. While a relatively uniform cloud field may be expected over scales of tens of km, such uniformity over hundreds of km as seen in the large idealised domain is unlikely to be representative of the real atmosphere. The small domain simulations (Figures 3.3g and 3.3h) exhibit uniformity in some scenes, and more varied cloud fields in others. However, their smaller size makes this a more limited representation of the varied cloud fields. The idealised cloud fields appear to develop more structure later in the simulations, also shown by Seifert et al. (2015), though still to a lesser extent than the realistic simulations. The cloud fraction in the satellite snapshots is also relatively large; a characteristic shared by the realistic simulations which tend to have a larger cloud fraction than the large domain idealised simulations.

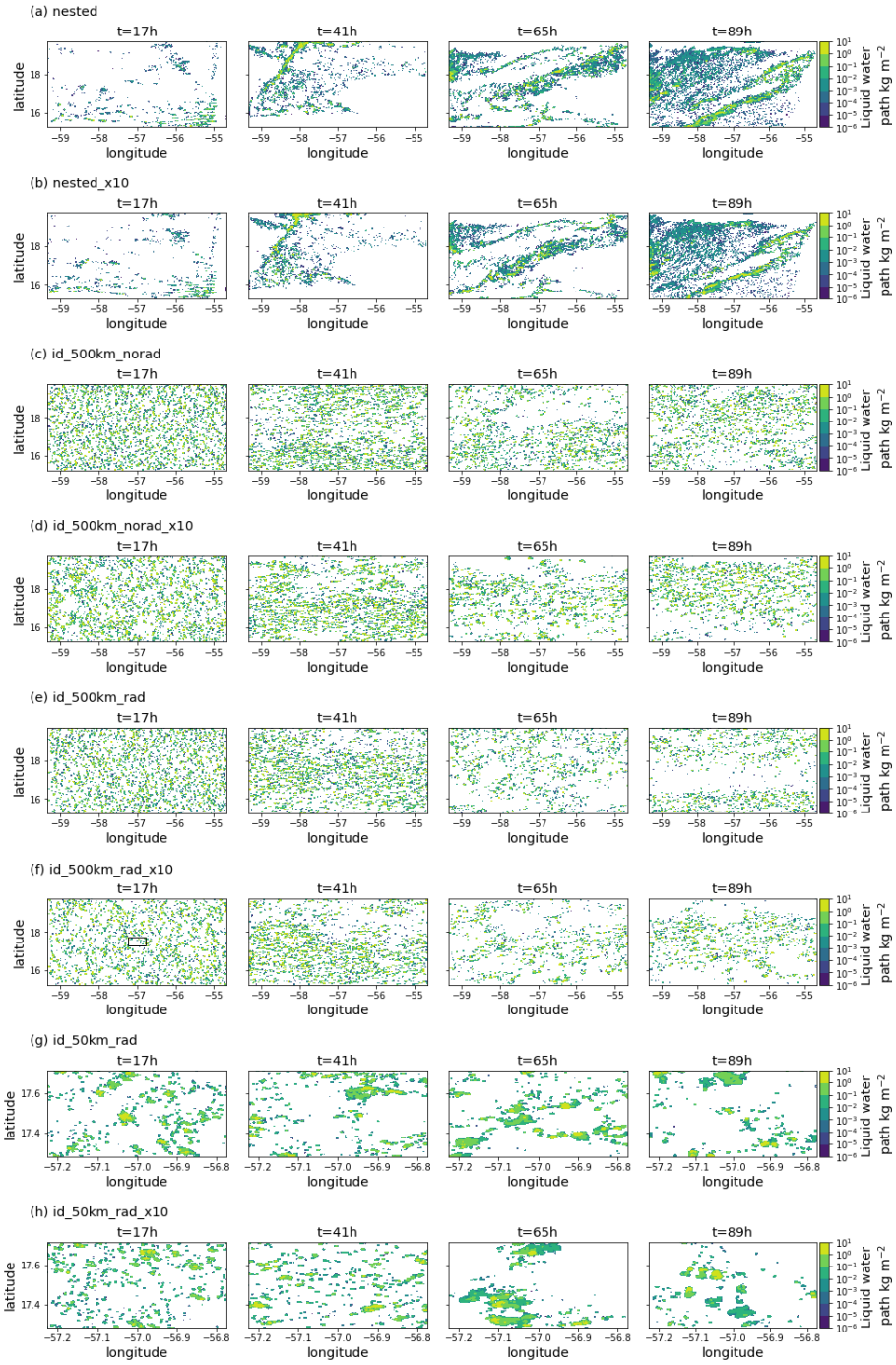

Figure 3.3: Snapshots of liquid water path at several times during each simulation: (a), (b) nested simulations, (c), (d) idealised simulations with no radiation scheme, (e), (f) with radiation, and (g), (h) small domain idealised simulations. Note that (g), (h) use a different spatial scale due to the smaller domain size of ~50km × ~50km, outlined in the first panel of (f).

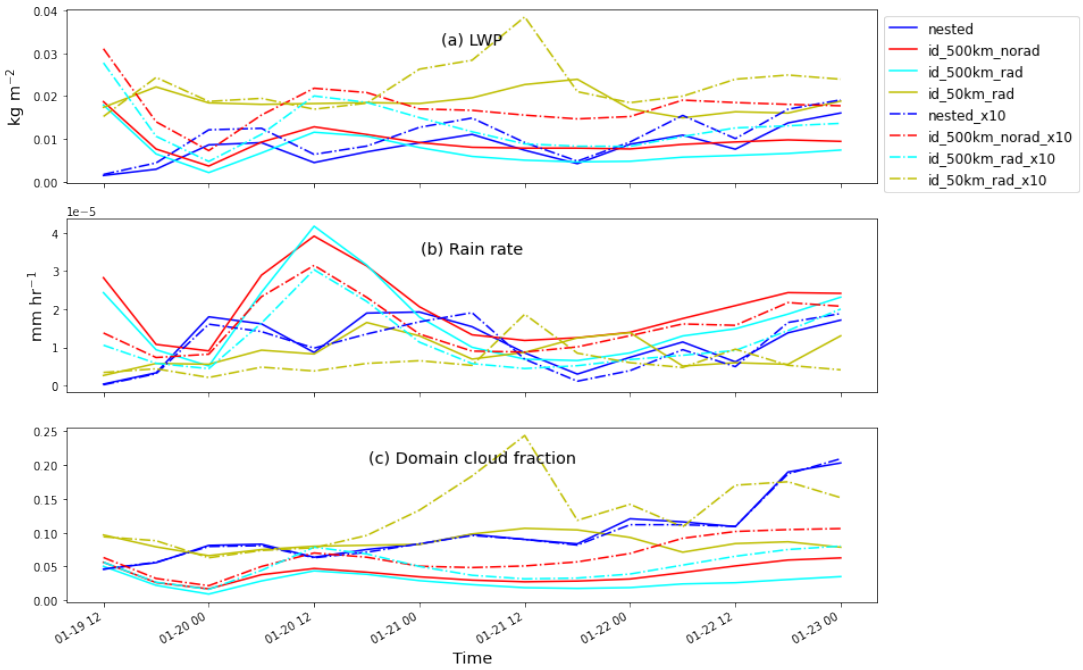

Figure 3.4: Timeseries of 6-hourly domain mean (a) liquid water path, (b) rain rate, (c) cloud fraction, for each simulation, starting after an initial 12h spin-up.

The simulations differ in their domain mean properties, and in these properties' response to the aerosol perturbations (Figure 3.4). Liquid water path increases with aerosol in all of the large domain simulations, particularly id_500km_norad_x10, while id_50km_rad_x10 shows an increase beginning in the second day. Precipitation is reduced with increased aerosol in the large domain idealised simulations, and through much of the first half of id_50km_rad_x10. This effect is smaller in the realistic simulations.

Notably, the cloud fraction in the realistic simulations is completely agnostic to the aerosol perturbation, while each idealised setup shows an increase in cloud fraction with increased aerosol (Figure 3.4c).

Vertical profiles of cloud fraction, domain mean and in-cloud liquid water, and updraught speeds show clearly the simulations' differing structure and response to aerosol (Figure 3.5). The in-cloud profiles are, at their highest and lowest altitudes, dominated by relatively few instances in the simulations, but

nonetheless provide insight into the in-cloud response. In the realistic simulations, these are a result of a number of large-scale, deeper, features. Applying a rolling filter, with a cloud-fraction threshold of 0.2, allows us to consider only a subset of smaller clouds, comparable to the idealised cloud fields. Under this approach, a moving average of cloud-fraction is calculated at each grid cell using a 50km window, and the cloud-fraction threshold is then applied. An alternative filter is applied to exclude clouds in the realistic simulations whose top heights exceed the maximum in the idealised simulations.

The idealised setups have larger mean in-cloud liquid water content (LWC) and updraught speeds, and display significant convective deepening and invigoration in response to increased aerosol, apparent in both domain mean and in-cloud profiles of LWC. While this effect is present in the realistic setup, it is muted in comparison. Applying the cloud-fraction threshold to the realistic simulations produces in-cloud profiles with a form similar to those in the idealised simulations, with more significant deepening than the unfiltered profile, though still less than the idealised simulations in the domain-mean. The cloud top height filter does little to affect the form of the profile, though produces slightly larger updraught speeds than the unfiltered profile.

Histograms of cloud top height (Figures 3.5e-3.5h) further highlight the differences in the cloud populations produced, and the response to increased aerosol. The occurrence of lower cloud top heights is suppressed in all perturbed simulations, though to a greater extent in nested_x10. All simulations also show an increase in the number of higher cloud top heights.

Figure 3.6 shows the evolution of temperature and humidity profiles in each simulation. The stark contrast between the realistic and idealised setups, and their responses to the aerosol perturbation, is evident. The perturbed idealised simulations have increased cooling towards the top of and above the cloud layer, and increases in moisture at the top of the cloud layer. This is what one might

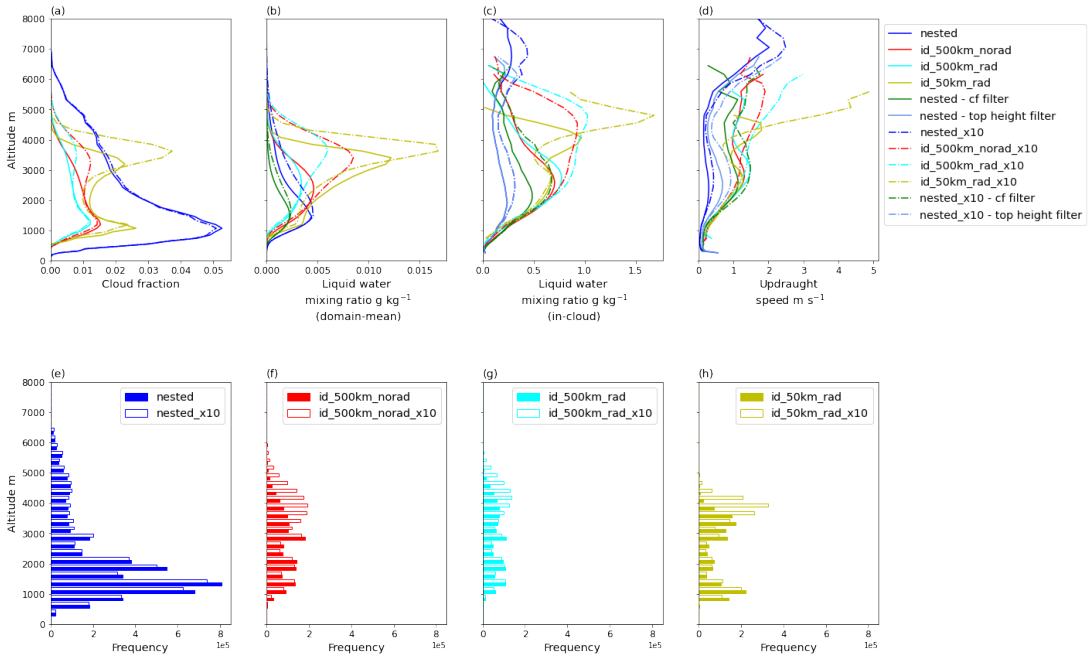

Figure 3.5: Vertical profiles of (a) cloud fraction, (b) domain mean cloud liquid water mixing ratio, (c) in-cloud mean liquid water mixing ratio, (d) updraught speed, and (e)-(h) histograms of cloud top height. A liquid water mixing ratio threshold of 0.01 g kg^{-1} is used to define a cloudy grid box. A rolling cloud fraction filter of 0.2, and a filter excluding clouds with top heights greater than maximum in the idealised simulations, are applied to the nested simulations, to produce additional profiles in (b)-(d), labelled with the suffixes '- cf filter' and '- top height filter'.

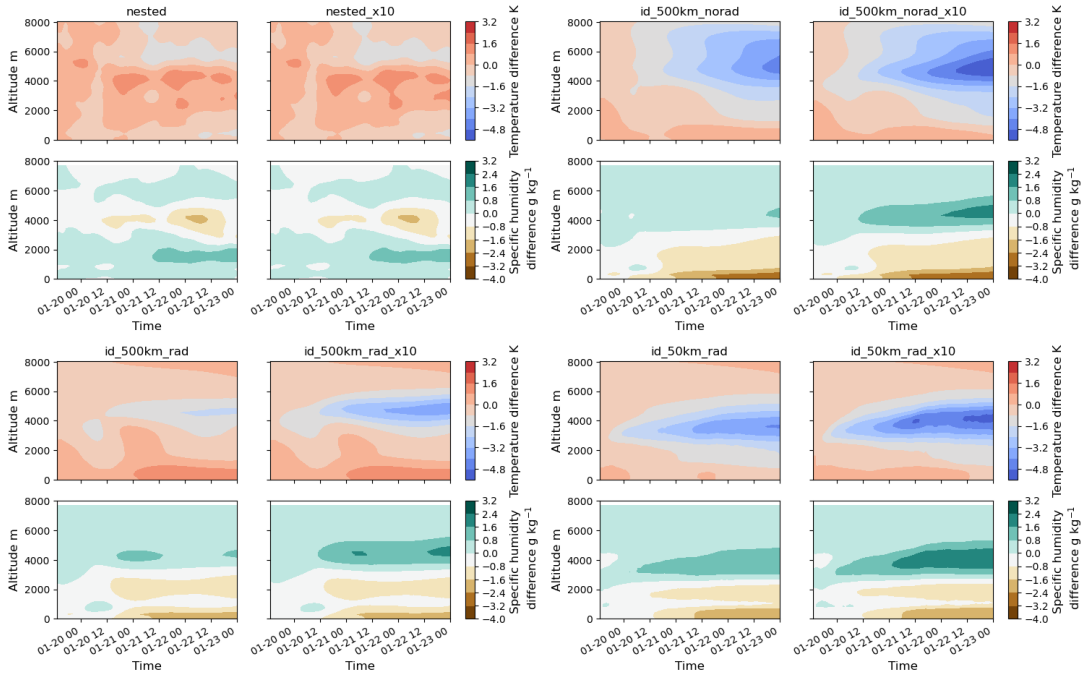

Figure 3.6: Hovmöller plots showing the temporal evolution of profiles of domain mean temperature and specific humidity. These show the difference between the mean temperature or specific humidity at each time in the simulation and the first time point after the 12h spin-up. The nested and nested_x10 simulations are in the top left quadrant, id_500km_norad and id_500km_norad_x10 in the top right, id_500km_rad and id_500km_rad_x10 in the bottom left, and id_50km_rad and id_50km_rad_x10 in the bottom right.

expect to see from buffering effects; with greater cooling allowing the deepening of the cloud layer, and more moisture being lofted higher in the atmosphere (Albrecht, 1993; Seifert et al., 2015; Dagan et al., 2016). The realistic simulations, however, show almost no thermodynamic response to the aerosol perturbation, consistent with the muted deepening and invigoration response.

3.4 Discussion

We have presented simulations of trade wind cumuli using different configurations of the Unified Model, highlighting the differences between idealised simulations, with fixed forcing and periodic boundaries, and more realistic simulations with open boundaries and varying large sale forcing. These configurations are chosen to eliminate as much model uncertainty as possible, and focus on examining the difference in aerosol-cloud interactions between the periodic domains with fixed forcing, and nested domains with varying forcing.

Snapshots of liquid water path show that the idealised and realistic simulations produce dramatically different cloud fields over large scales. The realistic simulations produce cloud fields with more evident structure, while the idealised simulations produce notably more uniform cloud fields. Domain mean liquid water path, precipitation, and cloud fraction further highlight the differences between the response to aerosol perturbations. The realistic simulations show no change in cloud fraction in response to increased aerosol, in contrast to the increase in the idealised simulations.

Vertical profiles of cloud liquid water indicate that the idealised simulations experience significantly more convective deepening with increased aerosol. While realistic and idealised may produce clouds with similar structures, the response to the aerosol perturbation of those in the realistic simulations is much weaker.

The thermodynamic evolution of the domain is driven by the applied large-scale forcing, and processes including interactions between the clouds and their environment, which are closely coupled to the cloud vertical structure. In the idealised simulations, increased aerosol leads to marked changes in the thermodynamic evolution, as would be expected from the buffering mechanism discussed by Stevens and Feingold (2009). No significant changes are seen in the thermodynamic evolution of the realistic simulations. This suggests that the ther-

modynamic environment is determined predominately by the varying large-scale forcing, which, along with the open boundaries, does not allow the cloud field to exert such a strong effect. However, it should be noted that the large-scale forcing and boundary conditions supplied by the driving model are not affected by the aerosol perturbation. Aerosol effects are thus only realised inside the nested domain, while in the real atmosphere this may not be the case. Nonetheless, observational studies have reached similar conclusions regarding the significance of transient large-scale forcing in determining the state of the cloud field. Dagan et al. (2018a) show that cloud field properties and environmental conditions vary significantly over periods shorter than those required to reach an idealised equilibrium state.

Limited area idealised models are undoubtedly useful in studying atmospheric processes. However, our findings suggest that their ability to represent the transient behaviour of the real atmosphere may be limited in comparison to more realistic approaches.

Aerosol perturbations may have a number of effects on cumulus cloud fields, including minor convective deepening and invigoration, and increases in liquid water path. However, due to the importance of the large-scale forcing, these are limited, perhaps explaining the unchanged cloud fraction.

Understanding the role of shallow clouds in the atmosphere is of critical importance, and with ever improving capabilities and methods, so too is understanding the differences, shortcomings, and advantages of modelling approaches.

Chapter 4

Aerosol-cloud interactions in a trade wind cloud field: differing responses of different cloud types

This chapter is based on a manuscript in preparation for submission to a peer-reviewed journal as:

Spill, G., Stier, P., Field, P. R., and Dagan, G. Aerosol-cloud interactions in a trade wind cloud field: differing responses of different cloud types.

I designed the study together with the co-authors. I carried out the simulations, which are extensions of those described in Chapter 2, with input from the co-authors. I designed the analysis, and wrote the manuscript, with input from the co-authors.

Abstract

The effects of aerosol on trade wind clouds remain poorly understood. Here we apply a cloud tracking algorithm to analyse large-domain, high resolution simulations based on a RICO case study, performed with the Met Office Unified

Model. Using this approach, we are able to explore aerosol effects on clouds with different characteristics. Tracked clouds are classified according to depth, updraught speed, and size. We find that increasing aerosol leads to a reduction in the number of the shallowest clouds, which dominate the cloud field, and an increase in the occurrence of higher liquid water paths. For shallow cumuli, cloud depths are relatively unaffected by increasing aerosol, whereas cumuli congestus become deeper, with higher cloud top heights. Though the onset of precipitation is delayed for all types of cloud with increased aerosol, shallow cumuli with stronger updraughts and cumuli congestus remain likely to produce precipitation during their lifetime. In contrast, shallow cumuli with weak updraughts are far less likely to produce precipitation under increased aerosol. This analysis highlights the differing responses to aerosol that may be found in trade wind cloud fields, that are often composed of clouds with a range of characteristics.

4.1 Introduction

Clouds are a central feature of the atmosphere, influencing both water budgets and energy balance, and yet are a significant source of uncertainty in our understanding of the climate system. This is particularly true of the shallow cumulus clouds that are ubiquitous in trade wind regions of the oceans. The myriad scales over which cloud processes occur lead to rich behaviours that challenge both observational and modelling approaches to their study.

The trade wind region of the Atlantic has long been a focal point for the study of shallow convective clouds, due to the pristine environment and prevalence of shallow cumuli. A number of studies have, however, noted the multi-modal nature of tropical and trade wind convection (Johnson et al., 1999; Hohenegger & Stevens, 2013; van den Heever et al., 2011; Li et al., 2013; Sheffield et al., 2015; Saleeby et al., 2015). Johnson et al. (1999) describes the abundance of cumuli

congestus, in addition to shallow cumuli and cumulonimbus, in the Tropical Ocean Global Atmosphere Coupled Ocean–Atmosphere Response Experiment (Webster & Lukas, 1992). Nuijens et al. (2014) and Vial et al. (2019), too, both discuss the diversity present in trade wind cloud fields.

Aerosol particles play an important role as cloud condensation nuclei (CCN), facilitating the formation of cloud droplets, and affecting the microphysical processes via which cloud hydrometeors interact with one another and their environment. For a given liquid water content in an aerosol-limited cloud, an increase in aerosol acting as CCN will lead to a larger number of smaller droplets (Twomey, 1977), which also results in an increase in cloud albedo due to enhanced reflection of shortwave radiation. Smaller droplets may also inhibit the formation of precipitation, which Albrecht (1989) argued could lead to increased cloud lifetime. In contrast, it has also been suggested that enhanced evaporation of smaller droplets may reduce cloud lifetimes (Small et al., 2009).

Reductions in precipitation resulting from increased aerosol have been frequently reported by modelling studies (Jiang et al., 2006; Xue et al., 2008; van den Heever et al., 2011; Saleeby et al., 2015). Increases in peak precipitation rates have, however, also been found (Saleeby et al., 2015; Seifert et al., 2015). Increases in aerosol, and delayed onset of precipitation, may lead to convective invigoration and deepening (Albrecht, 1993; Koren et al., 2014; Dagan & Chemke, 2016), with deeper warm clouds able to produce stronger precipitation rates. Enhanced condensational latent heating due to the greater number of droplets can lead to stronger vertical development (Lebo & Seinfeld, 2011; Koren et al., 2014). Stevens and Feingold (2009) argue that a delay in the onset of precipitation can allow more moisture to be transported to the cloud top, where increased evaporation destabilises and supports the deepening of the cloud layer.

van den Heever et al. (2011) find that clouds in the different modes of tropical convection may respond quite differently to aerosol perturbations. They find

that liquid water path and precipitation contributions from shallower clouds are reduced with increased aerosol, while a mixed and opposite responses are found for intermediate and deeper clouds. Despite significant responses of the different modes, changes in domain-mean precipitation and cloud fraction are weak. Similarly, Saleeby et al. (2015) find that increased aerosol leads to fewer shallow cumuli and erosion of precipitating stratiform clouds, alongside the enhanced development of deeper, more heavily-precipitating, cumuli.

Despite extensive research exploring the effects of aerosols on shallow clouds, the majority of studies have focused on exploring the mean characteristics of cloud populations. While this approach undoubtedly allows a great deal of insight into aerosol-cloud interactions, several critical aspects are difficult to study in this way. Most particularly is exploring how cloud lifetime is affected. Stevens and Feingold (2009) note that investigation of the lifetime effect has led to many distinct hypotheses that often have little to do with cloud lifetime as such. The effects of aerosol on cloud lifetimes are often considered alongside changes in cloud liquid water and cloudiness, with increases in liquid water and cloudiness associated with longer lifetimes, and vice versa (Albrecht, 1989; Small et al., 2009). Cloud lifetimes may be directly quantified, however, through the use of tracking algorithms. An additional component of cloud responses to aerosol that is difficult to explore with a domain- or population-mean approach is how clouds with different characteristics are affected. It is possible to attribute, for example, changes in vertical profiles of liquid water to low-level or higher-level clouds, however this approach does not capture the life-cycle of these clouds. Cloud-tracking algorithms allow individual clouds to be identified and tracked over their lifetime, capturing their characteristics throughout their evolution. Recently, increasing computational capabilities have facilitated the use of such algorithms for larger populations of clouds. Cloud tracking has been used in a number of studies (Heus & Seifert, 2013; Seifert et al., 2015; Heiblum et al., 2016;

Heiblum et al., 2019; Sakradzija & Hohenegger, 2017; Igel, 2018) to investigate properties of cloud fields such as cloud lifetimes and morphology, as well as the evolution of processes such as precipitation.

Here, a cloud-tracking algorithm is applied to simulations of trade wind convective clouds, to investigate the response of the cloud population to aerosol perturbations. The simulations are carried out in a large domain, allowing the analysis of the entire cloud field. Furthermore, the simulated domain is nested in an external driving model, supplying time-varying boundary conditions and large-scale forcing.

4.2 Methods

4.2.1 Model setup

The simulation setup presented here is also described in Spill et al. (2021). The Met Office Unified Model (UM) is run in a nested configuration; the simulation domain has open lateral boundaries, nested in a global driving configuration of the UM (vn11.1, GA6.1), which supplies hourly boundary conditions and is initialised from ERA Interim reanalysis (Dee et al., 2011). The simulation domain is ~500km × ~500km, with a horizontal resolution of ~500m × ~500m, and a stretched vertical coordinate system with 70 levels below 40km, 30 of which are below 3km. A 3D Smagorinsky sub-grid turbulence scheme is employed in the UM (Boutle et al., 2014), but no cloud or convection schemes are used in these simulations.

The simulations are performed for a case study based on the Rain In Cumulus over the Ocean (Rauber et al., 2007) (RICO) campaign. The simulations are initialised for 00:00UTC 19 January 2005, and the domain is centred on 17.5°N, 57°W. The simulations are run for 96 hours, including a 12-hour spin-up. How-

ever, due to the high-frequency time output that is required for cloud tracking, the tracking is performed for just 12 hours (11:00-23:00UTC 22 January 2005), during which simulation data is output at a frequency of 1 minute.

A double-moment microphysics scheme, CASIM (Shipway & Hill, 2012; Grosvenor et al., 2017; Miltenberger et al., 2018b), is employed, with a droplet activation scheme following Shipway (2015). A one-way coupling is used such that aerosols affect droplet activation and are advected in the domain, but cloud processes do not modify the aerosol population. Further, aerosols do not interact with radiation via direct aerosol effects. Observations from RICO are used to provide vertical profiles of Aitken and accumulation mode aerosol concentration (Spill et al., 2019) for the baseline simulation, UM_CASIM. These profiles are used to initialise the domain, as well as for lateral boundary conditions. The aerosol profiles are increased by a factor of 10 for the perturbed simulation, UM_CASIM_x10.

4.2.2 Tracking

We employ the tobac (Tracking and Object-Based Analysis of Clouds) framework (Heikenfeld et al., 2019). In this framework, clouds are initially detected by applying a threshold to a 2D field, and individually labelling contiguous regions where this threshold is exceeded. Heikenfeld et al. (2019) apply an updraught speed threshold to identify the deep convective clouds that are their subject of interest. For trade wind cloud fields, however, we are also interested in clouds with weak updraughts, or that may be decaying, making updraught speed less appropriate for identifying the features of interest. Here, then, we apply a liquid water path (LWP) threshold of $20\,\mathrm{g\,m^{-2}}$ to detect a cloud, following Jiang et al. (2010). Following this detection, 3D cloud volumes are determined using a segmentation approach. 3D watershedding is applied surrounding columns that meet the 2D LWP threshold to label voxels that exceed a liquid water content

threshold of $0.01\,\mathrm{g\,kg^{-1}}$.

In order to produce cloud tracks, features in successive frames must be linked and associated with one another. Tobac achieves this by projecting a new position based on the velocity for previous frames, producing a search area around this new position, and comparing the similarity of candidate features. Tobac offers a number of options to define and restrict this area; here a maximum radius of 1500 m is specified.

Tobac thus provides features identified in each frame of the simulation, and these features are then labelled according to the track to which they belong. This allows clouds to be analysed both over their tracked life-cycle, and as a snapshot of the cloud at a given point in time.

This tracking approach has a number of limitations that are important to note. Perhaps most significantly, it is not able to account for splitting and merging of clouds, which may occur often (Heiblum et al., 2016). After such events occur, only one track is continued from before the event, and either a new track is started, in the case of a split, or one is ended, in the case of a merge. This is important when considering the analysis of cloud lifetimes, as well as the timing of processes relative to cloud lifetime. For splitting events, the new track will not retain the history of the initial cloud, and it will begin with a cloud that may already be developed. For merging events, however, one of the initial tracks will end prematurely. In either case, it will not be possible to track the entire life cycle of all clouds involved. Another limitation lies in the feature detection being performed in 2D, which does not allow clouds in multiple layers in a column to be identified. It is also worth noting that thresholds applied to perform tracking are somewhat arbitrary. While some consensus exists in the literature, which can aid making comparisons, there are often differences in both the methods, fields, and the threshold values used to identify clouds that should be borne in mind

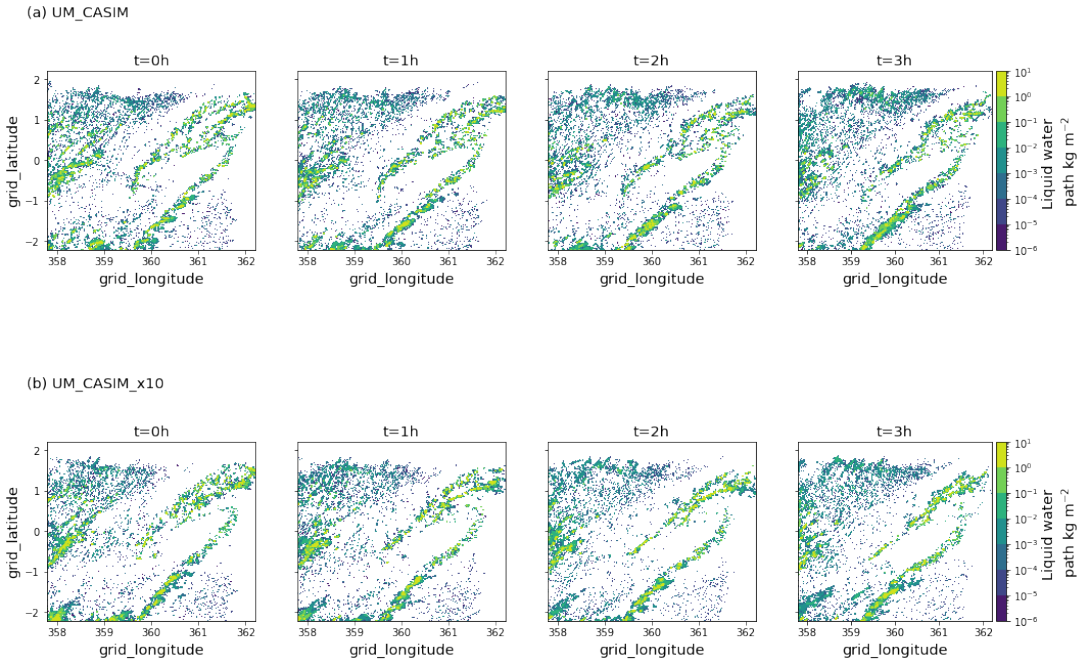

Figure 4.1: Snapshots of liquid water path at different times in each simulation: (a) UM_CASIM, (b) UM_CASIM_x10.

(Jiang et al., 2010; Heus & Seifert, 2013; Heiblum et al., 2016; Heikenfeld et al., 2019).

4.3 Results

Figure 4.1 shows snapshots of LWP at a number of times in each simulation, and gives an impression of the spatial structure of the cloud field. The spatial variability is clear, with large-scale patterns evident across the domain in both simulations. Also clear is the diversity in the clouds present, which Spill et al. (2021) note is a characteristic point of difference between realistic and idealised simulations of trade wind cloud fields.

Some illustrative examples of tracked clouds are shown in figure 4.2. Figure 4.2 (a) shows 5000 tracks from the UM_CASIM simulation, while 4.2 (b) shows the features identified in a single frame. The variation in the tracks across the

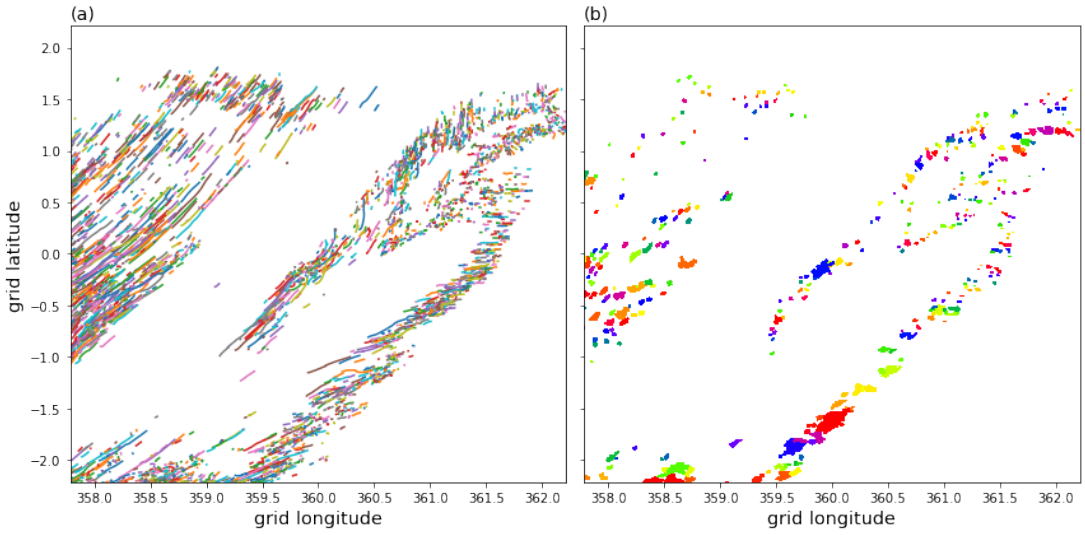

Figure 4.2: Illustrative examples of tracks and tracked clouds in the UM_CASIM simulation. (a) shows 5000 tracks from the UM_CASIM simulation. (b) shows examples of identified features in a single frame. Colours are arbitrary.

domain (figure 4.2 (a)) is indicative of the influence and spacing variability of the large-scale forcing. Comparing figure 4.2 (b) and figure 4.1, it is clear that the tracking algorithm does not identify all potential cloud features, due to the applied thresholds discussed in the previous section. Nevertheless, the algorithm does detect features that appear to have a range of different sizes and morphologies. In the UM_CASIM simulation, a total of 322,365 individual features are identified across all frames, with these features corresponding to 26,911 tracked clouds. The UM_CASIM_x10 simulation has 269,539 features, with 24,422 tracks.

Histograms in figure 4.3 show the statistics of a number of cloud properties. Cloud lifetime is defined as the duration for which a cloud is identified and tracked, and is dominated by short-lived clouds. Similarly, examining the baseline simulation, UM_CASIM, shows that low liquid water paths and small-area clouds are also the most common. Cloud tops between around 1.5km and 3km are the most frequently occurring, but a significant number have higher top heights reaching to around 6km in UM_CASIM. Figure 4.3 shows that clouds in

the perturbed and unperturbed simulations are largely quite similar. However, there are several noteworthy differences. While for both simulations the cloud population is dominated by low-LWP clouds, UM_CASIM_x10 shows a relative increase in the number of high-LWP clouds (figure 4.3 (b)). Additionally, there are increases in the number of clouds with greater top heights (figure 4.3 (d)), and greater depths (figure 4.3 (e)). It is also interesting to note that there is also an increase in the number of clouds with higher base heights in the perturbed simulation (figure 4.3 (f)), which may be remnants of deeper clouds. Figure 4.3 (a) shows that many tracked clouds have lifetimes that are much longer than might typically be expected for shallow cumuli. As the tracking and feature identification is performed using liquid water, some of these longer-lived tracks may be following the entire cloud life-cycle, during which they are not likely to be continuously convectively active. Merging clouds may also contribute to the tail of longer lifetimes. It is also likely due in part to the presence of other types of cloud in the domain, including deeper cumuli and larger stratiform clouds. Evidence of these stratiform clouds is also clear in figure 4.3, which shows that large-area clouds are not uncommon, despite smaller clouds dominating by number. It is particularly interesting to note that figure 4.3 (a) shows very little change in cloud lifetimes with increased aerosol.

Figure 4.4 shows some of the precipitation characteristics of the cloud population. We focus our analysis of precipitation on cloud-base precipitation rate, in order to more closely follow the changes to the tracked clouds, by reducing the influence of evaporation of rain below the cloud base on the analysis. Unless otherwise specified, precipitation rate herein refers to that at the cloud-base. Figure 4.4 (a) shows that both the perturbed and unperturbed simulations produce markedly similar precipitation rates, albeit with UM_CASIM_x10 showing a slight decrease in the frequency of intermediate intensity precipitation. In both simulations, weak precipitation rates are by far the most common. Joint

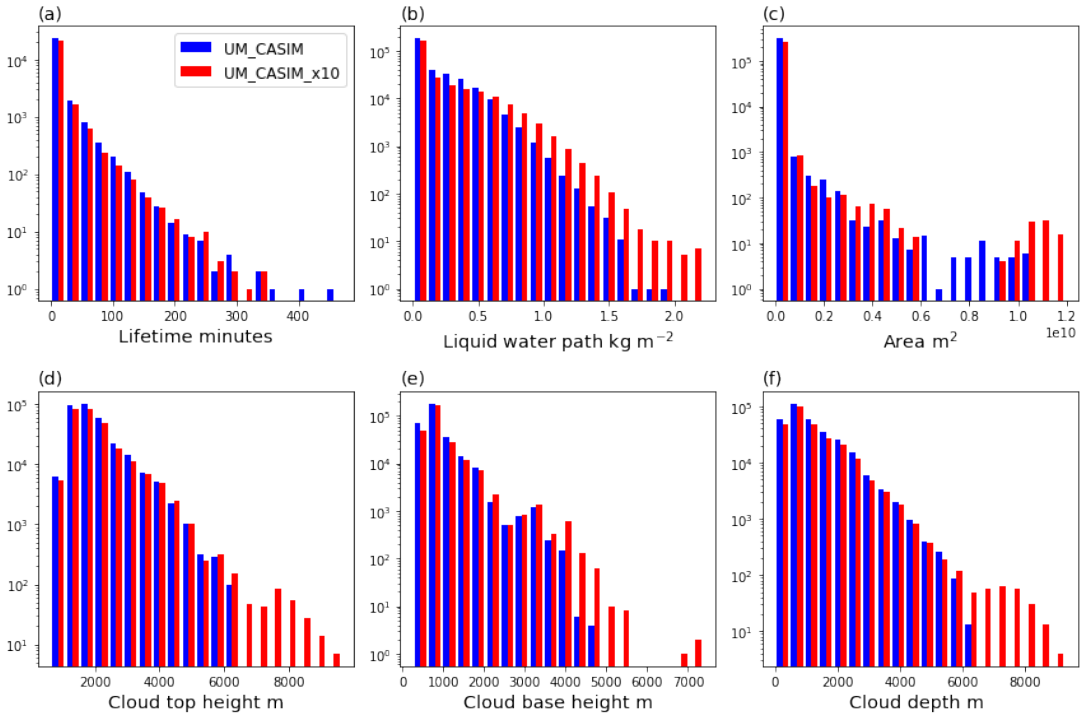

Figure 4.3: Histograms of (a) lifetime, (b) liquid water path, (c) area, (d) cloud top height, (e) cloud base height, and (f) cloud depth.

histograms of precipitation rate and cloud depth show, as expected, that precipitation rates increase with cloud depth in general. However, the deepest clouds in UM_CASIM_x10 do not produce the strongest precipitation.

The most significant difference between the perturbed an unperturbed simulations may be seen in figure 4.4 (d-f). In figure 4.4 (d) histograms are shown of the time of the onset of precipitation. This is the amount of time after a cloud is first tracked before it begins to produce a non-zero precipitation rate. The perturbed simulation has an extremely clear increase in the number of tracks with delayed onset of precipitation. The joint histograms in figure 4.4 (e-f) of onset of precipitation and cloud depth at this time show that this is most clear for shallower clouds. Clouds that are deeper when first detected by the tracking algorithm, however, tend to produce precipitation very early on. Due to the limitations of the tracking algorithm, for instance in treating splitting and merging

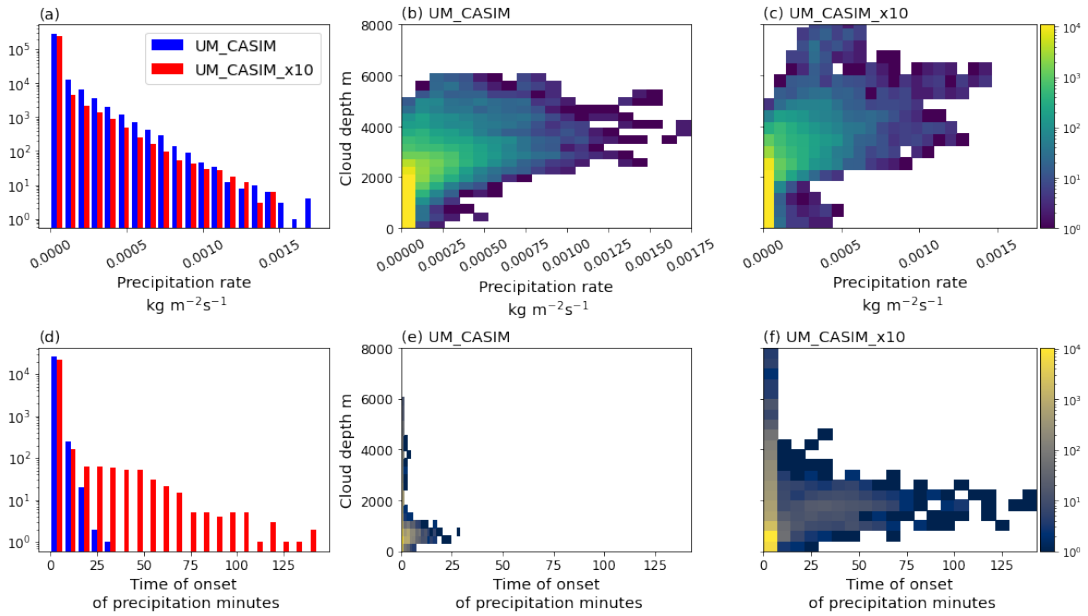

Figure 4.4: (a) Histograms of precipitation rate. (b, c) Joint histograms of precipitation rate and cloud depth for each simulation. (d) Histograms of time along track of the onset of precipitation. (e, f) joint histograms of time of onset of precipitation and cloud depth at the onset of precipitation. Onset of precipitation is defined as the first time at which a tracked cloud has a non-zero cloud-base precipitation rate.

events, some clouds are already quite developed, and may be precipitating, at the beginning of the track. For such cases, it is difficult to determine how onset of precipitation may have been affected by the aerosol perturbation. Given the large number of clouds and tracks, however, the number of these instances is relatively small.

Thus far we have considered the tracked cloud population in its entirety. However, as discussed, trade wind clouds fields are often composed of clouds with quite different characteristics, such as shallow cumuli, cumuli congestus, and stratiform clouds. Furthermore, these clouds may respond differently to aerosol perturbations. It is therefore useful to define a number of clusters, allowing the separate analysis of different cloud types. Given that our main interest is in convective clouds, we define a large-area cluster, cluster 0, to separate larger, stratiform-type clouds. We then define three further clusters: cluster 1 for shallow clouds with weak updraughts, cluster 2 for shallow clouds with stronger updraughts, and cluster 3 for deeper congestus clouds. Shallower convective clouds in clusters 1 and 2 are distinguished by a threshold of $3\,\mathrm{m\,s^{-1}}$ for the maximum updraught speed attained over the cloud's track. We follow a similar approach to Johnson et al. (1999) and Hohenegger and Stevens (2013) for defining congestus clouds. Hohenegger and Stevens (2013) define congestus as having top heights between 4 km and 9 km. However, it is possible for clouds to have varying base heights, and so we instead define congestus using cloud depth. The majority of clouds in the simulations have bases around 500 m, and so the cloud depth threshold applied is 3.5 km. The clusters and thresholds used to define them are summarised below.

- Cluster 0
  - maximum area $> 1 \times 10^9\,\mathrm{m^2}$
- Cluster 1

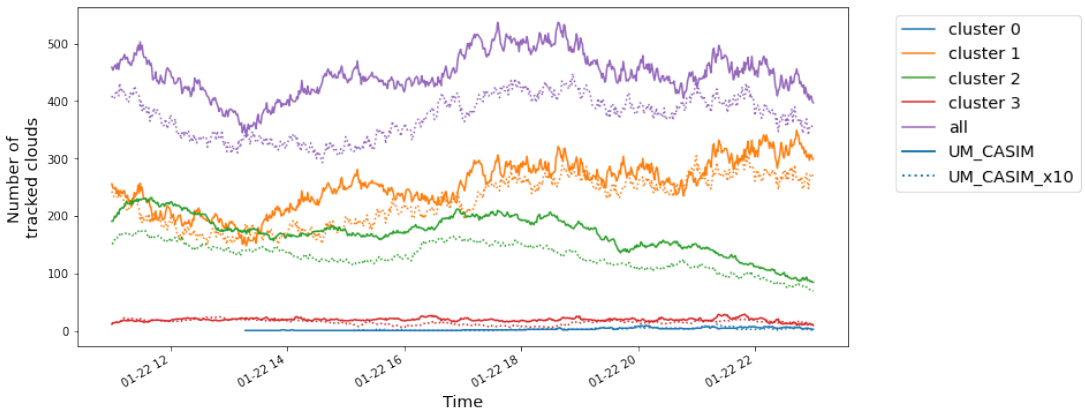

Figure 4.5: Timeseries of the total number of tracked clouds, and the number of tracked clouds in each cluster. Solid lines correspond to UM_CASIM, dotted lines to UM_CASIM_x10.

  - maximum area $< 1 \times 10^9\,\mathrm{m}^2$
  - maximum cloud depth $< 3500\,\mathrm{m}$
  - maximum updraught speed $< 3\,\mathrm{m\,s}^{-1}$

- Cluster 2
  - maximum area $< 1 \times 10^9\,\mathrm{m}^2$
  - maximum cloud depth $< 3500\,\mathrm{m}$
  - maximum updraught speed $> 3\,\mathrm{m\,s}^{-1}$

- Cluster 3
  - maximum area $< 1 \times 10^9\,\mathrm{m}^2$
  - maximum cloud depth $> 3500\,\mathrm{m}$

Figure 4.5 shows timeseries of the total number of tracked clouds, and the number of clouds in each cluster. Of note is the reduction in the number of clouds with increased aerosol. This change appears to be due to reductions in the number of clouds in clusters 1 and 2, the shallow cumuli, which are the

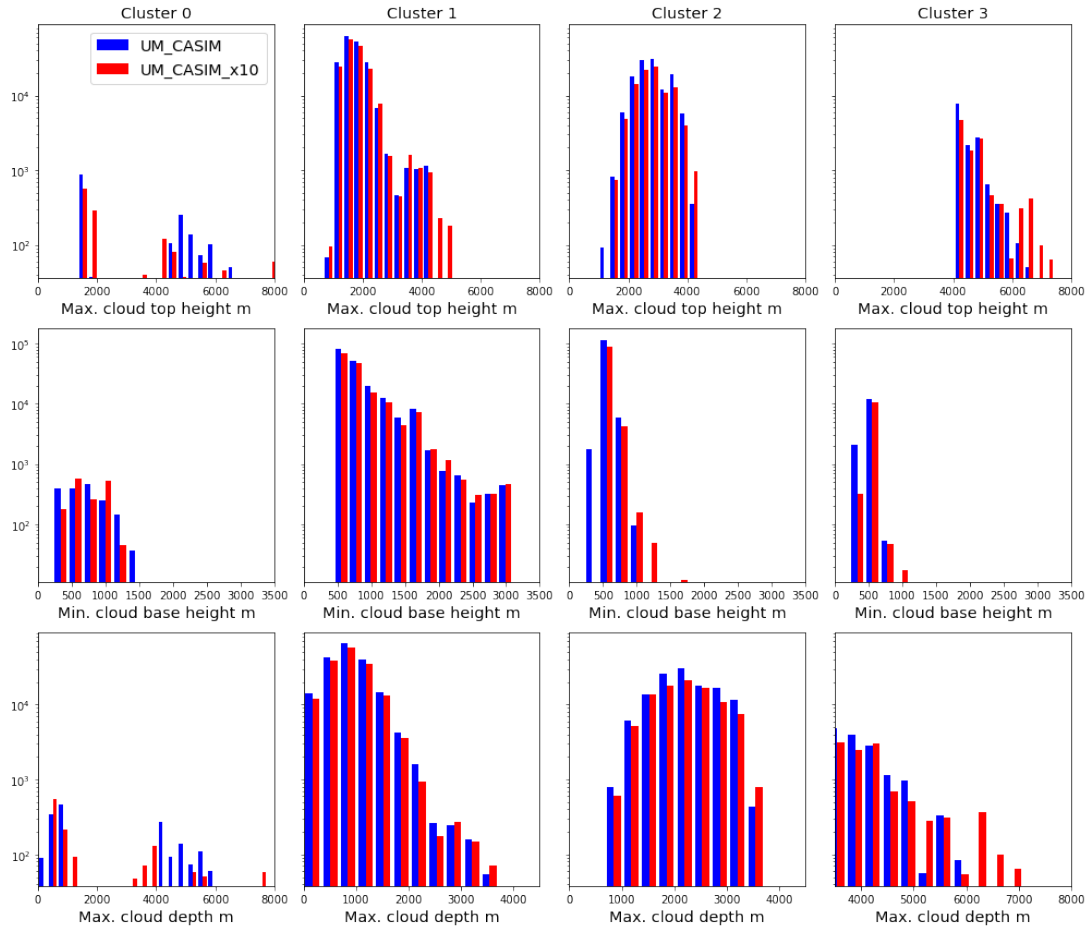

Figure 4.6: Histograms of maximum cloud top height (top row), minimum cloud base height (middle row), and maximum cloud depth (bottom row) for each cluster, arranged by column.

most frequently occurring. Cluster 3, the deeper congestus cluster, and cluster 0, the large-area cluster, account for a very small proportion of the total number of clouds. Further, there is little change in their numbers under the aerosol perturbation, with only a very small absolute decrease discernible for cluster 3.

Figure 4.6 shows details of the maximum top heights, minimum base heights, and maximum depths, for clouds in each of the clusters. There are few differences in the maximum cloud top heights (figure 4.6 top row) in clusters 1 and 2 between the perturbed and unperturbed simulations. For cluster 3, however, there is an increase in the number of clouds reaching greater heights, as well as an increase

in the maximum height reached. This is also reflected in the maximum depths achieved (figure 4.6 bottom row). The stronger-updraught clusters, 2 and 3, have cloud bases that are reasonably well confined to lower heights (figure 4.6 middle row). In contrast, cluster 1 displays cloud bases varying across a wide range. Cluster 0, the large-area cluster, has clouds with both low and high maximum top-heights and depths. In figure 4.7 we also see that high updraught speeds are reached. It is possible, then, that these clouds have not been tracked correctly, potentially due to difficulties in separating contiguous cloudy regions that may be more properly considered separately as congestus and stratiform. Some of these clouds may be congesutus that are embedded in a wider cloud deck. Close inspection of the characteristics of these clouds is indicative of this; with mean characteristics, such as mean precipitation rate, suggesting a stratiform type, and maxima that more closely resemble congestus. These instances are, however, still rare, and should not affect the interpretation of the analysis of the other clusters.

The histograms in figure 4.7 show more details of the clusters' characteristics. Cluster 0 shows the most pronounced dominance of shorter cloud lifetimes (figure 4.7 top row). Longer-lived clouds are more common in clusters 2 and 3, with stronger convection. Little difference in lifetimes can be discerned between the perturbed and unperturbed simulations. Stronger convection in clusters 2 and 3 is also apparent in the maximum updraught speeds (figure 4.7 middle row), with greater speeds reached in the deeper clouds of cluster 3 than in cluster 2. Again, there is relatively little difference between the perturbed and unperturbed simulations for clusters 1, 2, and 3. There is a notable presence of greater updraught speeds reached in cluster 0 in UM_CASIM_x10, however. In the bottom row of figure 4.7, histograms of clouds' nearest neighbour distance give an indication of the cloud field dynamics. Close neighbours are the most common for each cluster, other than cluster 0. Slight increases in the frequency of farther neighbours are

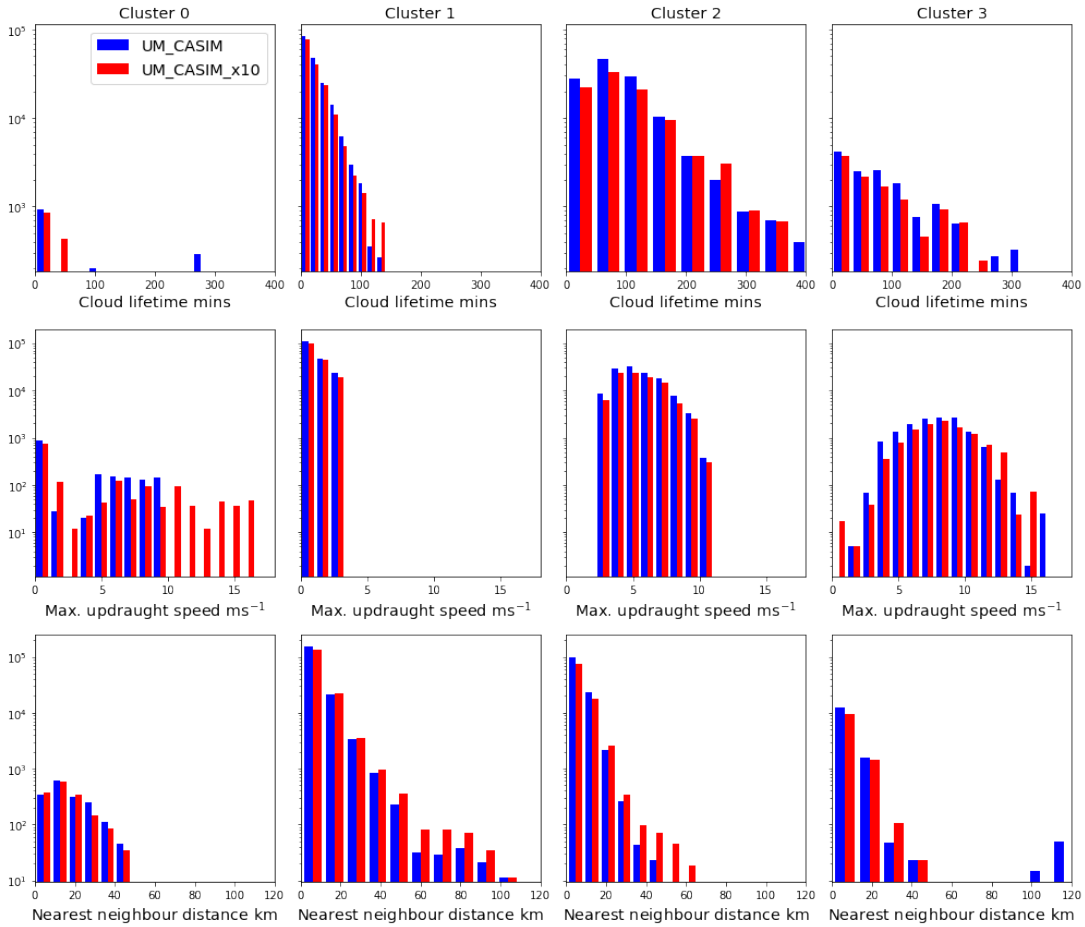

Figure 4.7: Histograms of cloud lifetime (top row), maximum updraught speed (middle row), and nearest neighbour distance (bottom row) for each cluster, arranged by column.

seen with increased aerosol, possibly due to the reduction in the total number of clouds. These are still, however, dominated by clouds with nearby neighbours.

The precipitation characteristics of the clusters are shown in figure 4.8. The shallow, weaker-updraught, clouds in cluster 1 produce only weak precipitation. Higher mean precipitation rates are achieved by the stronger-updraught in cluster 2, and deeper clouds in cluster 3. The middle row of figure 4.8 shows the maximum column precipitation rate rate reached for a tracked cloud. As might be expected, the highest precipitation rates are found for clouds in cluster 3. However, due to their greater prevalence, the precipitating shallow cumuli of

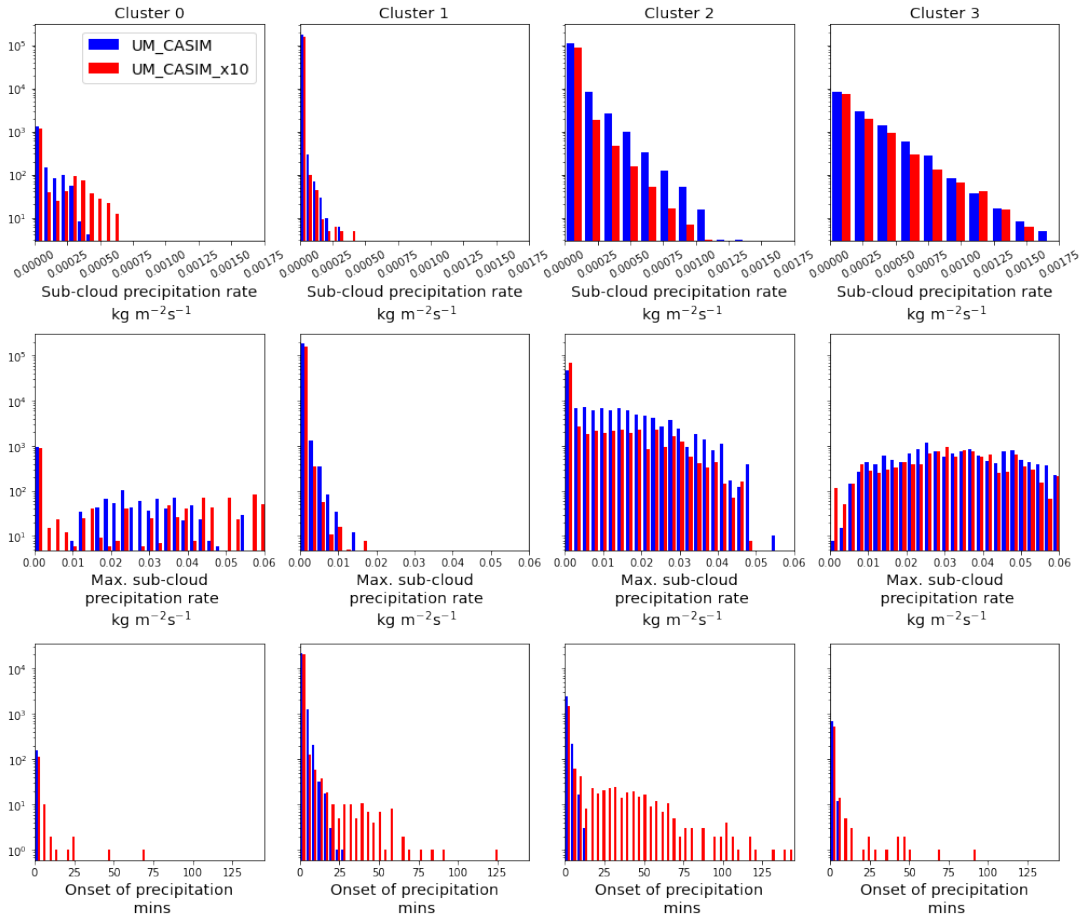

Figure 4.8: Histograms of sub-cloud precipitation rate (top row), maximum single-column sub-cloud precipitation rate along track (middle row), and time of onset of precipitation (bottom row) for each cluster, arranged by column.

cluster 2 produce a greater frequency of intermediate precipitation rates. Cluster 2 also seems to show the greatest response to the increase in aerosol, with reduced occurrences of stronger mean and maximum precipitation. As before, the histograms of the time of onset of precipitation in the bottom row of figure 4.8 show the most stark difference between the perturbed and unperturbed simulations. For all clusters, the increase in aerosol leads to a delay in the onset of precipitation. Cluster 1 is also most strongly affected in this regard. The deeper clouds in cluster 3, however, are much less affected.

Precipitation efficiency is a measure of how effectively a cloud converts con-

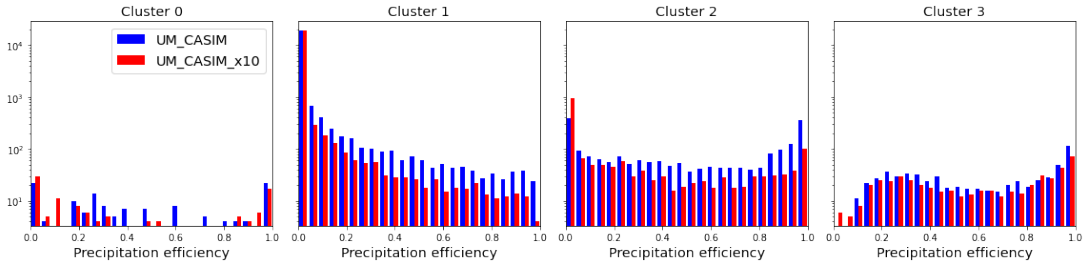

Figure 4.9: Histograms of precipitation efficiency for each cluster, arranged by column.

densed water into precipitation. Specific definitions of precipitation efficiency vary, depending on the perspective of the study. For example, it may defined in the large-scale as a ratio of surface precipitation rate and the sum of surface vapour convergence and evaporation (Tao et al., 2004; Sui et al., 2005). Microphysical definitions may use the ratio of precipitation to the sum of vapour condensation and evaporation rates, or even the ratio of hydrometeor masses (Sui et al., 2005; Sui et al., 2007).

While precipitation efficiency is often defined using surface precipitation, here we will continue to focus on sub-cloud precipitation, and use this in our calculation. Further, we employ a similar approach to Jiang et al. (2010), who use maximum values of liquid water path and precipitation rate in their calculations of precipitation susceptibility, allowing a greater range of values to be considered. Condensation is calculated by summing maximum precipitation and the change in maximum cloud liquid water path. Precipitation efficiency is then the ratio of accumulated precipitation to accumulated condensation, where both are accumulated over the cloud's tracked lifetime.

The histograms of precipitation efficiency for each cluster in figure 4.9 show that the clouds in clusters 2 and 3 produce relatively more instances of higher precipitation efficiency. For cluster 1, very low precipitation efficiencies are dominant. Increasing aerosol appears to have the strongest effect on the clouds in

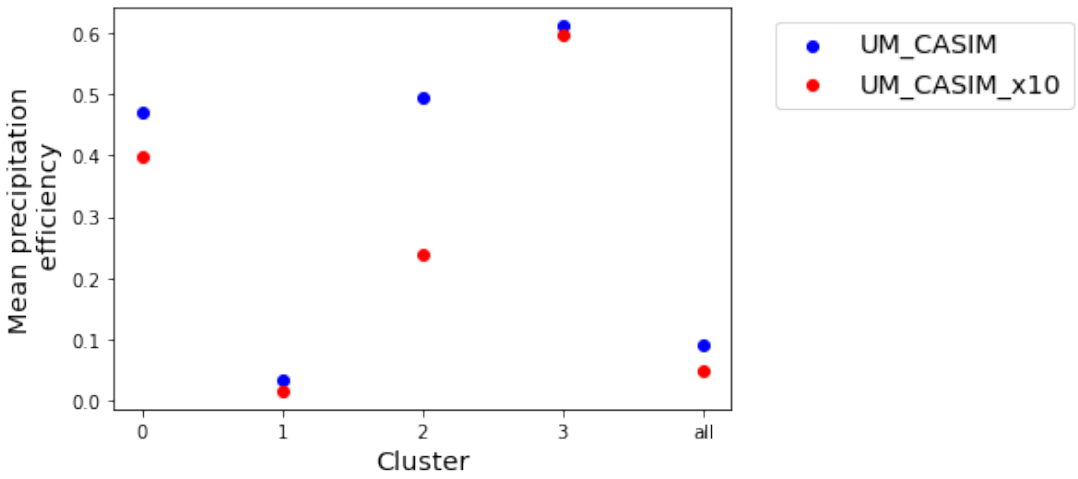

Figure 4.10: Mean precipitation efficiency calculated for all clouds, and for each cluster.

cluster 2, with a reduction in the number of clouds with higher efficiencies. Higher efficiencies also become less common for cluster 1. The deeper clouds in cluster 3 appear less affected by the perturbation. This is also clear from the mean precipitation efficiencies for the clusters, shown in figure 4.10. The mean value for cluster 1 is also not significantly reduced, as for both simulations it is dominated by low values. Cluster 2, shallow clouds with stronger updraughts, are most affected by the increase in aerosol. However, due to the cloud population itself being dominated by clouds in cluster 1, the impact on mean precipitation efficiency across all clouds is a relatively small reduction.

The probability of precipitation is a measure of the proportion of clouds that produce precipitation. It is calculated as the ratio of precipitating clouds to the total number of clouds. Two sets of probabilities are shown in figure 4.11. In figure 4.11 (a), the probability of precipitation is calculated using all individual clouds identified by the tracking algorithm, while in figure 4.11 (b) it is calculated for cloud tracks. Both show that increasing aerosol reduces the probability of precipitation. For individual clouds at a given time, this is most pronounced for clusters 1 and 2. However, when calculated over cloud tracks,

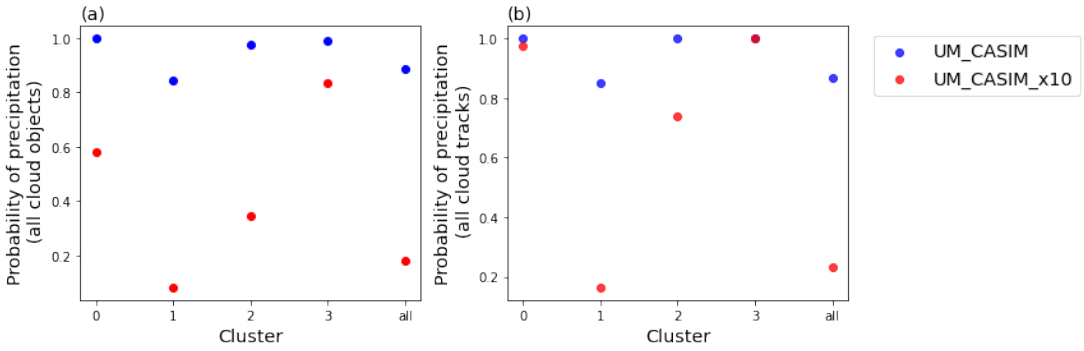

Figure 4.11: Probability of precipitation for (a) all cloud features across all times, and (b) for all cloud tracks. Probabilities are shown for features and tracks in each cluster, and in total.

the reduction for cluster 2 is smaller. A similar result is clear for cluster 3, and also for cluster 0. Increasing aerosol is therefore leading to less frequent precipitation, but not necessarily preventing clouds from precipitating altogether. However, as has already been noted for the precipitation efficiency, the behaviour of cluster 1 dominates the mean response across all clouds and tracks. In this mean, an increase in aerosol leads to a significant decrease in the probability of precipitation.

One of the most significant rapid adjustments of clouds to changes in aerosol is how the cloud droplet number concentration, and thus cloud albedo, is affected. Cloud albedo and cloud fraction determine the amount of shortwave radiation that clouds reflect, and are therefore of great importance in understanding the forcing associated with aerosol-cloud interactions. Seifert and Heus (2013) define a synthetic cloud albedo, A_c:

$$A_c = \frac{\tau}{6.8 + \tau}, \tag{4.1}$$

where τ is an estimate of the cloud optical depth as a function of liquid water

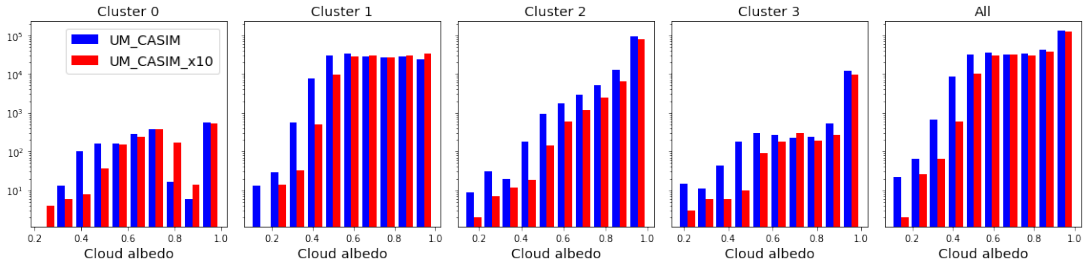

Figure 4.12: Histograms of cloud albedo for each cluster, and for all clouds.

path (LWP) and cloud droplet number concentration (N_d) (Zhang et al., 2005), given by

$$\tau = 0.19 LWP^{\frac{5}{6}} N_d^{\frac{1}{3}}. \tag{4.2}$$

Figure 4.12 shows histograms of the albedos of clouds in each cluster, and all clouds. Clear decreases in the frequency of lower-albedo clouds are seen with increased aerosol. In order to understand the impact that this may have for the domain as a whole, we also need to understand how the mean albedo changes, and how the cloud areas and cloud fraction change. In figure 4.13 we show timeseries of the difference in mean cloud albedo, cloud fraction, and scene albedo, between the perturbed and unperturbed simulations. These are shown for each cluster, and for all clouds. Cloud fraction is calculated by summing the areas of individual clouds, and taking the ratio with the domain area. Scene albedo is calculated using

$$A_{scene} = \frac{1}{a_{tot}} \left(\sum_i a_i A_{ci} \right) - (1 - C) A_b \tag{4.3}$$

where a_{tot} is the domain area, a_i are individual cloud areas, A_{ci} are individual cloud albedos, C is the domain cloud fraction, and A_b is the background

albedo. This is set to 0.05, as an estimate of the albedo of the sea surface for high zenith angles, following Seifert et al. (2015). It is important to note here that cloud fraction, which is given by the ratio of the total cloud area to the domain area, depends on the detection of clouds by the tracking algorithm. The application of the tracking, as discussed, will not detect all clouds in the domain. The cloud fraction calculated here will thus be an underestimate of the true value. We should therefore be cautious in interpreting the findings based on this. Koren et al. (2008) note the importance of the smallest clouds in determining the total reflectance in satellite observations of shallow cloud fields. Nevertheless, the algorithm identifies a large number of clouds, and it is interesting to understand the impact that changes to these clouds may have on the domain scene albedo. In figure 4.13 (a), we see that the mean cloud albedo is consistently higher in the perturbed simulation. The cloud fraction in figure 4.13 (b) is, on the whole, largely unchanged under the aerosol perturbation, except for an interval of around 2h in the middle of the analysed period, during which it is decreased. Changes in individual clusters' contribution to the cloud fraction are mostly noisy, however there is a notable decrease for cluster 2, and an increase for cluster 0 towards the end of the period. Changes in scene albedo (figure 4.13 (c)) appear to be largely driven by changes in cloud fraction. In particular, a decrease in scene albedo in the middle of the period following the decrease in cluster 2's cloud fraction, and an increase towards the end following the increase in cluster 0. The large-area clouds are unsurprisingly extremely important in determining the albedo characteristics of the domain. However, the small reduction in cloud fraction during times when the domain is mostly populated by cumuliform clouds, possibly due to the reduction in the number of clouds, is significant. The mean change in scene albedo is a decrease of 0.6% with the increase in aerosol. Small changes in cloud fraction thus appear to offset the increase in albedo due to increased droplet number. However, without more complete information re-

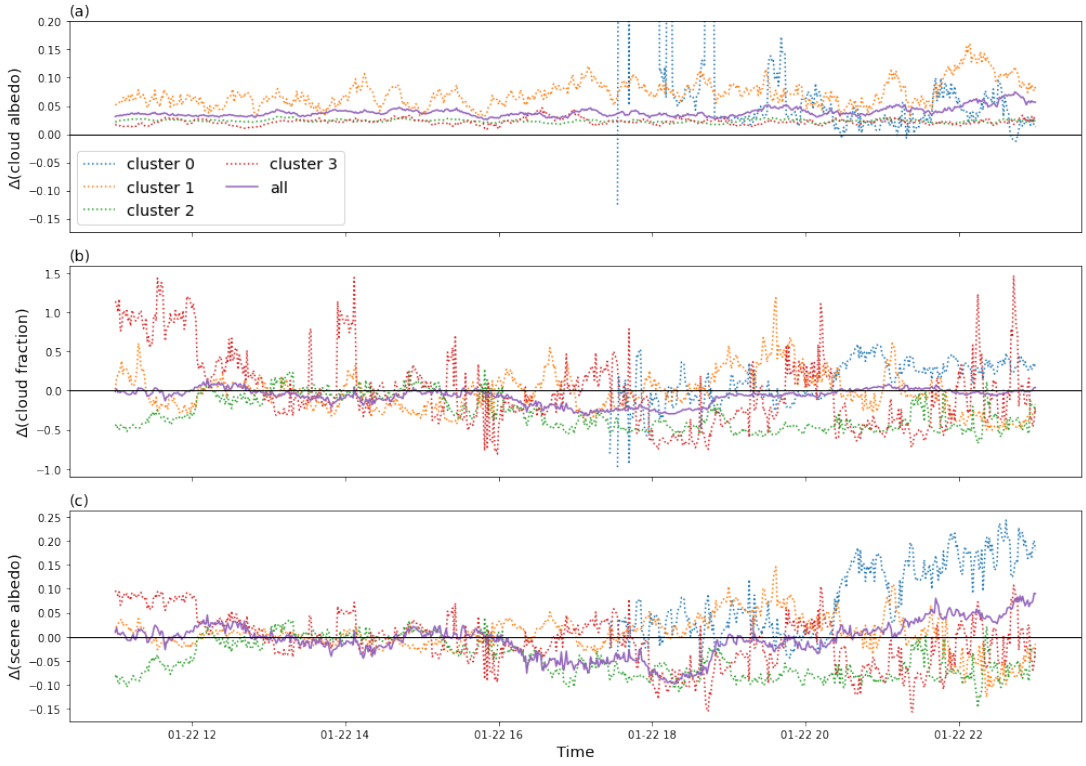

Figure 4.13: Timeseries of the relative change ((UM_CASIM_x10 − UM_-CASIM)/UM_CASIM) in (a) cloud albedo, (b) cloud fraction, and (c) scene albedo. Timeseries are shown for all clouds and for each cluster.

garding the total contribution of clouds to the scene albedo, an estimate of the forcing due to this change is difficult to make.

It is worth considering figure 4.5 again, in the context of the cloud fraction shown in figure 4.13 (b). Fewer clouds, but with a relatively similar cloud fraction, suggests a tendency towards clouds with larger areas, which may be linked to increased vertical development. However, as noted already, the contributions of individual clusters to changes in the total cloud fraction are quite noisy.

4.4 Discussion

We have presented simulations of trade wind convective clouds under different aerosol loadings, which are analysed using a cloud tracking algorithm. This al-

lows the cloud population to be decomposed into several clusters. These clusters are simply defined, in order to represent cloud types that may be familiar: shallow cumuli with weak updraughts, shallow cumuli with stronger updraughts, deeper cumuli congestus, and a cluster of large-area, potentially stratiform clouds. This approach is taken in order to understand the differing impacts of increased aerosol on the different cloud types.

Shallow cumuli are by far the most frequently occurring clouds in the simulations, with more weakly-updraught clouds. We find that an increase in aerosol leads to a decrease in the number of clouds identified by the tracking algorithm. This decrease is most prominent for the shallow cumuli with stronger updraughts. This finding is in agreement with Saleeby et al. (2015), who also find a reduction in the number of low-level cumuli with increased aerosol concentrations.

Increasing aerosol leads to an increase in the occurrence of higher liquid water paths, as well as cloud depths and cloud top heights. Analysis of the individual clusters shows that this increase in cloud depth is primarily a result of deepening congestus clouds, that penetrate the trade inversion base and marine boundary layer. Similar responses of congestus clouds deepening with increasing aerosol have been shown previously (van den Heever et al., 2011; Saleeby et al., 2015; Sheffield et al., 2015).

Cloud lifetimes show very little change with increased aerosol. This contrasts with the findings of Christensen et al. (2020), who employ a Lagrangian framework to investigate cloud lifetimes along stratus-to-cumulus transitions, finding that increased aerosol leads to longer lifetimes. Such differing results are indicative of the importance of cloud-type and regime in determining the impact of changing aerosol on clouds.

All clouds show a notable delay in the onset of precipitation with increased aerosol, though this is most pronounced for the stronger-updraught shallow cumuli. Precipitation efficiency is also most strongly affected for these clouds.

Analysis of the probability of precipitation reveals interesting differences between the cloud types. Under an increase in aerosol, shallow cumuli with weak updraughts, which typically produce weak precipitation, are much less likely to precipitate, and this behaviour dominates the mean for all cloud types. When the probability of precipitation is calculated for all detected clouds in a cluster, a reduction is also clear for the clouds with stronger updraughts. However, when calculated for clouds over their tracked lifetime, the decrease is smaller for these clouds, and no decrease is found for congestus clouds. While the onset of precipitation may be delayed in these clouds, it is not entirely suppressed. There is no indication that this delay leads to higher peak precipitation rates, as has been suggested for surface precipitation rates by a number of studies (Stevens & Feingold, 2009; Seifert et al., 2015; Saleeby et al., 2015).

Previous studies have discussed non-monotonic effects of aerosol on convective clouds (Dagan et al., 2017; Liu et al., 2019). While this can be considered as a function of aerosol concentration, it can also be considered in terms of cloud development. Here, we find that small, shallow clouds are suppressed by increased aerosol concentrations, while congestus clouds, in contrast, become deeper. The aerosol effect can then be considered non-monotonic in terms of cloud characteristics, rather than as a function of the aerosol loading itself.

The impact of higher aerosol concentrations on cloud albedo is of great interest. All clouds show an increase in albedo with increased aerosol, as a result of both higher cloud droplet number concentration and liquid water path. However, small changes in cloud fraction lead to a decrease, on average, of the scene albedo during the analysed period, which would imply a positive radiative forcing. The impact of changing aerosol on scene albedo is likely to be highly dependent on the composition and characteristic lifetime of the cloud field, due to the differing responses of different cloud types. Thus, a robust estimate of forcing is difficult

to make due to limitations of the tracking algorithm, and the short time period analysed.

Spill et al. (2021) argue that realistic and idealised simulations of trade wind clouds produce significantly different cloud fields, as well as different responses to increased aerosol concentration. A notable aspect of the differing cloud fields is the variability and diversity of the cloud population. Here, tracking individual clouds allows detailed investigation of the different components of the cloud field. We have shown that, within trade wind cloud fields that consist predominantly of shallow cumuli, the varied cloud population responds differently to aerosol perturbations. The shallowest clouds become less common, and are less likely to produce precipitation. In contrast, there is an increase in the number of deeper precipitating cumuli congestus, though these clouds do experience a delay in the onset of precipitation. As noted by Dagan et al. (2018a), the characteristic lifetime of these cloud fields is less than 12 hours, and their composition can be highly diverse (Nuijens et al., 2014; Vial et al., 2019). It is thus extremely important to consider the variability in the composition of trade wind cloud fields when considering the impact of aerosol perturbations.

Chapter 5

Conclusions

Clouds are self-evidently significant components of the Earth's atmosphere and climate system. Their interactions with aerosols, which are themselves another key component of the atmosphere, have been the subject of intense study for many years, with early work still serving as the foundation for modern research (Twomey, 1977; Albrecht, 1989). Yet, aerosol-cloud interactions are still one of the most significant sources of uncertainty in anthropogenic radiative forcing (Boucher et al., 2013a; Myhre et al., 2013). Shallow convective clouds in trade wind regions over the Earth's oceans are the most commonly occurring clouds in the atmosphere, and as such play key roles in the climate system; transporting heat and moisture, and reflecting short wave radiation. Furthermore, they are a key element of improving our understanding of the atmosphere and climate due to the high uncertainties in their behaviour, and their large contribution to the uncertainty associated with aerosol-cloud interactions. These large uncertainties reflect the complexity and variety of the processes via which clouds and aerosols may affect one another, and the range of scales on which such processes occur. With the intense study of clouds and aerosols have come many different, and often conflicting, hypotheses regarding the effects of aerosol on shallow clouds (Albrecht, 1989; Small et al., 2009; Stevens & Feingold, 2009; Koren et al., 2014;

Seifert et al., 2015; Dagan et al., 2018a). The interactions between aerosol and shallow clouds thus remain poorly understood, and it is these interactions that are the subject of this thesis.

In this concluding chapter the findings of the previous chapters will be summarised, and their collective implications will be explored. Questions arising from the work in this thesis will also be discussed, along with potential avenues for further research.

In Chapter 2, simulations of shallow cumuli were performed using a large domain and high spatial resolution, in order to explore the effects of aerosol on an entire shallow convective cloud field. Previously, modelling studies of shallow convection and aerosol have been limited due to computational constraints; either resolving shallow convection with high spatial resolution and being limited to small domains of tens of km, or relying upon parameterisations of convection for large, even global, domains. However, the importance of the large-scale behaviour of shallow cloud fields has also become clear (Wood & Hartmann, 2006; Seifert et al., 2015; Bretherton & Blossey, 2017; Dagan et al., 2018a). The simulations in Chapter 2 were performed using the Met Office Unified Model, along with a 500km domain, 500m horizontal resolution, and were based on a case study from the RICO field campaign. A two-moment microphysics scheme, CASIM, was used, and simulations were run with perturbed aerosol concentrations. The analysis found several elements of the response to increasing aerosol that were consistent with existing research. Namely, with increased aerosol there were increases in cloud liquid water path, maximum updraught speeds, and cloud top heights. Convective invigoration and deepening in response to increased aerosol has been demonstrated a number of times (Kaufman et al., 2005; Koren et al., 2014; Seifert et al., 2015; Saleeby et al., 2015; Dagan et al., 2017). However, the analysis in Chapter 2 did not find that this led to a significant increase in the occurrence of higher precipitation rates, as has been found previously (Seifert et

al., 2015; Saleeby et al., 2015). Furthermore, the analysis showed that increased aerosol led to persistent changes in domain-mean precipitation and liquid water path, in contrast to the very small domain-mean effects found by others (van den Heever et al., 2011; Seifert et al., 2015; Yamaguchi et al., 2019). Some have argued that increased aerosol may also lead to significant effects on the thermodynamic evolution of the clouds' environment (Stevens & Feingold, 2009; Lee et al., 2012; Seifert et al., 2015). The simulations in Chapter 2, however, found no such change, with similar domain-mean thermodynamic evolution under all aerosol concentrations. The quasi-equilibrium cloud fields found by several studies (Lee et al., 2012; Seifert et al., 2015; Yamaguchi et al., 2019) are also not seen.

A significant difference between the simulations presented in Chapter 2 and those in most existing research lies in the approach to domain boundary conditions and large-scale forcing. Large-eddy simulations typically employ doubly-periodic lateral boundary conditions, with large-scale forcing given by constant tendencies of temperature and moisture, and imposed subsidence. The nested UM domain, in contrast, has open boundaries, and has time-varying large-scale forcing due to the external driving model. Based on the findings in Chapter 2, it was hypothesised that these differences in simulation approaches are responsible for the different responses to aerosol perturbations. This hypothesis served as the motivation for Chapter 3.

Chapter 3 investigates the effects of aerosol on trade wind convective clouds in simulations with differing approaches to boundary conditions and large-scale forcing, and explores the significance of these differences in influencing the effects. The RICO campaign was again used as a basis for a case study, with baseline and perturbed aerosol concentrations. In order to test the hypothesis that different simulation approaches lead to different responses to aerosol perturbations, the same model, the UM, was used in different configurations. One configuration

used the open lateral boundaries, and external driving model, as employed in Chapter 2. The other main configuration used the approach that has typically been employed in large eddy simulations of shallow convection. That is, the lateral boundaries were doubly-periodic, and constant tendencies of temperature and moisture were prescribed to represent the large-scale forcing. These setups are referred to as 'realistic' and 'idealised', respectively, due to these distinctions. Again, large domains of 500km with 500m resolution were used for the realistic simulations, and for two of the three idealised configurations. Three idealised configurations were used: one did not use a radiation scheme, relying only on prescribed tendencies to represent radiative cooling, while a radiation scheme was included in the two others. The third used a smaller domain of 100km, and a higher horizontal resolution of 100m, compared to 500m in the 500km domain. These configurations were designed to provide different degrees of realism, and to reflect those that have been used in existing studies. Radiation schemes are often not employed in LES, though radiative cooling is an important component of the thermodynamic evolution of a domain (Guichard & Couvreux, 2017). A smaller domain simulation with higher resolution allowed an additional point of comparison with existing LES studies using finer horizontal grids.

The differences between the cloud fields and response to aerosol perturbations for the simulation approaches are striking. On large scales, the idealised and realistic simulations produce very different cloud fields, with far more structure and large-scale features evident in the realistic simulations, in contrast to the more uniform cloud fields in the idealised simulations. The behaviour of the idealised cloud fields in this respect is consistent with findings of existing studies, with some large-scale structure emerging later in the simulations (Seifert et al., 2015). The realistic and idealised simulations also exhibited markedly different responses to increased aerosol concentrations. In the domain-mean, of particular note is the resiliency of the cloud fraction in the realistic simulations,

in contrast to the increases seen in the idealised simulations. Analysis of the vertical structure of liquid water and updraught speeds further highlighted the differences between the approaches. Stronger deepening and invigoration with increased aerosol were both clear in all of the idealised simulations, compared to the realistic simulations. The analysis also showed that low cloud-fraction parts of the cloud field in the realistic simulation responded similarly, though still more weakly, to the increase in aerosol, compared to the idealised cloud fields.

One of the most dramatic differences between the realistic and idealised simulations lies in their thermodynamic evolution. Under the increase in aerosol, the idealised simulations show increases in cooling and moisture at the top of the cloud layer. In contrast, the thermodynamic evolution of the realistic simulations is almost entirely unchanged by the aerosol perturbation. Under the mechanism of buffering by convective deepening and invigoration described by Stevens and Feingold (2009), a delay in the onset of precipitation may allow more moisture to be lofted to the cloud top, leading to increased cooling due to evaporation, and enhanced vertical development. Additionally, increased aerosol may allow more water to be condensed, also enhancing vertical development (Lebo & Seinfeld, 2011; Koren et al., 2014). Thus, the differing thermodynamic responses are as may be expected given the degree of convective deepening and invigoration seen for the two approaches. In the idealised simulations, the enhanced cooling and lofting of moisture to the cloud top, and strong convective deepening and invigoration, is in keeping with the buffering mechanism described by Stevens and Feingold (2009), whereas a weaker thermodynamic response is seen in the realistic simulations along with weaker deepening.

The findings of Chapter 3 show that the time-varying large-scale forcing, and open lateral boundaries, in the more realistic simulations lead to a significantly different response to aerosol perturbations, compared to the fixed forcing and

periodic boundaries of the idealised simulations. This supports the finding of Dagan et al. (2018a), who show that the characteristic lifetime of shallow convective cloud fields is much shorter than the time taken to reach the quasi-equilibrium state described by a number of other studies (Lee et al., 2012; Seifert et al., 2015; Yamaguchi et al., 2019). Future research must therefore consider carefully the representation of large-scale forcing when interpreting model simulations of aerosol effects on shallow convective cloud fields. That some components of the realistic cloud field showed a similar structure of response to the aerosol perturbation compared to the idealised cloud fields, suggests that understanding the variability in the cloud population is also of great importance to understand the effects of changes in aerosol. Indeed, the diversity of trade wind cloud fields has been noted previously (Nuijens et al., 2014; Vial et al., 2019), and several studies have found that different modes of trade wind convection, including shallow cumulus and cumulus congestus, may respond differently to aerosol (van den Heever et al., 2011; Saleeby et al., 2015; Seifert et al., 2015).

Chapter 4 explores in detail the properties and life-cycle of individual clouds in trade wind cloud fields, investigating how different components of the cloud population respond to changes in aerosol. The application of a cloud tracking algorithm allows such a detailed analysis of a short period of the realistic simulations first presented in Chapter 3. The cloud tracking allows the analysis to be carried out using properties of individual clouds, rather than of the cloud field as a whole. The analysis reveals that many aspects of the clouds' characteristics are similar under increased aerosol, though there are increases in the occurrence of higher liquid water paths, cloud top heights, and cloud depths. The most striking difference is the significant delay in the onset of precipitation. Clustering the cloud population with simple thresholds on cloud depth, updraught speed, and area, allows separate investigation of different components of the cloud field,

such as weakly-convective shallow cumuli, more strongly-convective shallow cumuli, deeper cumuli congestus, and large-area stratiform clouds. Shallow cumuli are by far the most dominant by number, with more weakly-convective clouds identified. The tracking also finds that the number of clouds is notably reduced with increased aerosol, with most of this reduction from shallow cumuli, particularly the more strongly-convective shallow cumuli. This is in agreement with previous findings (van den Heever et al., 2011; Saleeby et al., 2015). Analysis of the individual clusters also supports existing suggestions that congestus clouds are the most likely to deepen in response to increased aerosol, but does not show an increase in the occurrence of higher peak precipitation rates for these clouds (van den Heever et al., 2011; Saleeby et al., 2015; Seifert et al., 2015). The delay in the onset of precipitation with increased aerosol is clear for all clouds, most notably the more strongly-convective shallow cumuli. An interesting difference in the behaviour between clouds can be seen in the probability of precipitation. Weakly-convective clouds are less likely to produce precipitation under higher aerosol conditions, while the more strongly convective clouds, especially congestus, remain likely to precipitate at some point during their lifetime, even if it is delayed. Analysis of the changes in cloud and scene albedo shows that, while aerosol may lead to increases in cloud albedo, small changes in cloud fraction are hugely important in determining the change in scene albedo.

This thesis has investigated several questions surrounding the effects of aerosol on shallow convective cloud fields. A number of key themes have emerged from the analyses that have been presented, with interesting comparisons with existing research. Chapters 2 and 3 demonstrated that large-domain simulations of trade wind cloud fields exhibit a response to aerosol that differs from many existing studies making use of smaller domains. Chapter 3 extends this, postulating that these differing responses to aerosol perturbations are a result of

differing approaches in idealised and realistic model setups. Large-domain simulations with a realistic setup also produce cloud fields with greater structure and diversity in the cloud population. The significance of this diverse cloud population is emphasised in Chapter 4. Detailed analysis using a tracking algorithm demonstrates that clouds with different characteristics respond differently to increases in aerosol; the weakest convective clouds are reduced in number with increased aerosol concentrations, while cumuli congestus may become deeper. Furthermore, in order to make robust estimates of the radiative forcing due to aerosol perturbations, it is necessary to combine information about the cloud field composition with an understanding of how each component is affected.

The analyses in this thesis give rise to a number of further questions. One avenue stems from the findings of Chapter 3; that different representations of boundary conditions and large-scale forcing can lead to dramatically different responses of the cloud field. This naturally leads to the question of how this behaviour may vary under different large-scale forcing. Dagan and Stier (2020) begin to explore this with an ensemble of simulations based on the NARVAL campaign, though with perturbations of cloud droplet number concentration rather than aerosol, and with a relatively coarse resolution of 1200m. The NARVAL and EUREC^{4}A campaigns offer a wealth of possibilities for extending the case-study analysis presented in this thesis; exploring not only different large-scale forcings, but also a wider range of examples of trade wind cloud fields.

The effects of atmospheric aerosol on clouds due their role as CCN are mediated by a range of microphysical processes, through which aerosols and clouds may each affect one another. In this thesis, the representation of microphysics has focused on a one-way coupling between aerosols and clouds; that is, changes in the aerosol population affect clouds, but cloud processes do not affect the aerosol population. This is evidently a limited representation, and a more detailed treatment that includes, for example, the removal of aerosol by precipitation, would

undoubtedly be of value. Further, the mechanisms through which increases in aerosol may drive convective deepening and invigoration depend on enhanced condensation, cloud-top evaporation, and changes in precipitation. A detailed analysis of microphysical process rates in clouds subject to different large-scale forcings may shed further light on how processes across scales are coupled. It could also explore how changes in process rates under aerosol perturbations differ for different components of the cloud population. This analysis could be supported through the use of the tracking algorithm employed in Chapter 4.

The tracking algorithm also opens a number of exciting possibilities to investigate changes in the cloud field dynamics. Mesoscale organisation of shallow cloud fields has been shown to be an important characteristic (Dagan et al., 2018b; Rasp et al., 2020; Stevens et al., 2020; Denby, 2020), and may be affected by changes in the number, size, and spacing of clouds. Improving tracking algorithms, and developing understanding of how choices in identification thresholds affect tracking analyses would allow even more comprehensive study of cloud field dynamics. Further, changes in the timing of precipitation processes could impact cold pool dynamics, that are also a central component in determining the organisation of cloud fields. Applying the algorithm to both clouds and cold pools would allow a detailed analysis of how their dynamics may be affected by perturbations such as aerosol.

Increasing computational capabilities are leading to the development of global cloud-resolving models (GCRMs) (Stevens et al., 2019b; Satoh et al., 2019). Such models promise exciting developments in advancing our understanding of clouds, through their representation of the multi-scale interactions between clouds and large-scale circulations, with the questions of horizontal boundary conditions and large-scale forcing dealt with implicitly in global simulations. However, GCRMs typically have grid sizes of up to 5km, and are thus still unable to resolve shallow convection. While sub-kilometre global simulations have been

carried out (Miyamoto et al., 2013; Miyamoto et al., 2015; Kajikawa et al., 2016), their application to studying shallow clouds remains some way off. High resolution simulations of shallow clouds in large domains will thus continue to be an essential component of studying these clouds.

This thesis has explored the effects of aerosol on shallow convective clouds. The use of high-resolution, large-domain simulations, with realistic modelling configurations, has allowed a central theme to emerge; that realistic representation of the transient large-scale forcing, and of the diversity found in shallow fields on large scales, is key in influencing the response of shallow cloud fields to aerosol perturbations.

References

Abdul-Razzak, H., & Ghan, S. J. (2000). A parameterization of aerosol activation: 2. multiple aerosol types. *Journal of Geophysical Research: Atmospheres*, *105*(D5), 6837–6844. https://doi.org/10.1029/1999JD901161

Abel, S. J., & Shipway, B. J. (2007). A comparison of cloud-resolving model simulations of trade wind cumulus with aircraft observations taken during rico. *Quarterly Journal of the Royal Meteorological Society*, *133*(624), 781–794. https://doi.org/10.1002/qj.55

Ackerman, A. S., Toon, O. B., Stevens, D. E., Heymsfield, A. J., Ramanathan, V., & Welton, E. J. (2000). Reduction of tropical cloudiness by soot. *Science*, *288*(5468), 1042–1047. https://doi.org/10.1126/science.288.5468.1042

Albrecht, B. A. (1989). Aerosols, cloud microphysics, and fractional cloudiness. *Science*, *245*(4923), 1227–1230. https://doi.org/10.1126/science.245.4923.1227

Albrecht, B. A. (1993). Effects of precipitation on the thermodynamic structure of the trade wind boundary layer. *Journal of Geophysical Research*, *98*, 7327–7337.

Allen, R. J., Amiri-Farahani, A., Lamarque, J.-F., Smith, C., Shindell, D., Hassan, T., & Chung, C. E. (2019). Observationally constrained aerosol–cloud semi-direct effects. *npj Climate and Atmospheric Science*, *2*(1), 16. https://doi.org/10.1038/s41612-019-0073-9

Altaratz, O., Koren, I., Remer, L. A., & Hirsch, E. (2014). Review: Cloud invigoration by aerosols—Coupling between microphysics and dynamics.

Atmospheric Research, *140*, 38–60. https://doi.org/10.1016/j.atmosres.2014.01.009

Andreae, M. O. (2019). Emission of trace gases and aerosols from biomass burning – an updated assessment. *Atmospheric Chemistry and Physics*, *19*(13), 8523–8546. https://doi.org/10.5194/acp-19-8523-2019

Andreae, M. O., & Rosenfeld, D. (2008). Aerosol–cloud–precipitation interactions. part 1. the nature and sources of cloud-active aerosols. *Earth-Science Reviews*, *89*(1), 13–41. https://doi.org/10.1016/j.earscirev.2008.03.001

Andreae, M. O. (2007). Aerosols before pollution. *Science*, *315*(5808), 50–51. https://doi.org/10.1126/science.1136529

Ångström, A. (1962). Atmospheric turbidity, global illumination and planetary albedo of the earth.

Bannon, P. R. (1996). On the anelastic approximation for a compressible atmosphere. *Journal of Atmospheric Sciences*, *53*(23), 3618–3628. https://doi.org/10.1175/1520-0469(1996)053⟨3618:OTAAFA⟩2.0.CO;2

Bony, S., Dufresne, J.-L., Le Treut, H., Morcrette, J.-J., & Senior, C. (2004). On dynamic and thermodynamic components of cloud changes. *Climate Dynamics*, *22*(2), 71–86. https://doi.org/10.1007/s00382-003-0369-6

Bony, S., & Dufresne, J.-L. (2005). Marine boundary layer clouds at the heart of tropical cloud feedback uncertainties in climate models. *Geophysical Research Letters*, *32*(20). https://doi.org/10.1029/2005GL023851

Bony, S., Schulz, H., Vial, J., & Stevens, B. (2020). Sugar, gravel, fish, and flowers: Dependence of mesoscale patterns of trade-wind clouds on environmental conditions [e2019GL085988 10.1029/2019GL085988]. *Geophysical Research Letters*, *47*(7), https://agupubs.onlinelibrary.wiley.com/doi/pdf/10.1029/2019GL085e2019GL085988. https://doi.org/https://doi.org/10.1029/2019GL085988

Bony, S., Stevens, B., Frierson, D. M. W., Jakob, C., Kageyama, M., Pincus, R., Shepherd, T. G., Sherwood, S. C., Siebesma, A. P., Sobel, A. H.,

Watanabe, M., & Webb, M. J. (2015). Clouds, circulation and climate sensitivity. *Nature Geoscience*, *8*(4), 261–268. https://doi.org/10.1038/ngeo2398

Boucher, O., Randall, D., Artaxo, P., Bretherton, C., Feingold, G., Forster, P., Kerminen, V.-M., Kondo, Y., Liao, H., Lohmann, U., Rasch, P., Satheesh, S. K., Sherwood, S., Stevens, B., & Zhang, X. Y. (2013a). Clouds and aerosols. In *Climate change 2013: The physical science basis. contribution of working group i to the fifth assessment report of the intergovernmental panel on climate change* (pp. 571–657). Cambridge, UK, Cambridge University Press. https://doi.org/10.1017/CBO9781107415324.016

Boucher, O., Randall, D., Artaxo, P., Bretherton, C., Feingold, G., Forster, P., Kerminen, V.-M., Kondo, Y., Liao, H., Lohmann, U., Rasch, P., Satheesh, S. K., Sherwood, S., Stevens, B., & Zhang, X. Y. (2013b). Clouds and aerosols. In *Climate change 2013: The physical science basis. contribution of working group i to the fifth assessment report of the intergovernmental panel on climate change* (pp. 571–657). Cambridge, UK, Cambridge University Press. https://doi.org/10.1017/CBO9781107415324.016

Boutle, I. A., Eyre, J. E. J., & Lock, A. P. (2014). Seamless stratocumulus simulation across the turbulent gray zone. *Monthly Weather Review*, *142*(4), 1655–1668. https://doi.org/10.1175/MWR-D-13-00229.1

Bretherton, C. S., & Blossey, P. N. (2017). Understanding mesoscale aggregation of shallow cumulus convection using large-eddy simulation. *Journal of Advances in Modeling Earth Systems*, *9*(8), 2798–2821. https://doi.org/10.1002/2017MS000981

Bryan, G. H., Wyngaard, J. C., & Fritsch, J. M. (2003). Resolution requirements for the simulation of deep moist convection. *Monthly Weather Review*, *131*(10), 2394–2416. https://doi.org/10.1175/1520-0493(2003)131⟨2394:RRFTSO⟩2.0.CO;2

Carslaw, K. S., Boucher, O., Spracklen, D. V., Mann, G. W., Rae, J. G. L., Woodward, S., & Kulmala, M. (2010). A review of natural aerosol interactions and feedbacks within the earth system. *Atmospheric Chemistry and Physics*, *10*(4), 1701–1737. https://doi.org/10.5194/acp-10-1701-2010

Carslaw, K. S., Lee, L. A., Reddington, C. L., Pringle, K. J., Rap, A., Forster, P. M., Mann, G. W., Spracklen, D. V., Woodhouse, M. T., Regayre, L. A., & Pierce, J. R. (2013). Large contribution of natural aerosols to uncertainty in indirect forcing. *Nature*, *503*(7474), 67–71. https://doi.org/10.1038/nature12674

Cavalli, F., Facchini, M. C., Decesari, S., Mircea, M., Emblico, L., Fuzzi, S., Ceburnis, D., Yoon, Y. J., O'Dowd, C. D., Putaud, J.-P., & Dell'Acqua, A. (2004). Advances in characterization of size-resolved organic matter in marine aerosol over the north atlantic. *Journal of Geophysical Research: Atmospheres*, *109*(D24). https://doi.org/10.1029/2004JD005137

Charba, J. (1974). Application of gravity current model to analysis of squall-line gust front. *Monthly Weather Review*, *102*(2), 140–156.

Charlson, R. J., Schwartz, S. E., Hales, J. M., Cess, R. D., Coakley, J. A., Hansen, J. E., & Hofmann, D. J. (1992). Climate forcing by anthropogenic aerosols. *Science*, *255*(5043), 423–430. https://doi.org/10.1126/science.255.5043.423

Chen, T., Rossow, W. B., & Zhang, Y. (2000). Radiative effects of cloud-type variations. *Journal of Climate*, *13*(1), 264–286. https://doi.org/10.1175/1520-0442(2000)013⟨0264:REOCTV⟩2.0.CO;2

Christensen, M. W., Jones, W. K., & Stier, P. (2020). Aerosols enhance cloud lifetime and brightness along the stratus-to-cumulus transition. *Proceedings of the National Academy of Sciences*, *117*(30), 17591–17598. https://doi.org/10.1073/pnas.1921231117

Connolly, P. J., Topping, D. O., Malavelle, F., & McFiggans, G. (2014). A parameterisation for the activation of cloud drops including the effects of semi-volatile organics. *Atmospheric Chemistry and Physics*, *14*(5), 2289–2302. https://doi.org/10.5194/acp-14-2289-2014

Cotton, W. R., Bryan, G. H., & van den Heever, S. C. (2011). *Storm and cloud dynamics*. Academic Press.

Dagan, G., & Chemke, R. (2016). The effect of subtropical aerosol loading on equatorial precipitation. *Geophysical Research Letters*, *43*(20), 11, 048–11, 056. https://doi.org/10.1002/2016GL071206

Dagan, G., Koren, I., Altaratz, O., & Heiblum, R. H. (2017). Time-dependent, non-monotonic response of warm convective cloud fields to changes in aerosol loading. *Atmospheric Chemistry and Physics*, *17*(12), 7435–7444. https://doi.org/10.5194/acp-17-7435-2017

Dagan, G., & Stier, P. (2020). Ensemble daily simulations for elucidating cloud–aerosol interactions under a large spread of realistic environmental conditions. *Atmospheric Chemistry and Physics*, *20*(11), 6291–6303. https://doi.org/10.5194/acp-20-6291-2020

Dagan, G., Koren, I., Altaratz, O., & Heiblum, R. H. (2016). Aerosol effect on the evolution of the thermodynamic properties of warm convective cloud fields. *Scientific Reports*, *6*, 38769. http://dx.doi.org/10.1038/srep38769

Dagan, G., Koren, I., Altaratz, O., & Lehahn, Y. (2018a). Shallow convective cloud field lifetime as a key factor for evaluating aerosol effects. *iScience*, *10*, 192–202. https://doi.org/10.1016/j.isci.2018.11.032

Dagan, G., Koren, I., Kostinski, A., & Altaratz, O. (2018b). Organization and oscillations in simulated shallow convective clouds. *Journal of Advances in Modeling Earth Systems*, *10*(9), 2287–2299. https://doi.org/10.1029/2018MS001416

Davidi, A., Kostinski, A. B., Koren, I., & Lehahn, Y. (2012). Observational bounds on atmospheric heating by aerosol absorption: Radiative signature

of transatlantic dust. *Geophysical Research Letters*, *39*(4). https://doi.org/10.1029/2011GL050358

Davidson, B. (1968). The barbados oceanographic and meteorological experiment. *Bulletin of the American Meteorological Society*, *49*(9), 928–935. https://doi.org/10.1175/1520-0477-49.9.928

Dee, D. P., Uppala, S. M., Simmons, A. J., Berrisford, P., Poli, P., Kobayashi, S., Andrae, U., Balmaseda, M. A., Balsamo, G., Bauer, P., Bechtold, P., Beljaars, A. C. M., van de Berg, L., Bidlot, J., Bormann, N., Delsol, C., Dragani, R., Fuentes, M., Geer, A. J., ... Vitart, F. (2011). The era-interim reanalysis: Configuration and performance of the data assimilation system. *Quarterly Journal of the Royal Meteorological Society*, *137*(656), 553–597. https://doi.org/10.1002/qj.828

Denby, L. (2020). Discovering the importance of mesoscale cloud organization through unsupervised classification [e2019GL085190 10.1029/2019GL085190]. *Geophysical Research Letters*, *47*(1), e2019GL085190. https://doi.org/10.1029/2019GL085190

Ekman, A. M. L., Engström, A., & Wang, C. (2007). The effect of aerosol composition and concentration on the development and anvil properties of a continental deep convective cloud. *Quarterly Journal of the Royal Meteorological Society*, *133*(627), 1439–1452. https://doi.org/10.1002/qj.108

Fan, J., Wang, Y., Rosenfeld, D., & Liu, X. (2016). Review of aerosol-cloud interactions: Mechanisms, significance, and challenges. *Journal of the Atmospheric Sciences*, *73*(11), 4221–4252. https://doi.org/10.1175/JAS-D-16-0037.1

Feingold, G., Cotton, W. R., Kreidenweis, S. M., & Davis, J. T. (1999). The impact of giant cloud condensation nuclei on drizzle formation in stratocumulus: Implications for cloud radiative properties. *Journal of the Atmospheric Sciences*, *56*(24), 4100–4117. https://doi.org/10.1175/1520-0469(1999)056⟨4100:TIOGCC⟩2.0.CO;2

Gettelman, A., Schmidt, A., & Egill Kristjánsson, J. (2015). Icelandic volcanic emissions and climate. *Nature Geoscience*, *8*(4), 243–243. https://doi.org/10.1038/ngeo2376

Gilmore, M. S., & Straka, J. M. (2008). The berry and reinhardt autoconversion parameterization: A digest. *Journal of Applied Meteorology and Climatology*, *47*(2), 375–396. https://doi.org/10.1175/2007JAMC1573.1

Golaz, J.-C., Larson, V. E., & Cotton, W. R. (2002). A pdf-based model for boundary layer clouds. part i: Method and model description. *Journal of the Atmospheric Sciences*, *59*(24), 3540–3551. https://doi.org/10.1175/1520-0469(2002)059⟨3540:APBMFB⟩2.0.CO;2

Grabowski, W. W., Dziekan, P., & Pawlowska, H. (2018). Lagrangian condensation microphysics with twomey ccn activation. *Geoscientific Model Development*, *11*(1), 103–120. https://doi.org/10.5194/gmd-11-103-2018

Grabowski, W. W. (2001). Coupling cloud processes with the large-scale dynamics using the cloud-resolving convection parameterization (crcp). *Journal of the Atmospheric Sciences*, *58*(9), 978–997. https://doi.org/10.1175/1520-0469(2001)058⟨0978:CCPWTL⟩2.0.CO;2

Grassl, H. (1973). Aerosol influence on radiative cooling. *Tellus*, *25*(4), 386–395. https://doi.org/10.3402/tellusa.v25i4.9672

Gregory, D., & Rowntree, P. R. (1990). A mass flux convection scheme with representation of cloud ensemble characteristics and stability-dependent closure. *Monthly Weather Review*, *118*(7), 1483–1506. https://doi.org/10.1175/1520-0493(1990)118⟨1483:AMFCSW⟩2.0.CO;2

Grosvenor, D. P., Field, P. R., Hill, A. A., & Shipway, B. J. (2017). The relative importance of macrophysical and cloud albedo changes for aerosol-induced radiative effects in closed-cell stratocumulus: Insight from the modelling of a case study. *Atmospheric Chemistry and Physics*, *17*(8), 5155–5183. https://doi.org/10.5194/acp-17-5155-2017

Gryspeerdt, E., Quaas, J., & Bellouin, N. (2016). Constraining the aerosol influence on cloud fraction. *Journal of Geophysical Research: Atmospheres*, *121*(7), 3566–3583. https://doi.org/10.1002/2015JD023744

Guichard, F., & Couvreux, F. (2017). A short review of numerical cloud-resolving models. *Tellus A: Dynamic Meteorology and Oceanography*, *69*(1), 1373578. https://doi.org/10.1080/16000870.2017.1373578

Hansen, J., Sato, M., & Ruedy, R. (1997). Radiative forcing and climate response. *Journal of Geophysical Research: Atmospheres*, *102*(D6), 6831–6864. https://doi.org/10.1029/96JD03436

Hartmann, D. L., Ockert-Bell, M. E., & Michelsen, M. L. (1992). The effect of cloud type on earth's energy balance: Global analysis. *Journal of Climate*, *5*(11), 1281–1304. https://doi.org/10.1175/1520-0442(1992)005⟨1281:TEOCTO⟩2.0.CO;2

Haywood, J. M., Abel, S. J., Barrett, P. A., Bellouin, N., Blyth, A., Bower, K. N., Brooks, M., Carslaw, K., Che, H., Coe, H., Cotterell, M. I., Crawford, I., Cui, Z., Davies, N., Dingley, B., Field, P., Formenti, P., Gordon, H., de Graaf, M., ... Zuidema, P. (2021). The cloud–aerosol–radiation interaction and forcing: Year 2017 (clarify-2017) measurement campaign. *Atmospheric Chemistry and Physics*, *21*(2), 1049–1084. https://doi.org/10.5194/acp-21-1049-2021

Heiblum, R. H., Pinto, L., Altaratz, O., Dagan, G., & Koren, I. (2019). Core and margin in warm convective clouds – part 2: Aerosol effects on core properties. *Atmospheric Chemistry and Physics*, *19*(16), 10739–10755. https://doi.org/10.5194/acp-19-10739-2019

Heiblum, R. H., Altaratz, O., Koren, I., Feingold, G., Kostinski, A. B., Khain, A. P., Ovchinnikov, M., Fredj, E., Dagan, G., Pinto, L., Yaish, R., & Chen, Q. (2016). Characterization of cumulus cloud fields using trajectories in the center of gravity versus water mass phase space: 1. cloud tracking and

phase space description. *Journal of Geophysical Research: Atmospheres*, *121*(11), 6336–6355. https://doi.org/10.1002/2015JD024186

Heikenfeld, M., Marinescu, P. J., Christensen, M., Watson-Parris, D., Senf, F., van den Heever, S. C., & Stier, P. (2019). Tobac 1.2: Towards a flexible framework for tracking and analysis of clouds in diverse datasets. *Geoscientific Model Development*, *12*(11), 4551–4570. https://doi.org/10.5194/gmd-12-4551-2019

Heinze, R., Dipankar, A., Henken, C. C., Moseley, C., Sourdeval, O., Trömel, S., Xie, X., Adamidis, P., Ament, F., Baars, H., Barthlott, C., Behrendt, A., Blahak, U., Bley, S., Brdar, S., Brueck, M., Crewell, S., Deneke, H., Di Girolamo, P., ... Quaas, J. (2017). Large-eddy simulations over germany using icon: A comprehensive evaluation. *Quarterly Journal of the Royal Meteorological Society*, *143*(702), 69–100. https://doi.org/10.1002/qj.2947

Heus, T., & Seifert, A. (2013). Automated tracking of shallow cumulus clouds in large domain, long duration large eddy simulations. *Geoscientific Model Development*, *6*(4), 1261–1273. https://doi.org/10.5194/gmd-6-1261-2013

Hohenegger, C., & Stevens, B. (2013). Preconditioning deep convection with cumulus congestus. *Journal of the Atmospheric Sciences*, *70*(2), 448–464. https://doi.org/10.1175/JAS-D-12-089.1

Houze, R. A. (2014). *Cloud dynamics*. Academic Press.

Howard, L. (1803). On the modifications of clouds, and on the principles of their production, suspension, and destruction; being the substance of an essay read before the askesian society in the session 1802–3. *The Philosophical Magazine*, *16*(64), 344–357. https://doi.org/10.1080/14786440308676358

Howell, W. E. (1949). The Growth of Cloud Drops in Uniformly Cooled Air. *Journal of Atmospheric Sciences*, *6*(2), 134–149. https://doi.org/10.1175/1520-0469(1949)006\textless{}0134:TGOCDI\textgreater{}2.0.CO;2

Hu, Z., Bruintjes, R. T., & Betterton, E. A. (1998). Sensitivity of cloud droplet growth to collision and coalescence efficiencies in a parcel model. *Journal of the Atmospheric Sciences*, *55*(15), 2502–2515. https://doi.org/10.1175/1520-0469(1998)055⟨2502:SOCDGT⟩2.0.CO;2

Igel, M. R. (2018). Lagrangian cloud tracking and the precipitation-column humidity relationship. *Atmosphere*, *9*(8). https://doi.org/10.3390/atmos9080289

Jiang, H., & Feingold, G. (2005). Effect of aerosol on warm convective clouds: Aerosol-cloud-surface flux feedbacks in a new coupled large eddy model. *Journal of Geophysical Research: Atmospheres*, *111*(D1). https://doi.org/10.1029/2005JD006138

Jiang, H., Feingold, G., & Koren, I. (2009). Effect of aerosol on trade cumulus cloud morphology. *Journal of Geophysical Research: Atmospheres*, *114*(D11). https://doi.org/10.1029/2009JD011750

Jiang, H., Feingold, G., & Sorooshian, A. (2010). Effect of aerosol on the susceptibility and efficiency of precipitation in warm trade cumulus clouds. *Journal of the Atmospheric Sciences*, *67*(11), 3525–3540. https://doi.org/10.1175/2010JAS3484.1

Jiang, H., Xue, H., Teller, A., Feingold, G., & Levin, Z. (2006). Aerosol effects on the lifetime of shallow cumulus. *Geophysical Research Letters*, *33*(14). https://doi.org/10.1029/2006GL026024

Johnson, D. B. (1982a). The role of giant and ultragiant aerosol particles in warm rain initiation. *Journal of Atmospheric Sciences*, *39*(2), 448–460. https://doi.org/10.1175/1520-0469(1982)039⟨0448:TROGAU⟩2.0.CO;2

Johnson, D. B. (1982b). The role of giant and ultragiant aerosol particles in warm rain initiation. *Journal of Atmospheric Sciences*, *39*(2), 448–460.

Johnson, R. H., Rickenbach, T. M., Rutledge, S. A., Ciesielski, P. E., & Schubert, W. H. (1999). Trimodal characteristics of tropical convection. *Journal of Climate*, *12*(8), 2397–2418. https://doi.org/0.1175/1520-0442(1999)012⟨2397:TCOTC⟩2.0.CO;2

Jung, E., Albrecht, B. A., Sorooshian, A., Zuidema, P., & Jonsson, H. H. (2016). Precipitation susceptibility in marine stratocumulus and shallow cumulus from airborne measurements. *Atmospheric Chemistry and Physics*, *16*(17), 11395–11413. https://doi.org/10.5194/acp-16-11395-2016

Jung, E., Albrecht, B., Prospero, J. M., Jonsson, H. H., & Kreidenweis, S. M. (2013). Vertical structure of aerosols, temperature, and moisture associated with an intense african dust event observed over the eastern caribbean. *Journal of Geophysical Research: Atmospheres*, *118*(10), 4623–4643. https://doi.org/10.1002/jgrd.50352

Kajikawa, Y., Miyamoto, Y., Yoshida, R., Yamaura, T., Yashiro, H., & Tomita, H. (2016). Resolution dependence of deep convections in a global simulation from over 10-kilometer to sub-kilometer grid spacing. *Progress in Earth and Planetary Science*, *3*(1), 1–14. https://doi.org/10.1186/s40645-016-0094-5

Kanji, Z. A., Ladino, L. A., Wex, H., Boose, Y., Burkert-Kohn, M., Cziczo, D. J., & Krämer, M. (2017). Overview of ice nucleating particles. *Meteorological Monographs*, *58*, 1.1–1.33. https://doi.org/10.1175/AMSMONOGRAPHS-D-16-0006.1

Kaufman, Y. J., Koren, I., Remer, L. A., Rosenfeld, D., & Rudich, Y. (2005). The effect of smoke, dust, and pollution aerosol on shallow cloud development over the atlantic ocean. *Proceedings of the National Academy of Sciences*, *102*(32), 11207–11212. https://doi.org/10.1073/pnas.0505191102

Khain, A. P., Beheng, K. D., Heymsfield, A., Korolev, A., Krichak, S. O., Levin, Z., Pinsky, M., Phillips, V., Prabhakaran, T., Teller, A., den Heever, S. C., & Yano, J.-I. (2015). Representation of microphysical processes in cloud-resolving models: Spectral (bin) microphysics versus bulk parameterization. *Reviews of Geophysics*, *53*(2), 247–322. https://doi.org/10.1002/2014RG000468

Khain, A. P., BenMoshe, N., & Pokrovsky, A. (2008). Factors determining the impact of aerosols on surface precipitation from clouds: An attempt at classification. *Journal of the Atmospheric Sciences*, *65*(6), 1721–1748. https://doi.org/10.1175/2007JAS2515.1

Khain, A. P., & Pinsky, M. B. (1997). Turbulence effects on the collision kernel. ii: Increase of the swept volume of colliding drops. *Quarterly Journal of the Royal Meteorological Society*, *123*(542), 1543–1560. https://doi.org/10.1002/qj.49712354205

Khairoutdinov, M. F., Krueger, S. K., Moeng, C.-H., Bogenschutz, P. A., & Randall, D. A. (2009). Large-eddy simulation of maritime deep tropical convection. *Journal of Advances in Modeling Earth Systems*, *1*(4). https://doi.org/10.3894/JAMES.2009.1.15

Khairoutdinov, M. F., & Randall, D. A. (2001). A cloud resolving model as a cloud parameterization in the ncar community climate system model: Preliminary results. *Geophysical Research Letters*, *28*(18), 3617–3620. https://doi.org/10.1029/2001GL013552

Khairoutdinov, M., & Kogan, Y. (2000). A new cloud physics parameterization in a large-eddy simulation model of marine stratocumulus. *Monthly Weather Review*, *128*(1), 229–243. https://doi.org/10.1175/1520-0493(2000)128⟨0229:ANCPPI⟩2.0.CO;2

King, M. D., Platnick, S., Menzel, W. P., Ackerman, S. A., & Hubanks, P. A. (2013). Spatial and temporal distribution of clouds observed by modis onboard the terra and aqua satellites. *IEEE Transactions on Geoscience and Remote Sensing*, *51*(7), 3826–3852. https://doi.org/10.1109/TGRS.2012.2227333

Klocke, D., Brueck, M., Hohenegger, C., & Stevens, B. (2017). Rediscovery of the doldrums in storm-resolving simulations over the tropical atlantic. *Nature Geoscience*, *10*(12), 891–896. https://doi.org/10.1038/s41561-017-0005-4

Koffi, B., Schulz, M., BrÃ©on, F.-M., Dentener, F., Steensen, B. M., Griesfeller, J., Winker, D., Balkanski, Y., Bauer, S. E., Bellouin, N., Berntsen, T., Bian, H., Chin, M., Diehl, T., Easter, R., Ghan, S., Hauglustaine, D. A., Iversen, T., Kirkevåg, A., ... Zhang, K. (2016). Evaluation of the aerosol vertical distribution in global aerosol models through comparison against caliop measurements: Aerocom phase ii results. *Journal of Geophysical Research: Atmospheres*, *121*(12), 7254–7283. https://doi.org/10.1002/2015JD024639

Köhler, H. (1936). The nucleus in and the growth of hygroscopic droplets. *Transactions of the Faraday Society*, (32), 1152–1161.

Koren, I., Oreopoulos, L., Feingold, G., Remer, L. A., & Altaratz, O. (2008). How small is a small cloud? *Atmospheric Chemistry and Physics*, *8*(14), 3855–3864. https://doi.org/10.5194/acp-8-3855-2008

Koren, I., Altaratz, O., & Dagan, G. (2015). Aerosol effect on the mobility of cloud droplets. *Environmental Research Letters*, *10*(10), 104011. https://doi.org/10.1088/1748-9326/10/10/104011

Koren, I., Dagan, G., & Altaratz, O. (2014). From aerosol-limited to invigoration of warm convective clouds. *Science*, *344*(6188), 1143–1146. https://doi.org/10.1126/science.1252595

Koren, I., Kaufman, Y. J., Remer, L. A., & Martins, J. V. (2004). Measurement of the effect of amazon smoke on inhibition of cloud formation. *Science*, *303*(5662), 1342–1345.

Korhonen, H., Carslaw, K. S., Spracklen, D. V., Mann, G. W., & Woodhouse, M. T. (2008). Influence of oceanic dimethyl sulfide emissions on cloud condensation nuclei concentrations and seasonality over the remote southern hemisphere oceans: A global model study. *Journal of Geophysical Research: Atmospheres*, *113*(D15). https://doi.org/10.1029/2007JD009718

Lamarck, J.-B. (1802). Sur la forme des nuages. *Annuaire Météorologique pour l'an X de la République Française*, *3*, 149–164.

Langhans, W., Schmidli, J., & Schär, C. (2012). Bulk convergence of cloud-resolving simulations of moist convection over complex terrain. *Journal of the Atmospheric Sciences*, *69*(7), 2207–2228. https://doi.org/10.1175/JAS-D-11-0252.1

Larson, V. E., & Golaz, J.-C. (2005). Using probability density functions to derive consistent closure relationships among higher-order moments. *Monthly Weather Review*, *133*(4), 1023–1042. https://doi.org/10.1175/MWR2902.1

Lasher-Trapp, S. G., Cooper, W. A., & Blyth, A. M. (2005). Broadening of droplet size distributions from entrainment and mixing in a cumulus cloud. *Quart. J. Roy. Meteor. Soc.*, *131*, 195–220.

Lau, K. M., & Wu, H. T. (2003). Warm rain processes over tropical oceans and climate implications. *Geophysical Research Letters*, *30*(24). https://doi.org/10.1029/2003GL018567

Lebo, Z. J., Morrison, H., & Seinfeld, J. H. (2012). Are simulated aerosol-induced effects on deep convective clouds strongly dependent on saturation adjustment? *Atmospheric Chemistry and Physics*, *12*(20), 9941–9964. https://doi.org/10.5194/acp-12-9941-2012

Lebo, Z. J., & Seinfeld, J. H. (2011). Theoretical basis for convective invigoration due to increased aerosol concentration. *Atmospheric Chemistry and Physics*, *11*(11), 5407–5429. https://doi.org/10.5194/acp-11-5407-2011

Lee, S.-S., Feingold, G., & Chuang, P. Y. (2012). Effect of aerosol on cloud–environment interactions in trade cumulus. *Journal of the Atmospheric Sciences*, *69*(12), 3607–3632. https://doi.org/10.1175/JAS-D-12-026.1

Li, X., Tao, W.-K., Masunaga, H., Gu, G., & Zeng, X. (2013). Aerosol effects on cumulus congestus population over the tropical pacific: A cloud-resolving modeling study. *Journal of the Meteorological Society of Japan. Ser. II*, *91*(6), 817–833. https://doi.org/10.2151/jmsj.2013-607

Li, Z., Zuidema, P., & Zhu, P. (2014). Simulated convective invigoration processes at trade wind cumulus cold pool boundaries. *Journal of the Atmospheric Sciences*, *71*(8), 2823–2841. https://doi.org/10.1175/JAS-D-13-0184.1

Liu, H., Guo, J., Koren, I., Altaratz, O., Dagan, G., Wang, Y., Jiang, J. H., Zhai, P., & Yung, Y. L. (2019). Non-monotonic aerosol effect on precipitation in convective clouds over tropical oceans. *Scientific Reports*, *9*(1), 7809. https://doi.org/10.1038/s41598-019-44284-2

Loeb, N. G., Doelling, D. R., Wang, H., Su, W., Nguyen, C., Corbett, J. G., Liang, L., Mitrescu, C., Rose, F. G., & Kato, S. (2018). Clouds and the earth?s radiant energy system (ceres) energy balanced and filled (ebaf) top-of-atmosphere (toa) edition-4.0 data product. *Journal of Climate*, *31*(2), 895–918. https://doi.org/10.1175/JCLI-D-17-0208.1

Lohmann, U., & Feichter, J. (2005). Global indirect aerosol effects: A review. *Atmospheric Chemistry and Physics*, *5*(3), 715–737. https://doi.org/10.5194/acp-5-715-2005

Lohmann, U., Lüönd, F., & Mahrt, F. (2016). *An introduction to clouds: From the microscale to climate*. Cambridge University Press. https://doi.org/10.1017/CBO9781139087513

Mace, G. G., & Abernathy, A. C. (2016). Observational evidence for aerosol invigoration in shallow cumulus downstream of mount kilauea. *Geophysical Research Letters*, *43*(6), 2981–2988. https://doi.org/10.1002/2016GL067830

Malkus, J. S., & Riehl, H. (1964). Cloud structure and distributions over the tropical pacific ocean1. *Tellus*, *16*(3), 275–287. https://doi.org/10.1111/j.2153-3490.1964.tb00167.x

Mann, G. W., Carslaw, K. S., Ridley, D. A., Spracklen, D. V., Pringle, K. J., Merikanto, J., Korhonen, H., Schwarz, J. P., Lee, L. A., Manktelow, P. T., Woodhouse, M. T., Schmidt, A., Breider, T. J., Emmerson, K. M., Reddington, C. L., Chipperfield, M. P., & Pickering, S. J. (2012). Intercomparison of modal and sectional aerosol microphysics representations within

the same 3-d global chemical transport model. *Atmospheric Chemistry and Physics*, *12*(10), 4449–4476. https://doi.org/10.5194/acp-12-4449-2012

Markowicz, K. M., Flatau, P. J., Ramana, M. V., Crutzen, P. J., & Ramanathan, V. (2002). Absorbing mediterranean aerosols lead to a large reduction in the solar radiation at the surface. *Geophysical Research Letters*, *29*(20), 29-1-29–4. https://doi.org/10.1029/2002GL015767

Masunaga, H., & Kummerow, C. D. (2006). Observations of tropical precipitating clouds ranging from shallow to deep convective systems. *Geophysical Research Letters*, *33*(16). https://doi.org/10.1029/2006GL026547

McCormick, R. A., & Ludwig, J. H. (1967). Climate modification by atmospheric aerosols. *Science*, *156*(3780), 1358–1359. https://doi.org/10.1126/science.156.3780.1358

McGee, C. J., & van den Heever, S. C. (2014). Latent heating and mixing due to entrainment in tropical deep convection. *Journal of the Atmospheric Sciences*, *71*(2), 816–832. https://doi.org/10.1175/JAS-D-13-0140.1

Medeiros, B., & Nuijens, L. (2016). Clouds at barbados are representative of clouds across the trade wind regions in observations and climate models. *Proceedings of the National Academy of Sciences*, *113*(22), E3062–E3070. https://doi.org/10.1073/pnas.1521494113

Medeiros, B., Stevens, B., & Bony, S. (2015). Using aquaplanets to understand the robust responses of comprehensive climate models to forcing. *Climate Dynamics*, *44*(7), 1957–1977. https://doi.org/10.1007/s00382-014-2138-0

Medeiros, B., Stevens, B., Held, I. M., Zhao, M., Williamson, D. L., Olson, J. G., & Bretherton, C. S. (2008). Aquaplanets, climate sensitivity, and low clouds. *Journal of Climate*, *21*(19), 4974–4991. https://doi.org/10.1175/2008JCLI1995.1

Miltenberger, A. K., Field, P. R., Hill, A. A., Rosenberg, P., Shipway, B. J., Wilkinson, J. M., Scovell, R., & Blyth, A. M. (2018a). Aerosol–cloud

interactions in mixed-phase convective clouds – part 1: Aerosol perturbations. *Atmospheric Chemistry and Physics*, *18*(5), 3119–3145. https://doi.org/10.5194/acp-18-3119-2018

Miltenberger, A. K., Field, P. R., Hill, A. A., Rosenberg, P., Shipway, B. J., Wilkinson, J. M., Scovell, R., & Blyth, A. M. (2018b). Aerosol–cloud interactions in mixed-phase convective clouds – part 1: Aerosol perturbations. *Atmospheric Chemistry and Physics*, *18*(5), 3119–3145. https://doi.org/10.5194/acp-18-3119-2018

Miyamoto, Y., Kajikawa, Y., Yoshida, R., Yamaura, T., Yashiro, H., & Tomita, H. (2013). Deep moist atmospheric convection in a subkilometer global simulation. *Geophysical Research Letters*, *40*(18), 4922–4926. https://doi.org/10.1002/grl.50944

Miyamoto, Y., Yoshida, R., Yamaura, T., Yashiro, H., Tomita, H., & Kajikawa, Y. (2015). Does convection vary in different cloud disturbances? *Atmospheric Science Letters*, *16*(3), 305–309. https://doi.org/10.1002/asl2.558

Morrison, H., & Grabowski, W. W. (2008). Modeling supersaturation and subgrid-scale mixing with two-moment bulk warm microphysics. *Journal of the Atmospheric Sciences*, *65*(3), 792–812. https://doi.org/10.1175/2007JAS2374.1

Morrison, H., van Lier-Walqui, M., Fridlind, A. M., Grabowski, W. W., Harrington, J. Y., Hoose, C., Korolev, A., Kumjian, M. R., Milbrandt, J. A., Pawlowska, H., Posselt, D. J., Prat, O. P., Reimel, K. J., Shima, S.-I., van Diedenhoven, B., & Xue, L. (2020). Confronting the challenge of modeling cloud and precipitation microphysics [e2019MS001689 2019MS001689]. *Journal of Advances in Modeling Earth Systems*, *12*(8), e2019MS001689. https://doi.org/10.1029/2019MS001689

Myhre, G., Shindell, D., Bréon, F.-M., Collins, W., Fuglestvedt, J., Huang, J., Koch, D., Lamarque, J.-F., Lee, D., Mendoza, B., Nakajima, T., Robock, A., Stephens, G., Takemura, T., & Zhang, H. (2013). Anthropogenic and

natural radiative forcing. In T. F. Stocker, D. Qin, G.-K. Plattner, M. Tignor, S. K. Allen, J. Doschung, A. Nauels, Y. Xia, V. Bex, & P. M. Midgley (Eds.), *Climate change 2013: The physical science basis. contribution of working group i to the fifth assessment report of the intergovernmental panel on climate change* (pp. 659–740). Cambridge, UK, Cambridge University Press. https://doi.org/10.1017/CBO9781107415324.018

Nair, U. S., Weger, R. C., Kuo, K. S., & Welch, R. M. (1998). Clustering, randomness, and regularity in cloud fields: 5. the nature of regular cumulus cloud fields. *Journal of Geophysical Research: Atmospheres*, *103*(D10), 11363–11380. https://doi.org/10.1029/98JD00088

Naumann, A. K., Stevens, B., Hohenegger, C., & Mellado, J. P. (2017). A conceptual model of a shallow circulation induced by prescribed low-level radiative cooling. *Journal of the Atmospheric Sciences*, *74*(10), 3129–3144. https://doi.org/10.1175/JAS-D-17-0030.1

Neale, R. B., Richter, J., Conley, A., Park, S., Lauritzen, P., Gettelman, A., Williamson, D., Rasch, P., Vavrus, S., Taylor, M., Et al. (2010). Description of the ncar community atmosphere model (cam 4.0), ncar tech. *Note, TN–485*, 212.

Neggers, R. A. J., Neelin, J. D., & Stevens, B. (2007). Impact mechanisms of shallow cumulus convection on tropical climate dynamics. *Journal of Climate*, *20*(11), 2623–2642. https://doi.org/10.1175/JCLI4079.1

Nuijens, L., Serikov, I., Hirsch, L., Lonitz, K., & Stevens, B. (2014). The distribution and variability of low-level cloud in the north atlantic trades. *Quarterly Journal of the Royal Meteorological Society*, *140*(684), 2364–2374. https://doi.org/10.1002/qj.2307

Nuijens, L., Stevens, B., & Siebesma, A. P. (2009). The environment of precipitating shallow cumulus convection. *Journal of the Atmospheric Sciences*, *66*(7), 1962–1979. https://doi.org/10.1175/2008JAS2841.1

O'Dowd, C. D., Lowe, J. A., Smith, M. H., & Kaye, A. D. (1999). The relative importance of non-sea-salt sulphate and sea-salt aerosol to the marine cloud condensation nuclei population: An improved multi-component aerosol-cloud droplet parameterization. *Quart. J. Roy. Meteor. Soc*, *125*, 1295–1313.

Onishi, R., & Takahashi, K. (2012). A warm-bin–cold-bulk hybrid cloud microphysical model. *Journal of the atmospheric sciences*, *69*(5), 1474–1497.

Perlwitz, J., & Miller, R. L. (2010). Cloud cover increase with increasing aerosol absorptivity: A counterexample to the conventional semidirect aerosol effect. *Journal of Geophysical Research: Atmospheres*, *115*(D8). https://doi.org/10.1029/2009JD012637

Pinsky, M., & Khain, A. (1997). Turbulence effects on droplet growth and size distribution in clouds - a review. *Journal of Aerosol Science*, *28*(7), 1177–1214. https://doi.org/10.1016/S0021-8502(97)00005-0

Pruppacher, H. R., & Klett, J. D. (2012). *Microphysics of clouds and precipitation: Reprinted 1980*. Springer Science & Business Media.

Qu, X., Hall, A., Klein, S. A., & Caldwell, P. M. (2015). The strength of the tropical inversion and its response to climate change in 18 cmip5 models. *Climate Dynamics*, *45*(1-2), 375–396.

Rasp, S., Schulz, H., Bony, S., & Stevens, B. (2020). Combining crowdsourcing and deep learning to explore the mesoscale organization of shallow convection. *Bulletin of the American Meteorological Society*, *101*(11), E1980–E1995. https://doi.org/10.1175/BAMS-D-19-0324.1

Rauber, R. M., Stevens, B., Ochs, H. T., Knight, C., Albrecht, B. A., Blyth, A. M., Fairall, C. W., Jensen, J. B., Lasher-Trapp, S. G., Mayol-Bracero, O. L., Vali, G., Anderson, J. R., Baker, B. A., Bandy, A. R., Burnet, E., Brenguier, J.-L., Brewer, W. A., Brown, P. R. A., Chuang, R., ... Zuidema, P. (2007). Rain in shallow cumulus over the ocean: The rico

campaign. *Bulletin of the American Meteorological Society*, *88*(12), 1912–1928. https://doi.org/10.1175/BAMS-88-12-1912

Reid, J. S., Lagrosas, N. D., Jonsson, H. H., Reid, E. A., Atwood, S. A., Boyd, T. J., Ghate, V. P., Xian, P., Posselt, D. J., Simpas, J. B., Et al. (2016). Aerosol meteorology of maritime continent for the 2012 7seas southwest monsoon intensive study–part 2: Philippine receptor observations of fine-scale aerosol behavior. *Atmospheric Chemistry and Physics*, *16*(22), 14057–14078.

Reutter, P., Su, H., Trentmann, J., Simmel, M., Rose, D., Gunthe, S., Wernli, H., Andreae, M., & Pöschl, U. (2009). Aerosol-and updraft-limited regimes of cloud droplet formation: Influence of particle number, size and hygroscopicity on the activation of cloud condensation nuclei (ccn). *Atmospheric Chemistry and Physics*, *9*(18), 7067–7080.

Rossow, W. B., & Schiffer, R. A. (1999). Advances in understanding clouds from isccp. *Bull. Amer. Meteorol. Soc.*, *80*, 2261–2288. https://doi.org/10.1175/1520-0477(1999)080⟨2261:AIUCFI⟩2.0.CO;2

Sakradzija, M., & Hohenegger, C. (2017). What determines the distribution of shallow convective mass flux through a cloud base? *Journal of the Atmospheric Sciences*, *74*(8), 2615–2632. https://doi.org/10.1175/JAS-D-16-0326.1

Saleeby, S. M., & Cotton, W. R. (2008). A binned approach to cloud-droplet riming implemented in a bulk microphysics model. *Journal of Applied Meteorology and Climatology*, *47*(2), 694–703. https://doi.org/10.1175/2007JAMC1664.1

Saleeby, S. M., Herbener, S. R., van den Heever, S. C., & L'Ecuyer, T. (2015). Impacts of cloud droplet–nucleating aerosols on shallow tropical convection. *Journal of the Atmospheric Sciences*, *72*(4), 1369–1385. https://doi.org/10.1175/JAS-D-14-0153.1

Sassen, K., & Wang, Z. (2008). Classifying clouds around the globe with the cloudsat radar: 1-year of results. *Geophysical Research Letters*, *35*(4). https://doi.org/10.1029/2007GL032591

Sassen, K., Wang, Z., & Liu, D. (2009). Cirrus clouds and deep convection in the tropics: Insights from calipso and cloudsat. *Journal of Geophysical Research: Atmospheres*, *114*(D4). https://doi.org/10.1029/2009JD011916

Satoh, M., Stevens, B., Judt, F., Khairoutdinov, M., Lin, S.-J., Putman, W. M., & Düben, P. (2019). Global cloud-resolving models. *Current Climate Change Reports*, *5*(3), 172–184. https://doi.org/10.1007/s40641-019-00131-0

Satoh, M., Tomita, H., Yashiro, H., Kajikawa, Y., Miyamoto, Y., Yamaura, T., Miyakawa, T., Nakano, M., Kodama, C., Noda, A. T., Nasuno, T., Yamada, Y., & Fukutomi, Y. (2017). Outcomes and challenges of global high-resolution non-hydrostatic atmospheric simulations using the k computer. *Progress in Earth and Planetary Science*, *4*(1), 13. https://doi.org/10.1186/s40645-017-0127-8

Schalkwijk, J., Jonker, H. J. J., Siebesma, A. P., & Meijgaard, E. V. (2015). Weather forecasting using gpu-based large-eddy simulations. *Bulletin of the American Meteorological Society*, *96*(5), 715–723. https://doi.org/10.1175/BAMS-D-14-00114.1

Schneider, T., Teixeira, J., Bretherton, C. S., Brient, F., Pressel, K. G., Schär, C., & Siebesma, A. P. (2017). Climate goals and computing the future of clouds. *Nature Climate Change*, *7*(1), 3–5. https://doi.org/10.1038/nclimate3190

Schumacher, C., & Houze, R. A. (2003). The trmm precipitation radar's view of shallow, isolated rain. *Journal of Applied Meteorology*, *42*(10), 1519–1524. https://doi.org/10.1175/1520-0450(2003)042⟨1519:TTPRVO⟩2.0.CO;2

Schutgens, N., Tsyro, S., Gryspeerdt, E., Goto, D., Weigum, N., Schulz, M., & Stier, P. (2017). On the spatio-temporal representativeness of obser-

vations. *Atmospheric Chemistry and Physics*, *17*(16), 9761–9780. https://doi.org/10.5194/acp-17-9761-2017

Seifert, A., & Heus, T. (2013). Large-eddy simulation of organized precipitating trade wind cumulus clouds. *Atmospheric Chemistry and Physics*, *13*(11), 5631–5645. https://doi.org/10.5194/acp-13-5631-2013

Seifert, A., Köhler, C., & Beheng, K. D. (2012). Aerosol-cloud-precipitation effects over germany as simulated by a convective-scale numerical weather prediction model. *Atmospheric Chemistry and Physics*, *12*(2), 709–725. https://doi.org/10.5194/acp-12-709-2012

Seifert, A., Heus, T., Pincus, R., & Stevens, B. (2015). Large-eddy simulation of the transient and near-equilibrium behavior of precipitating shallow convection. *Journal of Advances in Modeling Earth Systems*, *7*(4), 1918–1937. https://doi.org/10.1002/2015MS000489

Seigel, R. B. (2014). Shallow cumulus mixing and subcloud-layer responses to variations in aerosol loading. *Journal of the Atmospheric Sciences*, *71*(7), 2581–2603. https://doi.org/10.1175/JAS-D-13-0352.1

Seinfeld, J. H., Bretherton, C., Carslaw, K. S., Coe, H., DeMott, P. J., Dunlea, E. J., Feingold, G., Ghan, S., Guenther, A. B., Kahn, R., Kraucunas, I., Kreidenweis, S. M., Molina, M. J., Nenes, A., Penner, J. E., Prather, K. A., Ramanathan, V., Ramaswamy, V., Rasch, P. J., ... Wood, R. (2016). Improving our fundamental understanding of the role of aerosol-cloud interactions in the climate system. *Proceedings of the National Academy of Sciences*, *113*(21), 5781–5790. https://doi.org/10.1073/pnas.1514043113

Seinfeld, J. H., & Pandis, S. N. (2016). *Atmospheric chemistry and physics: From air pollution to climate change*. John Wiley & Sons, Incorporated.

Sheffield, A. M., Saleeby, S. M., & Heever, S. C. (2015). Aerosol-induced mechanisms for cumulus congestus growth. *Journal of Geophysical Research: Atmospheres*, *120*(17), 8941–8952. https://doi.org/10.1002/2015JD023743

Sherwood, S. C., Bony, S., & Dufresne, J.-L. (2014). Spread in model climate sensitivity traced to atmospheric convective mixing. *Nature*, *505*(7481), 37–42. https://doi.org/10.1038/nature12829

Shima, S., Kusano, K., Kawano, A., Sugiyama, T., & Kawahara, S. (2009). The super-droplet method for the numerical simulation of clouds and precipitation: A particle-based and probabilistic microphysics model coupled with a non-hydrostatic model. *Quarterly Journal of the Royal Meteorological Society*, *135*(642), 1307–1320. https://doi.org/10.1002/qj.441

Shima, S., Sato, Y., Hashimoto, A., & Misumi, R. (2020). Predicting the morphology of ice particles in deep convection using the super-droplet method: Development and evaluation of scale-sdm 0.2.5-2.2.0, -2.2.1, and -2.2.2. *Geoscientific Model Development*, *13*(9), 4107–4157. https://doi.org/10.5194/gmd-13-4107-2020

Shipway, B. J. (2015). Revisiting twomey's approximation for peak supersaturation. *Atmospheric Chemistry and Physics*, *15*(7), 3803–3814. https://doi.org/10.5194/acp-15-3803-2015

Shipway, B. J., & Hill, A. A. (2012). Diagnosis of systematic differences between multiple parametrizations of warm rain microphysics using a kinematic framework. *Quarterly Journal of the Royal Meteorological Society*, *138*(669), 2196–2211. https://doi.org/10.1002/qj.1913

Short, D. A., & Nakamura, K. (2000). Trmm radar observations of shallow precipitation over the tropical oceans. *Journal of Climate*, *13*(23), 4107–4124.

Simpson, E., Connolly, P., & McFiggans, G. (2014). An investigation into the performance of four cloud droplet activation parameterisations. *Geoscientific Model Development*, *7*(4), 1535–1542. https://doi.org/10.5194/gmd-7-1535-2014

Simpson, J. (1969). A comparison between laboratory and atmospheric density currents. *Quarterly Journal of the Royal Meteorological Society*, *95*(406), 758–765.

Small, J. D., Chuang, P. Y., Feingold, G., & Jiang, H. (2009). Can aerosol decrease cloud lifetime? *Geophysical Research Letters*, *36*(16). https://doi.org/10.1029/2009GL038888

Smith, R. N. B. (1990). A scheme for predicting layer clouds and their water content in a general circulation model. *Quarterly Journal of the Royal Meteorological Society*, *116*(492), 435–460. https://doi.org/10.1002/qj.49711649210

Spill, G., Stier, P., Field, P. R., & Dagan, G. (2019). Effects of aerosol in simulations of realistic shallow cumulus cloud fields in a large domain. *Atmospheric Chemistry and Physics*, *19*(21), 13507–13517. https://doi.org/10.5194/acp-19-13507-2019

Spill, G., Stier, P., Field, P. R., & Dagan, G. (2021). Contrasting responses of idealised and realistic simulations of shallow cumuli to aerosol perturbations. *Geophysical Research Letters*, *48*(13), e2021GL094137. https://doi.org/10.1029/2021GL094137

Stephens, G. L., Li, J., Wild, M., Clayson, C. A., Loeb, N., Kato, S., L'Ecuyer, T., Stackhouse, P. W., Lebsock, M., & Andrews, T. (2012). An update on earth's energy balance in light of the latest global observations. *Nature Geoscience*, *5*(10), 691–696. https://doi.org/10.1038/ngeo1580

Stevens, B., Bony, S., Farrell, D., Ament, F., Blyth, A., Fairall, C., Karstensen, J., Quinn, P. K., Speich, S., Acquistapace, C., Aemisegger, F., Albright, A. L., Bellenger, H., Bodenschatz, E., Caesar, K.-A., Chewitt-Lucas, R., de Boer, G., Delanoë, J., Denby, L., ... Zöger, M. (2021). EUREC^{4}A. *Earth System Science Data Discussions*, *2021*, 1–78. https://doi.org/10.5194/essd-2021-18

Stevens, B. (2005). Atmospheric moist convection. *Annual Review of Earth and Planetary Sciences*, *33*(1), 605–643. https://doi.org/10.1146/annurev.earth.33.092203.122658

Stevens, B., Ament, F., Bony, S., Crewell, S., Ewald, F., Gross, S., Hansen, A., Hirsch, L., Jacob, M., Kölling, T., Konow, H., Mayer, B., Wendisch, M., Wirth, M., Wolf, K., Bakan, S., Bauer-Pfundstein, M., Brueck, M., Delanoë, J., ... Zinner, T. (2019a). A high-altitude long-range aircraft configured as a cloud observatory: The narval expeditions. *Bulletin of the American Meteorological Society*, *100*(6), 1061–1077. https://doi.org/10.1175/BAMS-D-18-0198.1

Stevens, B., Bony, S., Brogniez, H., Hentgen, L., Hohenegger, C., Kiemle, C., L'Ecuyer, T. S., Naumann, A. K., Schulz, H., Siebesma, P. A., Vial, J., Winker, D. M., & Zuidema, P. (2020). Sugar, gravel, fish and flowers: Mesoscale cloud patterns in the trade winds. *Quarterly Journal of the Royal Meteorological Society*, *146*(726), 141–152. https://doi.org/10.1002/qj.3662

Stevens, B., Farrell, D., Hirsch, L., Jansen, F., Nuijens, L., Serikov, I., Brügmann, B., Forde, M., Linne, H., Lonitz, K., & Prospero, J. M. (2016). The barbados cloud observatory: Anchoring investigations of clouds and circulation on the edge of the itcz. *Bulletin of the American Meteorological Society*, *97*(5), 787–801. https://doi.org/10.1175/BAMS-D-14-00247.1

Stevens, B., & Feingold, G. (2009). Untangling aerosol effects on clouds and precipitation in a buffered system. *Nature*, *461*, 607–613. http://dx.doi.org/10.1038/nature08281

Stevens, B., Satoh, M., Auger, L., Biercamp, J., Bretherton, C. S., Chen, X., Düben, P., Judt, F., Khairoutdinov, M., Klocke, D., Kodama, C., Kornblueh, L., Lin, S.-J., Neumann, P., Putman, W. M., Röber, N., Shibuya, R., Vanniere, B., Vidale, P. L., ... Zhou, L. (2019b). Dyamond: The dynamics of the atmospheric general circulation modeled on non-hydrostatic

domains. *Progress in Earth and Planetary Science*, *6*(1), 61. https://doi.org/10.1186/s40645-019-0304-z

Stier, P., Feichter, J., Kinne, S., Kloster, S., Vignati, E., Wilson, J., Ganzeveld, L., Tegen, I., Werner, M., Balkanski, Y., Schulz, M., Boucher, O., Minikin, A., & Petzold, A. (2005). The aerosol-climate model echam5-ham. *Atmospheric Chemistry and Physics*, *5*(4), 1125–1156. https://doi.org/10.5194/acp-5-1125-2005

Stier, P., Seinfeld, J. H., Kinne, S., & Boucher, O. (2007). Aerosol absorption and radiative forcing. *Atmospheric Chemistry and Physics*, *7*(19), 5237–5261. https://doi.org/10.5194/acp-7-5237-2007

Stier, P., Feichter, J., Kloster, S., Vignati, E., & Wilson, J. (2006). Emission-induced nonlinearities in the global aerosol system: Results from the echam5-ham aerosol-climate model. *Journal of Climate*, *19*(16), 3845–3862. https://doi.org/10.1175/JCLI3772.1

Stjern, C. W., Samset, B. H., Myhre, G., Forster, P. M., Hodnebrog, Ø., Andrews, T., Boucher, O., Faluvegi, G., Iversen, T., Kasoar, M., Kharin, V., Kirkevåg, A., Lamarque, J.-F., Olivié, D., Richardson, T., Shawki, D., Shindell, D., Smith, C. J., Takemura, T., & Voulgarakis, A. (2017). Rapid adjustments cause weak surface temperature response to increased black carbon concentrations. *Journal of Geophysical Research: Atmospheres*, *122*(21), 11, 462–11, 481. https://doi.org/10.1002/2017JD027326

Stossmeister, G. (2008). Goes-east 1km rico-domain hdf data. version 1.0 [Accessed 29 May 2018. Data provided by NCAR/EOL under the sponsorship of the National Science Foundation. https://data.eol.ucar.edu/].

Stubenrauch, C. J., Rossow, W. B., Kinne, S., Ackerman, S., Cesana, G., Chepfer, H., Girolamo, L. D., Getzewich, B., Guignard, A., Heidinger, A., Maddux, B. C., Menzel, W. P., Minnis, P., Pearl, C., Platnick, S., Poulsen, C., Riedi, J., Sun-Mack, S., Walther, A., ... Zhao, G. (2013). Assessment of global cloud datasets from satellites: Project and database initiated by the gewex

radiation panel. *Bulletin of the American Meteorological Society*, *94*(7), 1031–1049. https://doi.org/10.1175/BAMS-D-12-00117.1

Sui, C.-H., Li, X., & Yang, M.-J. (2007). On the definition of precipitation efficiency. *Journal of the Atmospheric Sciences*, *64*(12), 4506–4513. https://doi.org/10.1175/2007JAS2332.1

Sui, C.-H., Li, X., Yang, M.-J., & Huang, H.-L. (2005). Estimation of oceanic precipitation efficiency in cloud models. *Journal of the atmospheric sciences*, *62*(12), 4358–4370.

Sundqvist, H., Berge, E., & Kristjánsson, J. E. (1989). Condensation and cloud parameterization studies with a mesoscale numerical weather prediction model. *Monthly Weather Review*, *117*(8), 1641–1657. https://doi.org/10.1175/1520-0493(1989)117⟨1641:CACPSW⟩2.0.CO;2

Tao, W. K., Johnson, D., Shie, C. L., & Simpson, J. (2004). The atmospheric energy budget and large-scale precipitation efficiency of convective systems during toga coare, gate, scsmex, and arm: Cloud-resolving model simulations. *Journal of Atmospheric Sciences*, *61*(20), 2405–2423.

Tao, W.-K., Chen, J.-P., Li, Z., Wang, C., & Zhang, C. (2012). Impact of aerosols on convective clouds and precipitation. *Reviews of Geophysics*, *50*(2). https://doi.org/10.1029/2011RG000369

Tiedtke, M. (1989). A comprehensive mass flux scheme for cumulus parameterization in large-scale models. *Monthly Weather Review*, *117*(8), 1779–1800. https://doi.org/10.1175/1520-0493(1989)117⟨1779:ACMFSF⟩2.0.CO;2

Twomey, S. (1977). The influence of pollution on the shortwave albedo of clouds. *Journal of the Atmospheric Sciences*, *34*(7), 1149–1152. https://doi.org/10.1175/1520-0469(1977)034⟨1149:TIOPOT⟩2.0.CO;2

van den Heever, S. C., Stephens, G. L., & Wood, N. B. (2011). Aerosol indirect effects on tropical convection characteristics under conditions of radiative–convective equilibrium. *Journal of the Atmospheric Sciences*, *68*(4), 699–718. https://doi.org/10.1175/2010JAS3603.1

vanZanten, M. C., Stevens, B., Nuijens, L., Siebesma, A. P., Ackerman, A. S., Burnet, F., Cheng, A., Couvreux, F., Jiang, H., Khairoutdinov, M., Kogan, Y., Lewellen, D. C., Mechem, D., Nakamura, K., Noda, A., Shipway, B. J., Slawinska, J., Wang, S., & Wyszogrodzki, A. (2011). Controls on precipitation and cloudiness in simulations of trade-wind cumulus as observed during rico. *Journal of Advances in Modeling Earth Systems*, *3*(2). https://doi.org/10.1029/2011MS000056

Vial, J., Bony, S., Dufresne, J.-L., & Roehrig, R. (2013). Coupling between lower-tropospheric convective mixing and low-level clouds: Physical mechanisms and dependence on convection scheme. *Journal of Advances in Modeling Earth Systems*, *8*(4), 1892–1911. https://doi.org/10.1002/2016MS000740

Vial, J., Vogel, R., Bony, S., Stevens, B., Winker, D. M., Cai, X., Hohenegger, C., Naumann, A. K., & Brogniez, H. (2019). A new look at the daily cycle of trade wind cumuli. *Journal of Advances in Modeling Earth Systems*, *11*(10), 3148–3166. https://doi.org/10.1029/2019MS001746

Vogel, R., Konow, H., Schulz, H., & Zuidema, P. (2021). A climatology of trade-wind cumulus cold pools and their link to mesoscale cloud organization. *Atmospheric Chemistry and Physics*, *21*(21), 16609–16630. https://doi.org/10.5194/acp-21-16609-2021

Vogel, R., Nuijens, L., & Stevens, B. (2020). Influence of deepening and mesoscale organization of shallow convection on stratiform cloudiness in the downstream trades. *Quarterly Journal of the Royal Meteorological Society*, *146*(726), 174–185. https://doi.org/10.1002/qj.3664

Walters, D., Boutle, I., Brooks, M., Melvin, T., Stratton, R., Vosper, S., Wells, H., Williams, K., Wood, N., Allen, T., Bushell, A., Copsey, D., Earnshaw, P., Edwards, J., Gross, M., Hardiman, S., Harris, C., Heming, J., Klingaman, N., ... Xavier, P. (2017). The met office unified model global atmosphere 6.0/6.1 and jules global land 6.0/6.1 configurations. *Geoscientific Model*

Development, *10*(4), 1487–1520. https://doi.org/10.5194/gmd-10-1487-2017

Warner, J. (1969a). The microstructure of cumulus cloud. part i. general features of the droplet spectrum. *J. Atmos. Sci.*, *26*, 1049–1059.

Warner, J. (1969b). The microstructure of cumulus cloud. part ii. the effect on droplet size distribution of the cloud nucleus spectrum and updraft velocity. *J. Atmos. Sci.*, *26*, 1272–1282.

Watson-Parris, D., Bellouin, N., Deaconu, L. T., Schutgens, N. A. J., Yoshioka, M., Regayre, L. A., Pringle, K. J., Johnson, J. S., Smith, C. J., Carslaw, K. S., & Stier, P. (2020). Constraining uncertainty in aerosol direct forcing [e2020GL087141 2020GL087141]. *Geophysical Research Letters*, *47*(9), e2020GL087141. https://doi.org/10.1029/2020GL087141

Webster, P. J., & Lukas, R. (1992). Toga coare: The coupled ocean–atmosphere response experiment. *Bulletin of the American Meteorological Society*, *73*(9), 1377–1416. http://www.jstor.org/stable/26230157

Whitby, K. T. (1978). The physical characteristics of sulfur aerosols [Proceedings of the International Symposium]. *Atmospheric Environment (1967)*, *12*(1), 135–159. https://doi.org/10.1016/0004-6981(78)90196-8

White, B., Gryspeerdt, E., Stier, P., Morrison, H., Thompson, G., & Kipling, Z. (2017). Uncertainty from the choice of microphysics scheme in convection-permitting models significantly exceeds aerosol effects. *Atmospheric Chemistry and Physics*, *17*(19), 12145–12175. https://doi.org/10.5194/acp-17-12145-2017

Wilcox, E. M. (2010). Stratocumulus cloud thickening beneath layers of absorbing smoke aerosol. *Atmospheric Chemistry and Physics*, *10*(23), 11769–11777. https://doi.org/10.5194/acp-10-11769-2010

Wood, R. (2012). Stratocumulus clouds. *Monthly Weather Review*, *140*(8), 2373–2423. https://doi.org/10.1175/MWR-D-11-00121.1

Wood, R., & Hartmann, D. L. (2006). Spatial variability of liquid water path in marine low cloud: The importance of mesoscale cellular convection. *Journal of Climate*, *19*(9), 1748–1764. https://doi.org/10.1175/JCLI3702.1

World Meteorological Organization. (2017). International cloud atlas. https://cloudatlas.wmo.int/

Xue, H., Feingold, G., & Stevens, B. (2008). Aerosol effects on clouds, precipitation, and the organization of shallow cumulus convection. *Journal of the Atmospheric Sciences*, *65*(2), 392–406. https://doi.org/10.1175/2007JAS2428.1

Yamaguchi, T., Feingold, G., & Kazil, J. (2019). Aerosol-cloud interactions in trade wind cumulus clouds and the role of vertical wind shear. *Journal of Geophysical Research: Atmospheres*, *124*(22), 12244–12261. https://doi.org/10.1029/2019JD031073

Yau, M. K., & Rogers, R. R. (1996). *A short course in cloud physics*. Elsevier Science.

Yu, P., Toon, O. B., Bardeen, C. G., Mills, M. J., Fan, T., English, J. M., & Neely, R. R. (2015). Evaluations of tropospheric aerosol properties simulated by the community earth system model with a sectional aerosol microphysics scheme. *Journal of Advances in Modeling Earth Systems*, *7*(2), 865–914. https://doi.org/10.1002/2014MS000421

Yuan, T., Remer, L. A., & Yu, H. (2011). Microphysical, macrophysical and radiative signatures of volcanic aerosols in trade wind cumulus observed by the a-train. *Atmospheric Chemistry and Physics*, *11*(14), 7119–7132. https://doi.org/10.5194/acp-11-7119-2011

Zhang, X. Y., Wang, Y. Q., Niu, T., Zhang, X. C., Gong, S. L., Zhang, Y. M., & Sun, J. Y. (2012). Atmospheric aerosol compositions in china: Spatial/temporal variability, chemical signature, regional haze distribution

and comparisons with global aerosols. *Atmospheric Chemistry and Physics*, *12*(2), 779–799. https://doi.org/10.5194/acp-12-779-2012

Zhang, Y., Pun, B., Vijayaraghavan, K., Wu, S.-Y., Seigneur, C., Pandis, S. N., Jacobson, M. Z., Nenes, A., & Seinfeld, J. H. (2004). Development and application of the model of aerosol dynamics, reaction, ionization, and dissolution (madrid). *Journal of Geophysical Research: Atmospheres*, *109*(D1). https://doi.org/10.1029/2003JD003501

Zhang, Y., Stevens, B., & Ghil, M. (2005). On the diurnal cycle and susceptibility to aerosol concentration in a stratocumulus-topped mixed layer. *Quarterly Journal of the Royal Meteorological Society*, *131*(608), 1567–1583. https://doi.org/10.1256/qj.04.103

Zhu, P., & Bretherton, C. S. (2004). A simulation study of shallow moist convection and its impact on the atmospheric boundary layer. *Monthly Weather Review*, *132*(10), 2391–2409. https://doi.org/10.1175/1520-0493(2004)132⟨2391:ASSOSM⟩2.0.CO;2

Zuidema, P., Li, Z., Hill, R. J., Bariteau, L., Rilling, B., Fairall, C., Brewer, W. A., Albrecht, B., & Hare, J. (2012). On trade wind cumulus cold pools. *Journal of the Atmospheric Sciences*, *69*(1), 258–280. https://doi.org/10.1175/JAS-D-11-0143.1